DEVELOPMENT OF A PRACTICAL 3D DDA PROGRAM FOR HAZARD ASSESSMENT OF EARTHQUAKE INDUCED LANDSLIDES

井, 培登

https://doi.org/10.15017/1785383

DEVELOPMENT OF A PRACTICAL 3D DDA PROGRAM FOR HAZARD ASSESSMENT OF EARTHQUAKE INDUCED LANDSLIDES

Jing Peideng

2016

DEVELOPMENT OF A PRACTICAL 3D DDA PROGRAM FOR HAZARD ASSESSMENT OF EARTHQUAKE INDUCED LANDSLIDE

Doctoral Dissertation

Submiitted to Graduate School of Engineering, Kyushu University

In Partial Fulfillment of the Requirements for the Degree of

Doctor of Engineering

By

Jing Peideng

Supervisor

Prof. Guangqi CHEN, Dr. Sci.

DEPARTMENT OF CIVIL AND STRUCTURAL ENGINEERING

KYUSHU UNIVERSITY

2016

CERTIFICATE

The undersigned hereby certify that they have read and recommended to the Graduate School of Engineering for the acceptance of this thesis entitled, ‘‘***Development of a practical 3D DDA program for hazard assessment of earthquake induced lanslides***” by **Jing Peideng** in partial fulfillment of the requirements for the degree of **Doctor of Engineering**.

Dated: May, 2016

Thesis Supervisor:

_____

Prof. Guangqi CHEN, Dr. Sci.

Examining Committee:

_____

Prof. Yasuhiro MITANI

_____

Prof. Takahiro KUBA

ABSTRACT

Earthquake induced landslide is one of the most serious geo-hazards. Especially, for the coastal area with potential tsunami, evacuation sites and access roads for tsunami are generally located upland and surrounded by slopes. Since an earthquake can induce not only tsunami but also landslides, it is obvious that the tsunami evacuation sites and access roads are threatened by the potential earthquake induced landslides. Therefore, it is important and necessary to assess the hazard of earthquake induced landslides so as to secure the safety of tsunami evacuation sites and access roads.

Hazard assessment of earthquake induced landslides includes slope stability analysis under seismic loading, landslide runout estimation and the evaluation of preventive effectivity such as anchor-reinforcement for a dangerous slope. With the development of the computer and computing sciences, various numerical simulation methods have been developed and shown their powerful capability in the landslide research. Discontinuous deformation analysis (DDA) is one of these simulation methods and has shown its advantage in theory and practice. There have been many research achievements reported by using 2D DDA. In order to overcome the limitation of 2D analysis, the development of 3D DDA is also undertaken. However, there still exist some key problems, which inhibit its practical application, in the development of 3D DDA program. For example, there is no effective tool for 3D DDA model construction; it is unavailable to perform slope stability analysis under seismic loading and with the anchor reinforcement.

This study aims at (1) developing a practical 3D DDA program by solving the above problems and (2) applying the new 3D DDA to the practical hazard assessment of potential earthquake induced landslides in a coastal area with potential tsunami of Oita prefecture, Japan. The new 3D DDA includes (1) developing an effective pre-processor for the 3D model construction; (2) adding the function of seismic loading and (3) adding the function of using anchor reinforcement.

The contents of this thesis are organized as follows:

Chapter 1 introduces the background, objective and organization of the thesis. The existing numerical simulation methods for landslide study are reviewed. The development of DDA in theory and practical application is briefly introduced and the advantages of DDA are clarified.

Chapter 2 provides an overview on 3D DDA. The 3D DDA formulation, contact principle, and program structure are illustrated in detail. The following unsolved problems of the existing 3D DDA program are discussed: (1) without an effective pre-processor for complex slope model construction, which is especially fundamental and necessary for practical application to landslide study; (2) unable to perform slope stability analysis and landslide runout simulation under a potential earthquake; (3) unable to evaluate the preventive effect of using anchor reinforcement.

Chapter 3 performs a close comparison between the 2D and 3D DDA to reveal the limitation of the 2D analysis and the necessity of 3D DDA. Their advantages and disadvantages are illustrated based on slope stability analysis and run-out simulation. The current 2D DDA program contains effective user friendly pre-processor and post-processor, which are powerful and necessary for practical slope study. There have been many achievements reported from practical 2D DDA applications. However, the limitations of 2D analysis also become obvious. Since lateral effect of a 2D slope section model cannot be considered, the factor of safety is often underestimated and lateral spread movement cannot be estimated in run-out analysis. On the other hand, the lateral friction and the lateral spread movement can be considered in 3D DDA analysis, the factor of safety can be estimated and the reasonable run-out can be simulated more accurately. But, a practical 3D DDA program has not been developed.

Chapter 4 develops a practical pre-processor to easily construct a complex 3D slope model for the 3D DDA program. Since construction of a complex 3D slope model is always a troublesome problem which including the following two big issues: (1) how to cut the blocks; (2) how to generate blocks of the 3D slope

terrain. The developed pre-processor solves these problems by taking the advantage of the commonly used commercial software: 3ds Max and ArcGIS. Arbitrary-shaped 3D bocks are made with 3ds Max and complex slope terrain mesh data are obtained from the ArcGIS. A pre-process program is developed to combine the output data from both 3ds Max and ArcGIS and translate them to the 3D DDA model format. It has been shown that a 3D DDA slope model can be easily and effectively made for any real slope with complex terrain by using the newly developed 3D DDA pre-processor, which makes it possible for applying 3D DDA to practical landslide study.

Chapter 5 extends the existing 3D DDA program by adding the function of seismic loading and the function of anchor reinforcement. The stability analysis and run-out estimation of a potential earthquake induced landslide need the function of dealing with seismic loading in a 3D DDA program. The added seismic loading function can use either displacement wave or acceleration wave, which depends on the data available. In addition, when a slope is judged unstable under a potential earthquake, the slope should be reinforced in general. Rock anchor reinforcement is one of typical preventive methods. Thus, it is necessary to evaluate the preventive effect and provide the useful information for optimum design of the size and number of rock anchors. By adding these two functions, the new 3D DDA program makes it possible to assess the hazard of earthquake induced landslides for securing the safety of tsunami evacuation sites and access roads.

Chapter 6 applies the new 3D DDA program to practical hazard assessment of earthquake induced landslides for securing the safety of tsunami evacuation sites and access roads in the coastal area of Oita prefecture. The Daiganji slope is taken as an example. An access road to a tsunami evacuation site and several houses are located at the slope downward. At first, the slope stability is analyzed by using both 2D and 3D DDA. The results are compared with those from the commonly used limit equilibrium method. The adaptability of DDA and the difference between 2D and 3D analysis are shown. Secondly, the factor of safety is analyzed by using earthquake loading. And the influence of seismic directivity on the slope stability is

analyzed. The landslide run-out is estimated by using the new 3D DDA program under the condition of the earthquake. It is shown that the access road and some houses are threatened by the potential landslide. Finally, the stability analysis of an anchor reinforced slope is performed to evaluate the preventive effect. It has been shown that the new 3D DDA is very useful and powerful enough for hazard assessment of earthquake induced landslides.

Chapter 7 summarizes the results and achievements of this study. The problems for the future study are highlighted.

ACKNOWLEDGEMENTS

I owe a debt of gratitude to many people when the dissertation is completed. Without their trust, patient guidance and constant encouragement, this study would have never been done.

First and foremost, I am most grateful to my supervisor, Prof. Dr. Guangqi Chen. His wisdom, knowledge and commitment to the highest standards inspired and motivated me. I benefited a lot from each conversation with him and I also learned how to purse my study and career. He provided me many opportunities to take part in international conferences, which makes me more confident in meeting the challenge in my later life and work. He not only taught me professional knowledge, but also scientific way of thinking and technical skills required in research. Without his valuable and timely comments, it would be very difficult for me to complete this dissertation.

I owe a special appreciation to Dr. Genhua Shi for his help and guidance in understanding DDA method and key discussions on developing the 3D-DDA code. I would like to extend my thanks to PhD candidate Wei Wang, Suhua Zhou and Long Zhang for their insightful discussions and useful C++ programming tips in this research.

I would like to express my sincerely gratitude to members of my dissertation committee, Prof. Dr. Guangqi Chen, Prof. Yasuhiro Mitani and Prof. Takahiro Kuba for their reviews, evaluation and valuable comments on my dissertation.

I am deeply indebted to Prof. Dr. Hongxing Wang, my former supervisor, in China University of Geosciences, for recommending me further study in Japan.

I also deeply appreciate Assoc. Prof. Kiyonobu Kasama, Staff Yuichi Yahiro for their enthusiastic and great help.

I would like to thank all the colleagues who I have been studying with in Geodiaster Prevention Laboratory where I really enjoyed my study in Japan. I would like to extend my thanks to all my friends in China, Japan and some other countries. They are always helping me, caring about me and encouraging me to

keep on this hard but happy journey.

I would like to extend my grateful acknowledgement to China Scholarship Council (CSC) for providing me the opportunity and scholarship to pursue my PhD at Kyushu University.

Finally and the most sincerely, I am grateful to my parents who always support me and encourage me.

TABLE OF CONTENTS

CHAPTER 1

INTRODUCTION

1.1 BACKGROUND

1.1.1 LANDSLIDE

The word “landslide” is normally used to describe the movement of the slope such as the falling, sliding and toppling or the combination of them. The materials that forming the landslide can be soil, rock or some artificial materials according to the references (Jackson, 1997) and other refers(Varnes, 1974; Hutchinson, 1988; WP/WLI, 1990; Cruden and Varnes, 1996; Highland and Bobrowsky, 2008; Gokceoglu and Sezer, 2009).

Landslide is a global and frequently occurred disaster which can cause huge damages and casualties (UNEP, 1997; EM-DAT, 2003). Some huge landslides or landslide causing disasters happened are catastrophic for humankind such as more than sixty thousand landslides causing by the 2008 Wenchuan earthquake causing more than twenty thousand fatalities. As can be seen by Table 1.1, landslide takes the 7^{th} position of the global major natural hazards in EM-DAT (2003). Moreover, it is normally think that the number fatalities caused by landslide in the database is underestimated because only the first triggers are recorded (Nadim et al., 2006; Yin et al, 2009).

Table 1. 1 The earthquake caused landslides.

Earthquake event	Date	Landslide number	Distribution area(km^2)	Reference
Iwate–Miyagi Nairiku, Japan	14 June 2008	4,161	600	Yagi et al. (2009)
Wenchuan, China	12 May 2008	60,000	20,000	Gorum et al. (2011)
Mid-Niigata, Japan	23 October 2004	4,438	275	Sekiguchi and Sato (2006)
Chi-Chi, Taiwan	21 September 1999	10,000	11,000	Liao and Lee (2000)
Northridge, California	17 January 1994	11,000	10,000	Harp and Jibson (1995, 1996)

1.1.2 LANDSLIDE-INDUCED DISASTERS

Landslides can induce secondary disasters, such as debris flows, landslide dams.

1.1.2.1 DEBRIS FLOW

The landslide induced by the earthquake is normally considered as a major sediment-supply for the mountainous area (Pearce et al., 1986). It is generally consider that the landslide deposit may transfer to debris flow if other factors are satisfied such as the heavy rainfall.

For example, the 2008 Wenchuan earthquake triggered more than 60,000 landslides in the mountainous areas in Sichuan Province, China. The rock materials and loose deposits of these landslides are distributed on steep slopes or in channels, and they can easily lead to debris flow in the moist season. In addition, the earthquake widely increased slope instability, providing lots of rock debris to initiate future debris flows.

A heavy rainfall triggered resulted in 72 debris flows in Beichuan County, Sichuan Province on September 23 and 24, 2008. These debris flows led to 42 people killed as well as great damages to roads and relocation area for people suffered from the earthquake.

Besides, a rainstorm triggerd 21 debris flows around Yingxiu Town, Sichuan Province on 14 August, 2010 (Figure 1.1). Among the 21 debris flows, the severest

one occurred in Hongchun Gully, Yingxiu Town. It carried large amount of sediment to Minjiang River and formed a natural debris dam, which is up to 10 m high, 100 m long and 150 m wide and subsequently changed the channel of Minjiang River and caused a flood in the newly reconstructed Yingxiu Town. The flood with a depth of about 2.5-3.0 m as estimated, lasted for 7 days and thus caused 13 people killed and 59 missing. Approximate 8,000 residents had to leave their residence communities.

Figure 1. 1 Aerial photograph showing debris flow fans produced by rainstorm near Yingxiu town on August 14, 2010 (taken by the Ministry of Land and Resources, PRC)

1.1.2.2 LANDSLIDE DAM

The river near the landslide may be blocked by the landslide forming the landslide dam. Once the dam break happens, the huge inventory and rapid stream may be a serious disaster for the people living downstream. An example of the landslide dam can be found in Figure 1.2.

Figure 1. 2 Helicopter view of the artificial spillway in the Tangjiashan landslide dam (adopted from Xinhua News Agency)

The failure of landslide dam can be found worldwide. As an typical example, the 2008 Wenchuan earthquake caused many landslide dams. The landslide dam caused by the earthquake is considered as one of the most serious earthquake induced disasters (Costa 1985; Costa and Schuster 1991; Kallen et al. 2006).

For conclusion, landslide or it induced disasters such as debris and landslide dam are huge threaten for humankind. It is meaningful and necessary to make a deep research on the landside-prone slope, such as its stability, run-out analysis and also the countermeasures such as the anchor reinforcement.

1.2 Research Methods

It is important to the capture the accurate or reasonable landslide movements in the landslide prevention engineering. Normally, there are three major research methods for studying the landslide movement: the experimental, the empirical and numerical method. Although there are some so-called analytical methods, because of some assumptions and simple models are used, it can be considered as one kind of numerical method. The following will show the detail review of the three research methods..

1.2.1 EXPERIMENTAL METHOD

Because the direct experiment is not easy to perform and it is dangerous and expensive, scale model is always been used for the experimental study of the landslide movements. Before scale modeling, some physical experiments are necessary, for instance the tri-axial test. According to the paper review, some artificial landslide mode experiment have been performed (Okura et al. 2000a, 2000b, 2002; Ochiai et al. 2004; Moriwaki et al. 2004; and others). Although some research result can be get by the experiment method, there are some limits. Firstly, as the material comparison is always heterogeneous, it is difficult to reflect the real material characteristics and the model has to be simplified. Secondly, it is nearly impossible to make a deep research of all the impact factors, as with one factor changes, the model should be rebuilt. Thirdly, it is obvious that it is time and money consuming. However, as it can get the qualitative data, it is fundamental and meaningful for the landslide research.

1.2.2 EMPIRICAL METHOD

As can be seen by the review of Hungr (2002), empirical method is very useful to estimate the runout distance of the landslide. These empirical methods normally estimate the run-out distance by creating the relation between the topography and the runout zone length. Generally, these methods can be called the statistical method

(Keylock and Domaas 1999). The *Fahrböschung* principle which is proposed by Heim (1932) is recommended and modified by many researchers such as Toppe (1987) and Hungr (1993) to estimate the runout zone. The basic theory of the *Fahrböschung* principle is to define the travel angle between the landslide source and the deposits, which results from the practical observations. Some modified principles have been proposed such as the minimum shadow angle by Evans and Hungr (1993), which follow the step of Lied (1977), which is the angle between the highest point of the slope and the deposit stop point. This theory has been testified and shown a good effect by Evans and Hungr (1993) depending on the practical study of sixty slopes in British.

A detail research has been conducted by Keylock and Dommas (1999), in which three kinds of models are used and compared. Its focus was on their ability to estimate the length of run-out are. The first mode that was used was the height function model, which can predict the runout length by building a connection with the height of rock face and the slope. The second model was theα-β model, proposed by Hsü (1975) and Köner (1980), which sources from the average energy theory. The last one was named as runout ratio model from McClung and Lied (1987), which can predict the horizontal runout distance according to the slope horizontal length and the rock face. This method was shown to be more accurate comparing with the other two methods according to the practical investigation.

Improved empirical model notable performing regressions on subsets with varying scopes were presented by Cannon (1993), Corominas (1996), Rickenman (2005) and others.

The empirical models can be used as a rudimentary evaluation and are meaningful for the landslide research, and besides the empirical models are easy for use. These models can be refined by other models if more detail research is needed. There are some disadvantages of the empirical models. Firstly, these models are over-simplified and cannot reflect the detail deformation and movement information of the landslide; Secondly, these models are born from the database of specific locations making them be very difficult for the general usage; Thirdly, although some

models have been created to try to consider the detail parameters(Japan Road Association 2000), it is impossible for these models to take the topography into consideration not to mention the properties of the landslide mass such as the water content, shear strength and et al.

1.2.3 ANALYTICAL METHOD

Generally, there are two major numerical methods for the landslide or the landslide-prone slope: the continuous method and the discontinuous method. When using the numerical method, the simulation sliding or slide-prone body is usually broken into small elements which can contact and influence with each other. The advantage is obvious that it can take the strength and interaction into consideration when simulation the source masses, and the entrainment can also be modeled during the runout. This allows for modeling the source mass with accounting for internal strength and entrainment throughout runout.

For the continuous methods, a typical and most used is the FEM (Finite Element Method). The FEM takes the simulation area as many small units connected by nodes which use the sub-domain approximation solution and can approach the infinite knowns by finite unknown variables. The FEM can be used to solve the linear problems and nonlinear issues. When simulating the debris, especially when the dimension of the elements is greatly smaller than the depth and length, the continuum method is more appreciate. A typical method called the Saint Venant method is built based on the average depth assuming the mass is incompressible, the relation between the mass and the the momentum equation is in form of depth-average. Some researchers (e.g., Soussa and Voight 1991; Takahashi et al. 1992; Cao et al. 1996) developed their simulation method according to the conventional Eulerian method. However, other published papers (e.g., Savage and Hutter 1989; Hungr 1995; Chen and Lee, 2000; Pirulli 2005 and McDougall 2006) value more another classical method which is based on the Lagrangian coordinate. The major differences of these re-built models are how to represent the resistance of the base and the constitutive models used to describe the mechanical performance of the simulated material.

For the landslide mass that is considered as large small fragments, the assembly of blocks can be used to model the sliding mass. When considering the individual block, the relevant constitutive law, the contact mechanism related to contacted block(s), the force applied can be reproduced, therefore, the movement characteristics such as velocity, displacements can be simulated and studied during a certain simulation period. In order to represent the simulated block, some researchers used the polygon shape model, while some recommended the circular shape mode (e.g., Poisel et al. 2008). For the polygon model, although it has the advantage of reflecting the real nature pattern, because of the inherent complexity of contact mechanism and the low computation efficiency, it is more appreciate for problems limited to limited blocks. For the circular model, it does not have the disadvantage of the polygon model, as a proximate method, when the block number is large enough, it can be used to simulate the runout process and evaluate the deposit value and position.

DDA method is a typical discontinuous method, in which the simulated subject can be an assembly of individual contacted blocks. The verification and usage of it has been worldwide. For instance the usage of DDA method in analysis the single blocks such as the rockfall and the assemble blocks such as the landslide can be found in the literatures such as Ohnishi et al. (1996), Koo and Chern (1998), Yang et al. (2004) and Ma et al. (2011). The obvious advantages of the numerical method in analysis the dynamic behavior of the landslide or the landslide-prone slope are:

1) The mass shape pattern can be accurately or similarly reflected.

2) The constitutive law of the block, the contact mechanism, and the complexity of the topography of landslide can be reflected.

3) Some other conditions such as the earthquake and the rainfall can be simulated

4) The dynamic behavior such as the single block’s deformation and the whole blocks’ movement can be captured and analysis directly.

1.1.3.4 NUMERICAL METHOD

Numerical methods break the failing volume into elements that may interact with each other. This allows for modeling the source mass with accounting for internal strength and entrainment throughout runout. These models mainly include continuum fluid mechanics models and discontinuum method.

When considering that the dimensions of a typical particle is much smaller than the depth and length of the debris, the debris mass is treated as continuum. According to depth averaged Saint Venant method, the material is assumed to be incompressible and the mass and momentum equations are written in a depth-averaged form. Some authors (e.g., Soussa and Voight 1991; Takahashi et al. 1992; Cao et al. 1996) configure their analysis in the conventional Eulerian framework, whereas others (e.g., Savage and Hutter 1989; Hungr 1995; Chen and Lee, 2000; Pirulli 2005 and McDougall 2006) prefer the Lagrangian coordinate. The primary differences are their representation of basal resistance force and the constitutive relations describing the mechanical behavior of the considered material.

When the landslide mass consists of large fragments and boulders, the runout mass is modelled as an assembly of blocks moving down a surface. By applying known individual constitutive properties, contact laws, velocities, displacements and body forces, their dynamic behavior can be studied over a selected period in time. Some authors take circular shape models for their runout analysis to evaluate maximum runout and final deposit position of past or potential events (e.g., Poisel et al. 2008). Although polygonal shapes have the disadvantages due to the complexity of the contact patterns and penalty in computational time, methods using non-circular shapes will be required for more real-world problems. It is more appropriate when problems are limited in finite blocks.

For example, recent utilisations of DDA in analysing falls of single blocks and block assemblies were described by Ohnishi et al. (1996), Koo and Chern (1998) , Yang et al. (2004) and Ma et al. (2011).

The most merits of movement behavior analysis using numerical methods are

that:

5) The internal strength of debris mass and complex conditions of landslide can be simulated;

6) Various conditions such as earthquake or intense rainfall can be considered without additional assumption;

7) The movement behaviors can be directly output.

1.3 COMPARISON BETWEEN DDA AND OTHER NUMERICAL METHODS

1.3.1 Compare with FEM

The FEM (Finite Element Method) is a typical continuum method, which can be used for dynamic pattern and nonlinear material analysis. It can be used for not only solid but also fluid. In rock engineering, if the rock mass is intact or heavily fractured, the FEM may be a reasonable as an approximation method. However, in practice, the mechanics of rock mass is controlled by the discontinuities including joints and fractures, which makes the FEM unreasonable because of its nature pattern (Zheng et al. 2013). Another problem is it cannot handle large deformation problems such as runout of the landslide and the rockfall because the continuum assumption and the elements distortion. Some attempts have been made to fix this problem, such as the re-mesh method. But the large deformation problem is so difficult for FEM and up to now no reliable method can be proposed. Besides, as the simulation mass is assumed as continuum material connected by elements, it cannot simulate the broken and discreteness of the simulation body.

If we look at the formulations of the DDA method, it can be found that the DDA method is actually a parallel method compared with FEM. The DDA method, as its name shows, simulates the system as discontinuous blocks. It uses the energy minimization principle method, using the displacements as the basic variables (for 2D DDA six variables, twelve for 3D). Then the equilibrium equation which is in matrix form can be solved and the detail movement pattern can be got in each simulation step. What is more, the DDA method can also absorb totally the

advantage of FEM method by discretizing the discrete blocks internally (Grayeli and Hatami 2008; Beyabanaki et al 2009a, b; Liu et al, 2012). As Wu (2010)mentioned, the easy introduction of simple or the high order deformation function to the discrete elements of DDA is one major advantage of DDA method when simulation rigid body movements.

1.3.2 Compare with DEM

The distinct element method (DEM) is a typical discontinuous method representing the simulated materials as independent discrete elements which can interact with contacted element(s). It has a major application advantages: it is suitable for simulating a system comprising of non-deformable elements such as the granular material. The DEM method was firstly proposed by Cundall and Strack (1979) in literature. Generally, the calculation procedure includes two major steps: 1) to compute the interact forces based on the “Force-displacement” method, in which the force is got from the penetration displacement. This kind of penetration represents the deformation of the contacted surface as pointed by Cundall and Hart (1992); 2) to obtain the acceleration of each distinct element based on the Newton’s second law. Then, the relevant velocity and displacement can be got by integration with time. Then the position of each element is updated during each simulation time step. This kind of process continues until the simulation is finished. This kind of numerical solution process is named as the MD (Molecular Dynamic) formalism.

There are three obvious differences between the DDA and the DEM：1）the time integration method. For the DDA, it uses the implicit version, while the DEM uses the explicit version; 2) the fundamental dynamic theory. For the DDA, it is based on the energy minimization principle, while Newton’s second law for the DEM; 3) the unknown variables. For the DDA, its unknowns are displacements (6 for 2D and 12 for 3D), while for the DEM, its unknowns are accelerations.

Although both the DDA and DEM can be considered as the members of the big family of discrete element method, the DDA method has its instinctive advantage compared with the DEM method, which owns the following five basic advantages

(Jing, 2003):

1) For the quasi-static problem, the DDA can satisfy the equilibrium conditions automatically, while for DEM, it has to use extra iteration process;

2) The system's failure pattern and numerical instability do not need to be preliminary introduced, making the simulation time can be very larger;

3) The Gaussian quadrature technique (a kind of discrete variable approximation method) is not need, as the DDA can perform the integration in a closed form;

The penalty method in contact mechanism is more reasonable compared with the "Force-displacement" method in DEM;

As mentioned above, the internal deformation pattern can be got by coupling the existed FEM code. This kind of process can be finished easily in DDA. Moreover, it can avoid the limitations of the FEM, such as the continuous geometry and low accuracy and efficiency when dealing with the dynamic problems. So, a perfect bridge connecting the continuous and discontinuous can be created. While for the DEM, it is not possible to do so.

1.3.3 Compare with NMM

The NMM (Numerical Manifold Method) was developed based on the DDA method and also absorb the characteristics of FEM. The NMM and DDA method have some common patterns such as using the minimization of potential energy when solving the equilibrium functions, the same contact detection technique and contact mechanism, also they are available for both static and dynamic simulation.

The difference between these two methods is obvious. The NMM uses the physical cover to represent the material boundary or the block boundary, and etc. Also, the weight function is used, which is just like the nodal shape function in FEM. In other words, the NMM will be exact the DDA when each of the simulated element is discretized to be finite cover, in this case, each element (or block) in DDA owns the displacement filed in a linear form.

However, as in the NMM, the degrees of freedom will be raised because of the existing of covers, which will cause the technique difficulty and lower efficiency problems especially for the 3D case. That is also the main reason why the 3D NMM is rare to be found in the practice use according to the literature research.

1.4 Development of the DDA method

The DDA (Discontinuous Deformation Analysis) (Shi, 1998, 2001), in theory, is a typical energy based numerical discrete method (by minimization the system's potential energy). It can be used for both the static and dynamic analysis. It is very available for simulation a system comprising of individual blocks that are separated by discontinuities, such as joints and rock faces. One of its major advantages is there is no need to assume the failure modes beforehand. Another obvious advantage is that when it is used for the rock engineering, each individual block's movements such as translation and rotation, and the deformation can be easily captured and reshown. Moreover，large scale movements such as the sliding relevant to discontinuities can be correctly represented.

Significant development has been achieved since DDA was first introduced as a two-dimensional (2D) numerical model (Shi and Goodman 1985) and the focus has been mainly on 2D state in the past decades. MacLaughlin and Doolin (2006) provided a review of more than one hundred published and unpublished validation studies on 2D DDA.

The original edition of 2D DDA technique focuses mainly on the deformable block by coupling the rigid body movements with the uniformed state of strain for the block can be in arbitrary shape. In order to represent the deformation pattern for each block in arbitrary shape, there are mainly three kinds of attempts has been made: 1) each block can be artificially divided into many sub-blocks (Lin et al, 1996), in which the artificial joints are used to glue the sub-blocks together glued together (Ke, 1993), (2) Coupling the FEM method represent the internal by using the finite elements such as (Shyu, 1993), (3) To make some modification of the displacement function by using polynomial terms such as (Koo and Chern, 1996;

Koo and Chen, 1997; Shyu, 1993; Ma et al, 1996; Hsiung, 2001).

Another technique that is necessary to be mentioned is the penalty method, which is used to avoid penetration and get the reasonable contact force for the contacted blocks. For the original 2D DDA edition, it uses almost the same penalty method just as the method used in the FEM (Campbell 1974; Felippa 1986; Munjiza and Andrews. 2000), using this method the block(s) will be pushed apart when the first entrance position is judged to avoid inter-penetration. In order to improve the accuracy of detection the contact force and also increase the efficiency of prevention of penetration of blocks, the ALM (Augmented Lagrangian Method) was used in the original 2D DDA program by Lin et al (1996). The good result can be got using this improvement and also the restriction of penalty number to be ten-thousand times the material's Young's modulus (Shi 1988) is not needed. In the original 2D DDA program, when considering the energy dissipation, the algorithm in DDA itself can represent it automatically. In order to capture the dissipation of energy more accurately, adding the viscosity coefficient has been made by Sasaki et al, 2005. This improvement makes the energy dissipation in the 2D DDA more physically reasonable.

However, if we use the 2D DDA in many practical problems, the results are unavoidable unreasonable because the slope is highly in 3D shape and orientation of the rock joints is also in 3D orientation. For example, in the slope stability analysis, when the 2D DDA method is used the lateral friction cannot be considered, which will lead the underestimation of the factor of safety compared with the 3D analyse. When the runout analysis is made, the 2D DDA method cannot consider the lateral spread in the real case. Therefore, the 2D DDA has its natural and unavoidable disadvantages, and the development of 3D DDA is very necessary and meaningful.

1.4.1 Development of the 2D DDA

The 2D DDA has been developed maturely not only in theory but also in the practical engineering usage. The very useful user-friendly pre-processor and post-processor has been developed (Chen et al, 1996; Doolin and Sitar, 2001), which

makes it convenient for the deep research and more widely used in the practical engineering problems. The practical usages of the 2D DDA can be listed as followings:

1) analyse of rock fall (Chen, 2003; Wu et al, 2005; Ma et al, 2011; Kaidi et al, 2012; Chen et al, 2013),

2) slope (landslide) (Sitar et al, 1997, 2005; Wu, 2007, 2010, 2011; Kveldsvik et al, 2009; Wu et al, 2009; Zhang et al, 2013),

3) the mining engineering and the tunnel (Yeung, 1993; Yeung and Leong, 1997; Law and Lam, 2003; Wu et al, 2004; Tesesarsky and Hatzor, 2006),

4) the underground openings' stability and failure (Hsiung and Shi, 2001; MacLaughlin and Clapp, 2002; Hatzor, Talesnick and Tsesarsky, 2002; Bakun-Mazor et al, 2009; Hatzor et al, 2010; Shi, 2014; Zhang et al, 2014),

5) stability analysis of dam (Dong et al, 1996; Kottenstette, 1999; Shi, 2009),

6) static and dynamic analysis of masonry structures (Bicanic and Stirling, 2001; Kamai and Hatzor et al, 2008; Rizzi et al, 2014),

7) fracture propagation in rock (Ning, Yang, An et al, 2011),

8) simulation of the process of rock blasting (Ning, Yang, Ma et al, 2011),

9) process of flow-stress (Kim et al, 1999; Jing et al, 2001; Rouainia et al, 2006; Koyama, 2011, Kaidi et al, 2012; Chen et al, 2013), and other practical engineering usages (Hatzor and Benary, 1997; Thomas and Bray, 1999).

Moreover, some remarkable engineering projects were researched by the 2D DDA, for example, the Three Gorges Dam project in China, Pueblo Damin Colorado, Yerba Buena tunnel portal in San Francisco, Gjovik Olympic Cavern in Norway, Masada National Monument in Isreal (Dong et al, 1996, Kottenstette, 1999, Law and Lam, 2003, Scheldt et al, 2002 Hatzor, Arzi and Tsesarsky, 2002; Hatzor et al, 2004)

1.4.2 Development of the 3D DDA

According to the literature review, compared with the 2D DDA method, much more few works on the 3D DDA can be found. There works are mainly focus on the basic contact theory development and some simple model verifications. The main developments of the 3D DDA can be summarized as followings:

1) The developments of the basic formulations. The basic formulations in 3D DDA for all kinds of potential terms' sub-matrices have been specified by Shi (2001) and Liu et al. (Liu, 2004). For the contact theory, a point to plane entrance model was illustrated by Jiang et al. (Jiang and Yeung, 2004). As a modification, a new contact theory called the frictionless point to plane contact algorithm was proposed by Wu et al. (Wu et al, 2005). Some researchers have made some contributions on the high order displacement formulations such as Beyabanaki Jafari and Yeung (2010) and Beyabanaki, Yeung et al (2010).

2) The improvements of contact detection method. An effective and efficient contact detection method PEM (Penetrated Edges Method) has been proposed by Chen et al. (2004), which is available for just convex 3D blocks. Another contact detection method related with the 3D convex block is the IB (Incision Body) scheme, which was used by Wang et al. (2006) for both the static and dynamic stability analysis. Moreover, the CPA (Closest Points Algorithm) and the MP (Main Plane) method have been proposed by Beyabanaki et al. (2008) and Keneti et al. (2008) separately, both of which are efficient for solving the contact detection problem between convex blocks in 3D DDA. Moreover, a virtual entrance plane based vertex to vertex contact algorithm was proposed by Ahn and Song (2011) called ISM (Inscribed Sphere Method). An unavoidable problem when dealing with the large scale 3D problem is the efficiency problem, in order to fix this, two techniques were used by Mikola and Sitar (2013). The first one is the usage of explicit formulation and the other is the FCP (Fast Common Plane) method.

3) Modify the contact constraints. The ALM (Augmented Lagrange Multiplier) method was adopted by Beyabanaki, Mikola et al (2009) to perfect the point to plane contact theories. A cross-line entrance model was presented by Yeung et al. (Yeung, 2007) and Wu (20008), which was modified by Beyabanaki, Ferdosi and Mohammadi (2009).

4) To couple with the FEM. The DDA method and FEM are typical methods for the discontinuous and continuum media respectively. The coupling between these two methods bridges these two methods and makes the simulation technique move to a new and high level. In order to solve the fissured elastic problem, Grayeli and Hatami (2008) applied the 4-noded tetrahedral elements in 3D DDA block to obtain the more accurate stresses and deformation distribution. The trilinear and serendipity hexahedron FE was introduced into the 3D DDA to improve the deformation ability of single block by Beyabanaki et al. (2009a, b). Moreover, the tetrahedron FEM was adopted and coupled with the 3D DDA by Liu et al. (2012), whose research has showed the powerful ability of the coupled method.

5) Practical applications. Actually, there are few applications relevant to the applications because of some technique barriers. The classical wedge model and key block theory were used by Yeung et al. (2003) and Bakun-Mazor (2012) et al. to clarify the availability of the 3D DDA program. The real 3D rock-fall problems were solved by Chen et al. (2013) using the 3D DDA combined with the 3D terrain created from the GIS (Geographic Information System) data. Moreover, the spherical-shaped materials can be simulated by the spherical-block 3D DDA by Other developments by Zhao (2000).

1.5 Scope and objective

Earthquake induced landslide is one of the most serious geo-hazards. Especially, for the coastal area with potential tsunami, evacuation sites and access roads for tsunami are generally located upland and surrounded by slopes. Since an earthquake can induce not only tsunami but also landslides, it is obvious that the tsunami

evacuation sites and access roads are threatened by the potential earthquake induced landslides. Therefore, it is important and necessary to assess the hazard of earthquake induced landslides so as to secure the safety of tsunami evacuation sites and access roads.

Hazard assessment of earthquake induced landslides includes slope stability analysis under seismic loading, landslide runout estimation and the evaluation of preventive effectivity such as anchor-reinforcement for a dangerous slope. With the development of the computer and computing sciences, various numerical simulation methods have been developed and shown their powerful capability in the landslide research. Discontinuous deformation analysis (DDA) is one of these simulation methods and has shown its advantage in theory and practice. There have been many research achievements reported by using 2D DDA. In order to overcome the limitation of 2D analysis, the development of 3D DDA is also undertaken. However, there still exist some key problems, which inhibit its practical application, in the development of 3D DDA program. For example, there is no effective tool for 3D DDA model construction; it is unavailable to perform slope stability analysis under seismic loading and with the anchor reinforcement.

This study aims at (1) developing a practical 3D DDA program by solving the above problems and (2) applying the new 3D DDA to the practical hazard assessment of potential earthquake induced landslides in a coastal area with potential tsunami of Oita prefecture, Japan. The new 3D DDA includes (1) developing an effective pre-processor for the 3D model construction; (2) adding the function of seismic loading and (3) adding the function of using anchor reinforcement.

1.6 Thesis organization

Chapter 1 introduces the background, objective and organization of the thesis. The existing numerical simulation methods for landslide study are reviewed. The development of DDA in theory and practical application is briefly introduced and the advantages of DDA are clarified.

Chapter 2 provides an overview on 3D DDA. The 3D DDA formulation,

contact principle, and program structure are illustrated in detail. The following unsolved problems of the existing 3D DDA program are discussed: (1) without an effective pre-processor for complex slope model construction, which is especially fundamental and necessary for practical application to landslide study; (2) unable to perform slope stability analysis and landslide runout simulation under a potential earthquake; (3) unable to evaluate the preventive effect of using anchor reinforcement.

Chapter 3 performs a close comparison between the 2D and 3D DDA to reveal the limitation of the 2D analysis and the necessity of 3D DDA. Their advantages and disadvantages are illustrated based on slope stability analysis and run-out simulation. The current 2D DDA program contains effective user friendly pre-processor and post-processor, which are powerful and necessary for practical slope study. There have been many achievements reported from practical 2D DDA applications. However, the limitations of 2D analysis also become obvious. Since lateral effect of a 2D slope section model cannot be considered, the factor of safety is often underestimated and lateral spread movement cannot be estimated in run-out analysis. On the other hand, the lateral friction and the lateral spread movement can be considered in 3D DDA analysis, the factor of safety can be estimated and the reasonable run-out can be simulated more accurately. But, a practical 3D DDA program has not been developed.

Chapter 4 develops a practical pre-processor to easily construct a complex 3D slope model for the 3D DDA program. Since construction of a complex 3D slope model is always a troublesome problem which including the following two big issues: (1) how to cut the blocks; (2) how to generate blocks of the 3D slope terrain. The developed pre-processor solves these problems by taking the advantage of the commonly used commercial software: 3ds Max and ArcGIS. Arbitrary-shaped 3D bocks are made with 3ds Max and complex slope terrain mesh data are obtained from the ArcGIS. A pre-process program is developed to combine the output data from both 3ds Max and ArcGIS and translate them to the 3D DDA model format. It has been shown that a 3D DDA slope model can be easily and effectively made for any

real slope with complex terrain by using the newly developed 3D DDA pre-processor, which makes it possible for applying 3D DDA to practical landslide study.

Chapter 5 extends the existing 3D DDA program by adding the function of seismic loading and the function of anchor reinforcement. The stability analysis and run-out estimation of a potential earthquake induced landslide need the function of dealing with seismic loading in a 3D DDA program. The added seismic loading function can use either displacement wave or acceleration wave, which depends on the data available. In addition, when a slope is judged unstable under a potential earthquake, the slope should be reinforced in general. Rock anchor reinforcement is one of typical preventive methods. Thus, it is necessary to evaluate the preventive effect and provide the useful information for optimum design of the size and number of rock anchors. By adding these two functions, the new 3D DDA program makes it possible to assess the hazard of earthquake induced landslides for securing the safety of tsunami evacuation sites and access roads.

Chapter 6 applies the new 3D DDA program to practical hazard assessment of earthquake induced landslides for securing the safety of tsunami evacuation sites and access roads in the coastal area of Oita prefecture. The Daiganji slope is taken as an example. An access road to a tsunami evacuation site and several houses are located at the slope downward. At first, the slope stability is analyzed by using both 2D and 3D DDA. The results are compared with those from the commonly used limit equilibrium method. The adaptability of DDA and the difference between 2D and 3D analysis are shown. Secondly, the factor of safety is analyzed by using earthquake loading. And the influence of seismic directivity on the slope stability is analyzed. The landslide run-out is estimated by using the new 3D DDA program under the condition of the earthquake. It is shown that the access road and some houses are threatened by the potential landslide. Finally, the stability analysis of a anchor reinforced slope is performed to evaluate the preventive effect. It has been shown that the new 3D DDA is very useful and powerful enough for hazard assessment of earthquake induced landslides.

Chapter 7 summarizes the results and achievements of this study. The problems

for the future study are highlighted.

REFERENCES

Ahn TY and Song JJ. (2011). New contact-definition algorithm using inscribed spheres for 3D discontinuous deformation analysis. International Journal of Computational Methods, 8(02), 171-191.

Ala G, Francomano E, Tortofici A, Toscano E and Viola F. (2007). Corrective meshless particle formulations for time domain Maxwell's equations. J Comput Appl Math 210(1-2):34-46

Ala G, Francomano E, Tortorici A, Toscano E, Viola F. (2006). Smoothed particle electromagnetics: a mesh-free solver for transients. J Comput Appl Math 191(2):194-205

Bakun-Mazor D, Hatzor YH and Dershowitz WS. (2009). Modelingmechanical layering effects on stability of underground openings in jointed sedimentary rocks. International Journal of Rock Mechanics and Mining Sciences, 46(2), 262-271.

Bakun-Mazor D, Hatzor YH and Glaser SD. (2012). Dynamic sliding of tetrahedral wedge: The role of interface friction. International Journal for Numerical and Analytical Methods in Geomechanics, 36(3), 327-343.

Bao H, Zhao Z and Tian Q. (2014). On the implementation of augmented Lagrangian method in the two-dimensional discontinuous deformation analysis. International Journal for Numerical and Analytical Methods in Geomechanics, 38(6), 551-571.

Campbell, J. S. (1974). A penalty function approach to the minimization of quadratic functionals in finite element analysis. Finite element

methods in engineering, 33-54.

Chen G, Zheng L, Zhang Y and Wu J. (2013). Numerical simulation in rockfall analysis: a close comparison of 2-D and 3-D DDA. Rock mechanics and rock engineering, 46(3), 527-541.

Chen G. (2003). Numerical modelingof rock fall using extended DDA. Chinese Journal of Rock Mechanics and Engineering, 22(6), 926-931.

Chen H, Zhao Z and Sun J. (2013). Coupled hydro-mechanical model for fractured rock masses using the discontinuous deformation analysis. Tunnelling and Underground Space Technology, 38, 506-516.

Chen JK, Beraun JE, Carney TC (1999) A corrective smoothed particle method for boundary value problems in heat conduction. Int J Numer Methods Eng 46:231-252

Chen JS, Pan C, Roque C and Wang HP. (1998). A Lagrangian reproducing kernel particle method for metal forming analysis. Comput Mech 22(3):289-307

Chen WS, Zheng H, Cheng YM and Ge XR. (2004). Detection of 3D rock block contacts by penetration edges. Chinese Journal of Rock Mechanics and Engineering, 23(4), 565-571. (in Chinese)

Chen, G, Miki S and Ohnishi Y. (1996). Practical improvement on DDA. Discontinuous deformation analysis (DDA) and simulations of discontinuous media, TSI Press, Albuquerque, NM, 302-309.

Cheng YM. (1998). Advancements and improvement in discontinuous deformation analysis. Computers and geotechnics, 22(2), 153-163.

Chikazawa Y, Koshizuka S, Oka Y. (2001). A particle method for elastic and visco-plastic structures and fluid-structure interactions. Comput

Mech 27(2):97-106

Cleary P, Ha J, Alguine V and Nguyen T. (2002). Flow modelling in casting processes. Appl Math Model 26(2):171-190.

Cleary PW. (1998). Modelling confined multi-material heat and mass flows using SPH. Appl Math Model 22(12):981-993.

Cleary PW and Ha J. (2000). Three dimensional modelling of high pressure die casting. Int J Cast Met Res 12(6):357-365.

Cleary PW, Ha J and Ahuja V. (2000). High pressure die casting simulation using smoothed particle hydrodynamics. Int J Cast Met Res 12(6):335-355.

Cleary PW, Prakash M. (2004). Discrete-element modelling and smoothed particle hydrodynamics: potential in the environmental sciences. Philos Trans R Soc A 362(1822):2003-2030.

Dalrymple RA and Rogers BD. (2006). Numerical modeling of water waves with the SPH method. Coast Eng 53(2-3):141-147

Dolag K, Bartelmann M and Lesch H. (1999). SPH simulations of magnetic fields in galaxy clusters. Astron Astrophys 348(2):351- 363

Fang HS, Bao K, Wei JA, Zhang H, Wu EH, Zheng LL (2009) Simulations of droplet spreading and solidification using an improved SPH model. Numer Heat Transfer A, Appl 55(2):124- 143

Gallati M, Braschi G, Falappi S. (2005). SPH simulations of the waves produced by a falling mass into a reservoir. Nuovo Cimento C, 28(2):129-140

Garg R, Narayanan C, Lakehal D and Subramaniam S. (2007). Accurate numerical estimation of interphase momentum transfer in

Lagrangian-Eulerian simulations of dispersed two-phase flows. Int J Multiph Flow, 33(12):1337-1364

Ghazali JN and Kamsin A. (2008). A real time simulation and modeling of flood hazard. In: 12th WSEAS international conference on systems, Heraklion, Greece.

Ha J, Cleary PW. (2000). Comparison of SPH simulations of high pressure die casting with the experiments and VOF simulations of Schmid and Klein. Int J Cast Met Res 12(6):409-418.

Ha J, Cleary PW. (2005). Simulation of high pressure die filling of a moderately complex industrial object using smoothed particle hydrodynamics. Int J Cast Met Res 18(2):81-92.

Hart R, Cundall PA and Lemos J. (1988, June). Formulation of a three-dimensional distinct element model—Part II. Mechanical calculations for motion and interaction of a system composed of many polyhedral blocks. In International Journal of Rock Mechanics and Mining Sciences and Geomechanics Abstracts (Vol. 25, No. 3, pp. 117-125). Pergamon.

Hatzor YH and Benary R. (1998). The stability of a laminated voussoir beam: back analysis of a historic roof collapse using DDA. International Journal of Rock Mechanics and Mining Sciences, 35(2), 165-181.

Hatzor YH, Arzi AA and Tsesarsky M. (2002). Realistic dynamic analysis of jointed rock slopes using DDA. In Proceedings of the 5th International Conference on Analysis of Discontinuous Deformation, 47-56.

Hatzor YH, Arzi AA, Zaslavsky Y and Shapira A. (2004). Dynamic

stability analysis of jointed rock slopes using the DDA method: King Herod's Palace, Masada, Israel. International Journal of Rock Mechanics and Mining Sciences, 41(5), 813-832.

Hatzor YH, Talesnick M and Tsesarsky M. (2002). Continuous and discontinuous stability analysis of the bell-shaped caverns at Bet Guvrin, Israel. International Journal of Rock Mechanics and Mining Sciences, 39(7), 867-886.

Hatzor YH, Wainshtein I and Bakun Mazor D. (2010). Stability of shallow karstic caverns in blocky rock masses. International Journal of Rock Mechanics and Mining Sciences, 47(8), 1289-1303.

Herrera PA, Massabo M and Beckie RD. (2009). A meshless method to simulate solute transport in heterogeneous porous media. Adv Water Resour 32(3):413-429.

Hieber SE (2004) Remeshed smoothed particle hydrodynamics simulation of the mechanical behavior of human organs. Technol Health Care 12(4):305-314.

Hong JM, Lee HY, Yoon JC and Kim CH. (2008). Bubbles alive. ACM Trans Graph 27(3).

Jeong JH, Jhon MS, Halow JS and Van Osdol J. (2003). Smoothed particle hydrodynamics: applications to heat conduction. Comput Phys Commun 153(1):71-84.

Ji SY, Li H, Shen HT, Wang RX, Yue QJ (2007) A hybrid Lagrangian-Eulerian numerical model for sea-ice dynamics. Acta Oceanol Sin 26:12-24.

Ji SY, Shen HT, Wang ZL, Shen HH and Yue QJ (2005) A viscoelastic-plastic constitutive model with Mohr-Coulomb yielding criterion for

sea ice dynamics. Acta Oceanol Sin 24(4):54-65.

Jiang F, Sousa ACM. (2006). SPH numerical modeling for ballistic-diffusive heat conduction. Numer Heat Transfer B, Fundam 50(6):499-515.

Jiang FM, Oliveira MSA and Sousa ACM. (2006). SPH simulation of transition to turbulence for planar shear flow subjected to a streamwise magnetic field. J Comput Phys 217(2):485-501.

Kaidi S, Ouahsine A, Sergent P and Rouainia M. (2012). Discontinuous Deformation Analysis to assess the stability of rockfill dams under seismic loading. Comptes rendus. Mécanique, 340(10), 731-738.

Kaidi S, Rouainia M and Ouahsine A. (2012). Stability of breakwaters under hydrodynamic loading using a coupled DDA/FEM approach. Ocean Engineering, 55, 62-70.

Kamai R and Hatzor YH. (2008). Numerical analysis of block stone displacements in ancient masonry structures: A new method to estimate historic ground motions. International journal for numerical and analytical methods in geomechanics, 32(11), 1321-1340.

Ke TC. (1993). Simulated test of two-dimensional heterogeneous and discontinuous rock mass using Discontinuous Deformation Analysis, PhD thesis, Department of Civil Engineering, University of California, Berkeley.

Ke TC. (1996). The issue of rigid-body rotation in DDA. In Proceedings of the First International Forum on Discontinuous Deformation Analysis (DDA) and Simulations of Discontinuous Media. Berkeley, California, USA, June 12-14, 1996, 318-325.

Keneti AR, Jafari A and Wu JH. (2008). A new algorithm to identify

contact patterns between convex blocks for three-dimensional discontinuous deformation analysis. Computers and Geotechnics, 35(5), 746-759.

Laigle D, Lachamp P and Naaim M. (2007). SPH-based numerical investigation of mudflow and other complex fluid flow interactions with structures. Comput Geosci 11(4):297-306.

Law HK and Lam IP. (2003). Evaluation of seismic performance for tunnel retrofit project. Journal of geotechnical and geoenvironmental engineering, 129(7), 575-589.

Law HK and Lam IP. (2003). Evaluation of seismic performance for tunnel retrofit project. Journal of geotechnical and geoenvironmental engineering, 129(7), 575-589.

Lee WH (2000) Newtonian hydrodynamics of the coalescence of black holes with neutron stars, III: irrotational binaries with a stiff equation of state. Mon Not R Astron Soc 318(2):606-624.

Lee WH and Kluzniak W. (1999). Newtonian hydrodynamics of the coalescence of black holes with neutron stars, II: tidally locked binaries with a soft equation of state. Mon Not R Astron Soc 308(3):780-794.

Li J, Xue J, Xiao J and Wang Y. (2012). Block theory on the complex combinations of free planes. Computers and Geotechnics, 40, 127-134.

Ma GC, Matsuyama H, Nishiyama S and Ohnishi Y. (2011). Practical studies on rockfall simulation by DDA. J Rock Mech Geotech Eng, 3(1), 57-63.

Ma MY, Zaman M and Zhou JH. (1996, June). Discontinuous deformation analysis using the third order displacement function. In Proc., First Int. Forum on Discontinuous Deformation Analysis (DDA) and Simulations

of Discontinuous Media (pp. 383-394). San Antonio, Tex.: TSI Press.

MacLaughlin MM and Clapp KK. (2002). Discrete element analysis of an underground opening in blocky rock: An investigation of the differences between UDEC and DDA results. Geotechnical Special Publication, 329-334.

MacLaughlin MM and Doolin DM. (2006). Review of validation of the discontinuous deformation analysis (DDA) method. International journal for numerical and analytical methods in geomechanics, 30(4), 271-305.

Maeda K, Sakai H. (2007). Seepage failure analysis with evolution of air bubbles by SPH. In: New frontiers in Chinese and Japanese geotechniques, proceedings of the 3rd Sino-Japan geotechnical symposium, Chongqing, China

McDougall S, Hungr O. (2004). A model for the analysis of rapid landslide motion across three-dimensional terrain. Can Geotech J 41(6):1084-1097

McDougall S, Hungr O. (2005). Dynamic modelling of entrainment in rapid landslides. Can Geotech J 42(5):1437-1448.

Meglicki Z. (1994). Verification and accuracy of smoothed particle magnetohydrodynamics. Comput Phys Commun 81(1-2):91- 104.

Melean Y and Sigalotti LD. (2005). Coalescence of colliding van der Waals liquid drops. Int J Heat Mass Transfer 48:4041-4061.

Melean Y and Sigalotti LDG. (2005). Coalescence of colliding van der Waals liquid drops. Int J Heat Mass Transfer 48(19-20):4041- 4061.

Panizzo A. (2005). SPH modelling of underwater landslide generated

waves. In: Proceedings of the 29th international conference on coastal engineering 2004, Lisbon, Portugal.

Password F. (2003). Cosmological smoothed particle hydrodynamics simulations: a hybrid multiphase model for star formation. Mon Not R Astron Soc 339(2):289-311.

Pastor M, Haddad B, Sorbino G, Cuomo S and Drempetic V. (2009). A depth-integrated, coupled SPH model for flow-like landslides and related phenomena. Int J Numer Anal Methods 33(2).

Randles PW and Libersky LD. (1996). Smoothed particle hydrodynamics: some recent improvements and applications. Comput Methods Appl Mech Eng 139(1):375-408.

Rhee SH and Engineer L. (2005). Unstructured grid based Reynoldsaveraged Navier-Stokes method for liquid tank sloshing. J Fluid Eng 127:572.

Ritchie BW and Pa Thomas. (2001). Multiphase smoothed-particle hydrodynamics. Mon Not R Astron Soc 323(3):743-756.

Sakai H and Maeda K. (2006). Seepage failure of granular ground accounting for soil-water-gas interaction. In: Geomechanics and geotechnics of particulatemedia, proceedings of the international symposium on geomechanics and geotechnics of particulate media, Ube, Yamaguchi, Japan.

Sasaki T, Hagiwara I, Sasaki K, Yoshinaka R, Ohnishi Y and Nishiyama S. (2004). Earthquake response analysis of rock-fall models by discontinuous deformation analysis. In Proceedings of third Asian rock mechanics symposium, Kyoto, 1267-1272.

Schafer C, Speith R and Kley W. (2007). Collisions between equalsized

ice grain agglomerates. Astron Astrophys 470(2):733-739.

Scheldt T, Lu M and Myrvang A. (2002). Numerical analysis of Gjovik cavern: A comparison of continuous and discontinuous results by using Phase 2 and DDA. In: Hatzor YH, editor. Fifth international conference on analysis of discontinuous deformation—stability of rock structures. Rotterdam: Balkema; 2002, 125-132.

Senz DG, Bravo E and Woosley SE (1999) Single and multiple detonations in white dwarfs. Astron Astrophys 349:177-188.

Shao SD. (2006). Incompressible SPH simulation of wave breaking and overtopping with turbulence modelling. Int J Numer Methods Fluids 50(5):597-621.

Shao SD. (2009). Incompressible SPH simulation of water entry of a free-falling object. Int J Numer Methods Fluids 59(1):91- 115.

CHAPTER 2

OVERVIEW ON THE 3D DDA METHOD

2.1 INTRODUCTION

In the rock engineering, the rock masses are inborn consisted of discontinuities such as joints and faults such as the Fig.2.1 shows. The size of the discontinuities such as the length and the width varies greatly and also the number and the directivity can be in many cases. As a result, the mechanism behavior of the rock mass is mainly controlled by the rock discontinuities, this point has become a common sense for rock engineering and has been proved by many researchers such as (Ohnishi, 1999; Hwang et al., 2002; Ohnishi, 2002; Hwang, 2003; Hwang and Ohnishi, 2003; Hwang et al., 2003; Hwang, 2004; Hwang et al., 2004).

Figure 2. 1 Dicontinuties in rock mass.

DDA was created by Shi (1998, 2001), which can simulate not only the

translation, rotation but also the strain characteristics of the individual simulated block just like the Figure 2.3 shows. For the 3D DDA, each kinds of displacement can own 3 subclasses on the relevant three direction, therefore for there will be twelve unknowns.

The DDA method just like its name shows is very adaptable for simulation the behavior of rock mass consisting of rock joints. As Figure 2.2 shows, two rock joints in three dimensions cut the rock into four parts, which can be modeled and simulated in 3D DDA method.

The major advantages or features can be summarized in the following five points: 1) the solution is unique without assuming the failure mode beforehand because of the minimization of potential energy of the whole system is used; 2) the simulation mode static or dynamic can be selected freely according to the simulation purpose; 3) the constitutive law of individual block can be adjusted and incorporated into the program easily; 4) the contact criteria, such as the classical Mohr-coulomb criteria, the boundary state, the loading state can be represent easily and accurately; 5) comparing the DEM, the simulation is more stable because of no damping terms are considered. All of these features make the 3D DDA method can capture the large displacements accurately and efficiently when simulating the discrete block(s).

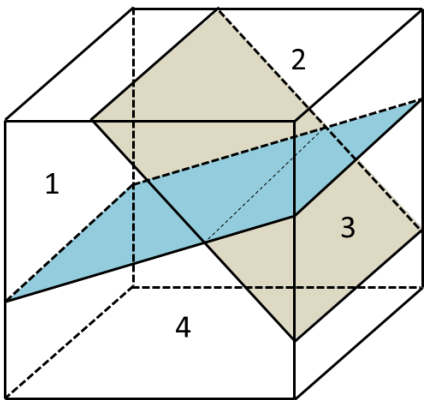

Figure 2. 2 The illustration of block cut by joints.

Since most geotechnical engineering problems are three dimensional, however, a two-dimensional representation is, at best, a crude approximation. In the case of slopes and tunnels, the orientation and geometry of discontinuities are unlikely to be

suitable for two-dimensional idealization, even though the dimension perpendicular to the plane of analysis may be large. To simulate the behavior of rock masses with discontinuities more precisely, the numerical method is required to consider the effects of the distributions of discontinuities, the terrains, the contacts among blocks, and the large displacements in three dimensions.

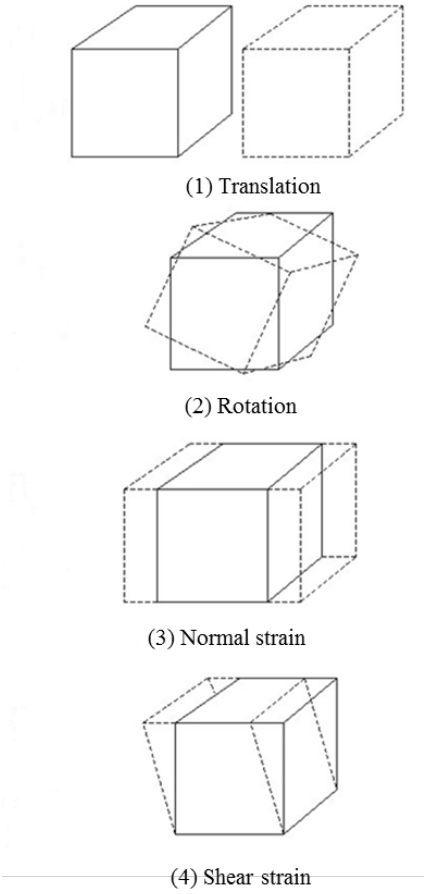

Figure2. 3 Displacements of the block in 3D DDA.

2.2 FUNDAMENTAL THEORY OF THE DDA

2.2.1 3D DDA FORMULATIONS

2.2.1.1 TIME INTEGRATION SCHEME

The equations related to motion in the 3D DDA method are originally derived from the theory of minimization of potential energy, which is just the similar as FEM. The sources of the potential energy can be all kinds of mechanisms such as the

internal force or the external loading, contact forces. If the U_i is used to represent all kinds of potential energy according to the deformation mechanism, K, the dynamic energy and W, means the energy that dissipated, the system's total energy E can be obtained by adding the energy together as the following equation:

$$E = \sum\left(U_i\right) + K - W \tag{2.1}$$

According to the theory of minimization potential energy of the whole system, the following equation can be found:

$$\frac{\partial E}{\partial D} = \frac{\partial\left(U_i\right) + \partial K - \partial W}{\partial D} = 0 \tag{2.2}$$

Actually, the Eq. (2.1) is just a weak formulation form of the system's equilibrium function that is used to describe the motion. If we expand all terms in Eq. (2.2), a general equation form for motion can be got:

$$\mathbf{M}\ddot{\mathbf{D}} + \mathbf{C}\dot{\mathbf{D}} + \mathbf{K}\mathbf{D} = \mathbf{F}\left(t, \mathbf{D}\right) \tag{2.3}$$

In the Eq. (2.3), **M** is the term of global mass, and **C** and **K** are matrices of damping and stiffness separately. The **F**(t, **D**) means the force vector which is time related. **D** is the displacement vector of the system, and accordingly, $\dot{\mathbf{D}}$ and $\ddot{\mathbf{D}}$ represent the velocity and the acceleration vectors for the simulation system respectively.

If we use the $\mathbf{D}_n$ to represent the displacement at the beginning of the time step **D**(t), and $\mathbf{D}_{n+1}$ represents the displacement after a time step Δt, **D**(t+Δt), the Eq. (2.3) comes

$$\mathbf{M}\ddot{\mathbf{D}}_{n+1} + \mathbf{C}\dot{\mathbf{D}}_{n+1} + \mathbf{K}\mathbf{D}_{n+1} = \mathbf{F}_{n+1} \tag{2.4}$$

The initial state is, **D**(0) = 0 and $\dot{\mathbf{D}}\left(0\right) = \mathbf{V}\left(0\right)$.

Using the Newmark's scheme, the displacement and the velocity can be represented in the following form:

$$\mathbf{D}_{n+1} = \mathbf{D}_n + \Delta t\dot{\mathbf{D}}_n + \frac{(\Delta t)^2}{2}\left[(1-2\beta)\ddot{\mathbf{D}}_n + 2\beta\ddot{\mathbf{D}}_{n+1}\right] \tag{2.5}$$

$$\dot{\mathbf{D}}_{n+1} = \dot{\mathbf{D}}_n + \Delta t\left[(1-\gamma)\ddot{\mathbf{D}}_n + \gamma\ddot{\mathbf{D}}_{n+1}\right] \tag{2.6}$$

In which, the β and γ are weight parameters for the velocity and acceleration individually.

Just as mentioned by Doolin and Sitar (2004), if the 3D DDA uses γ = 1 and β = 1 / 2, it will be an implicit iteration form, which is normally called the DDA Newmark-β method. By doing this, the Eq. (2.5) and (2.6) becomes:

$$\mathbf{D}_{n+1} = \mathbf{D}_n + \Delta t\dot{\mathbf{D}}_n + \frac{(\Delta t)^2}{2}\ddot{\mathbf{D}}_{n+1} \tag{2.7}$$

$$\dot{\mathbf{D}}_{n+1} = \dot{\mathbf{D}}_n + \Delta t\ddot{\mathbf{D}}_{n+1} \tag{2.8}$$

Another thing that is needed to mention is that in the 3D DDA simulation, for each time step, the deformation will be refreshed and the displacements are set to be zero $\mathbf{D}_n = 0$ at the beginning. Therefore, the Eq. (2.7) can generate the following two functions to obtain the accelerations and velocities.

$$\ddot{\mathbf{D}}_{n+1} = \frac{2}{(\Delta t)^2}\mathbf{D}_{n+1} - \frac{2}{\Delta t}\dot{\mathbf{D}}_n \tag{2.9}$$

$$\dot{\mathbf{D}}_{n+1} = \frac{2}{\Delta t}\mathbf{D}_{n+1} - \dot{\mathbf{D}}_n \tag{2.10}$$

Combining Eq. (2.9) with (2.10), the Eq. (2.4) can be created.

$$\left[\frac{2\mathbf{M}}{(\Delta t)^2} + \frac{2\mathbf{C}}{\Delta t} + \mathbf{K}\right]\mathbf{D}_{n+1} = \mathbf{F}_{n+1} + \left(\frac{2\mathbf{M}}{\Delta t} + \mathbf{C}\right)\dot{\mathbf{D}}_n \tag{2.11}$$

As the 3D DDA method uses an implicit integration method, the damping term $\mathbf{C}$ =0. Then the Eq. (2.11) can be rewrite in a simple expression as

$$\widehat{\mathbf{K}}\mathbf{D} = \widehat{\mathbf{F}} \tag{2.12}$$

Because Eq. (2.12) assembles the system's mass matrix and stiffness matrix, the iteration solver is normally used to solve the function.

2.2.1.2 DISPLACEMENT FUNCTION

In the 3D DDA program, the displacements of each block are obtained from the first-order approximation function Eq. (2.13). There are two main assumptions under this: 1) the displacement and deformation during each time step is small; 2) the stress and strain are both in uniform distribution.

$$\begin{cases} u = a_0 + a_1 x + a_2 y + a_3 z \\ v = b_0 + b_1 x + b_2 y + b_3 z \\ w = c_0 + c_1 x + c_2 y + c_3 z \end{cases} \tag{2.13}$$

In which, (x, y, z) are positions of a certain point, and (u, v, w) are its displacements for a block, moreover, $\begin{bmatrix} a_0 & a_1 & a_2 & a_3 \\ b_0 & b_1 & b_2 & b_3 \\ c_0 & c_1 & c_2 & c_3 \end{bmatrix}$ are constant terms.

If the gravity centroid is considered, the Eq. (2.13) will becomes:

$$\begin{cases} u_c = a_0 + a_1 x_c + a_2 y_c + a_3 z_c \\ v_c = b_0 + b_1 x_c + b_2 y_c + b_3 z_c \\ w_c = c_0 + c_1 x_c + c_2 y_c + c_3 z_c \end{cases} \tag{2.14}$$

In which (u_c, v_c, w_c) and (x_c, y_c, z_c) represent the same meaning as before, and c is on behalf of the centroid.

Combing Eq. (2.14) with Eq. (2.13), it comes:

$$\begin{cases} u = u_c + a_1 (x - x_c) + a_2 (y - y_c) + a_3 (z - z_c) \\ v = v_c + b_1 (x - x_c) + b_2 (y - y_c) + b_3 (z - z_c) \\ w = w_c + c_1 (x - x_c) + c_2 (y - y_c)_c + c_3 (z - z_c) \end{cases} \tag{2.15}$$

Then the parameters $\begin{bmatrix} a_0 & a_1 & a_2 & a_3 \\ b_0 & b_1 & b_2 & b_3 \\ c_0 & c_1 & c_2 & c_3 \end{bmatrix}$ can be transformed into the parameters $\begin{bmatrix} u_c & r_x & \varepsilon_x & \gamma_{yz} \\ v_c & r_y & \varepsilon_y & \gamma_{zx} \\ w_c & r_z & \varepsilon_z & \gamma_{xy} \end{bmatrix}$. In these parameters, (r_x, r_y, r_z) are the rotation angle related to the rotation center (x_c, y_c, z_c), $(\varepsilon_x, \varepsilon_y, \varepsilon_z)$ and $(\gamma_{yz}, \gamma_{zx}, \gamma_{xy})$ represent the normal and shear strain individually.

Then, the new parameters can be:

$$\begin{cases} a_1 = \varepsilon_x \\ b_2 = \varepsilon_y \\ c_3 = \varepsilon_z \\ c_2 = \frac{1}{2}\gamma_{yz} + r_x \\ b_3 = \frac{1}{2}\gamma_{yz} - r_x \\ a_3 = \frac{1}{2}\gamma_{zx} + r_y \\ c_1 = \frac{1}{2}\gamma_{zx} - r_y \\ b_1 = \frac{1}{2}\gamma_{xy} + r_z \\ a_2 = \frac{1}{2}\gamma_{xy} - r_z \end{cases} \tag{2.16}$$

Denoting the displacement function as

$$\mathbf{T}_i(x, y, z) = \begin{bmatrix} 1 & 0 & 0 & 0 & z - z_c & -(y - y_c) & x - x_c & 0 & 0 & 0 & \frac{z - z_c}{2} & \frac{y - y_c}{2} \\ 0 & 1 & 0 & -(z - z_c) & 0 & x - x_c & 0 & y - y_c & 0 & \frac{z - z_c}{2} & 0 & \frac{x - x_c}{2} \\ 0 & 0 & 1 & y - y_c & -(x - x_c) & 0 & 0 & 0 & z - z_c & \frac{y - y_c}{2} & \frac{x - x_c}{2} & 0 \end{bmatrix} \tag{2.17}$$

and $\mathbf{D}_i$ are the unknowns- displacements and deformations in the following form:

$$\mathbf{D}_i = \begin{bmatrix} u_c \\ v_c \\ w_c \\ r_x \\ r_y \\ r_z \\ \varepsilon_x \\ \varepsilon_y \\ \varepsilon_z \\ \gamma_{yz} \\ \gamma_{zx} \\ \gamma_{xy} \end{bmatrix} = \begin{bmatrix} d_{i1} \\ d_{i2} \\ d_{i3} \\ d_{i4} \\ d_{i5} \\ d_{i6} \\ d_{i7} \\ d_{i8} \\ d_{i9} \\ d_{i10} \\ d_{i11} \\ d_{i12} \end{bmatrix} \tag{2.18}$$

The displacements for all points in the *i* block can be represented using the following equation:

$$\begin{bmatrix} u \\ v \\ w \end{bmatrix} = \mathbf{T}_i(x, y, z) \cdot \mathbf{D}_i \tag{2.19}$$

2.2.1.3 GLOBAL EQUILIBRIUM EQUATIONS

As mentioned before, the 3D DDA's equilibrium equation is created by minimization the system's potential energy, which is also called the Lagrangian energy method. There are many kinds of potential energy sources. Generally, the potential energy for a single block can be summarized in the following seven kinds: (1) the elastic stress, (2) the initial constant stresses, (3) the point load, (4) the body forces, (5) the inertia forces, (6) the measured displacements and (7) contact forces between blocks. The total potential energy of an *n* blocks' system is formed as:

$$\Pi = \frac{1}{2}\begin{bmatrix}\mathbf{D}_1^T & \mathbf{D}_2^T & \cdots & \mathbf{D}_n^T\end{bmatrix}\begin{bmatrix}\mathbf{K}_{11} & \mathbf{K}_{12} & \cdots & \mathbf{K}_{1n}\\ \mathbf{K}_{21} & \mathbf{K}_{22} & \cdots & \mathbf{K}_{2n}\\ \vdots & \vdots & \vdots & \vdots\\ \mathbf{K}_{n1} & \mathbf{K}_{n2} & \cdots & \mathbf{K}_{nn}\end{bmatrix}\begin{bmatrix}\mathbf{D}_1\\ \mathbf{D}_2\\ \vdots\\ \mathbf{D}_n\end{bmatrix} + \begin{bmatrix}\mathbf{D}_1^T & \mathbf{D}_2^T & \cdots & \mathbf{D}_n^T\end{bmatrix}\begin{bmatrix}\mathbf{F}_1\\ \mathbf{F}_2\\ \vdots\\ \mathbf{F}_n\end{bmatrix} + Constant \tag{2.20}$$

where $\mathbf{K}_{ij}$ is a 12×12 stiffness sub-matrix of block *i*, $\mathbf{D}_i$ is 12×1 displacement sub-matrix and $\mathbf{F}_i$ is 12×1 load sub-matrix of *Block i*, respectively. The symmetries $\mathbf{K}_{ij} = \mathbf{K}_{ji}^T$ can be seen.

By minimizing the total potential energy, all terms of the differentiations of an *n* blocks' system assemble the simultaneous equilibrium equations as a matrix form as below:

$$\begin{bmatrix}\mathbf{K}_{11} & \mathbf{K}_{12} & \cdots & \mathbf{K}_{1n}\\ \mathbf{K}_{21} & \mathbf{K}_{22} & \cdots & \mathbf{K}_{2n}\\ \vdots & \vdots & \vdots & \vdots\\ \mathbf{K}_{n1} & \mathbf{K}_{n2} & \cdots & \mathbf{K}_{nn}\end{bmatrix}\begin{bmatrix}\mathbf{D}_1\\ \mathbf{D}_2\\ \vdots\\ \mathbf{D}_n\end{bmatrix} = \begin{bmatrix}\mathbf{F}_1\\ \mathbf{F}_2\\ \vdots\\ \mathbf{F}_n\end{bmatrix} \tag{2.21}$$

where sub-matrix $\mathbf{K}_{ii}$ depends on the material properties and $\mathbf{K}_{ij}$, $i \neq j$ depends on the contacts between *Block i* and *j*.

For *Block i*, equations

$$\begin{cases}\dfrac{\partial \Pi}{\partial u_c} = 0\\ \dfrac{\partial \Pi}{\partial v_c} = 0\\ \dfrac{\partial \Pi}{\partial w_c} = 0\end{cases} \tag{2.22}$$

represent the equilibrium of all loads and contact forces acting on the block along *x*, *y* and *z* directions respectively. Equations

$$\begin{cases} \dfrac{\partial \Pi}{\partial r_x} = 0 \\ \dfrac{\partial \Pi}{\partial r_y} = 0 \\ \dfrac{\partial \Pi}{\partial r_z} = 0 \end{cases} \tag{2.23}$$

represent the moment equilibrium of all loads and contact forces acting on the block. And equations

$$\begin{cases} \dfrac{\partial \Pi}{\partial \varepsilon_x} = 0 \\ \dfrac{\partial \Pi}{\partial \varepsilon_y} = 0 \\ \dfrac{\partial \Pi}{\partial \varepsilon_z} = 0 \\ \dfrac{\partial \Pi}{\partial \gamma_{yz}} = 0 \\ \dfrac{\partial \Pi}{\partial \gamma_{zx}} = 0 \\ \dfrac{\partial \Pi}{\partial \gamma_{xy}} = 0 \end{cases} \tag{2.24}$$

represent the equilibrium of all external forces and stresses on the block.

The differentiations

$$\frac{\partial^2 \Pi}{\partial d_{ir} \partial d_{js}},\ r, \mathrm{s} = 1, \cdots, 12 \tag{2.25}$$

are the sub-matrix $\mathbf{K}_{ij}$ in Eq. (2.21). The differentiations

$$-\frac{\partial \Pi(0)}{\partial d_{ir}},\ r = 1, \cdots, 12 \tag{2.26}$$

are the free terms of Eq. (2.21) after shifting to the right side of the equation,

which are the sub-matrix $\mathbf{F}_i$.

2.2.3.1.1 SUB-MATRIX OF ELASTIC STIFFNESS

The elastic strain energy generated by the elastic stresses of *Block i* is

$$\Pi_e = \iiint_{V_i} \frac{1}{2} \boldsymbol{\varepsilon}^T \boldsymbol{\sigma} \mathrm{d}x\mathrm{d}y\mathrm{d}z \tag{2.27}$$

where the integral domain V_i is the volume of *Block i*. For each time step, blocks are assumed as linearly elastic. The relations between stress and strain can be established as

$$\boldsymbol{\sigma} = \mathbf{E}\boldsymbol{\varepsilon} \tag{2.28}$$

where

$$\boldsymbol{\sigma} = \begin{pmatrix} 0 & 0 & 0 & 0 & 0 & 0 & \sigma_x & \sigma_y & \sigma_z & \tau_{xy} & \tau_{yz} & \tau_{zx} \end{pmatrix}^T \tag{2.29}$$

$$\boldsymbol{\varepsilon} = \begin{pmatrix} 0 & 0 & 0 & 0 & 0 & 0 & \varepsilon_x & \varepsilon_y & \varepsilon_z & \gamma_{xy} & \gamma_{yz} & \gamma_{zx} \end{pmatrix}^T \tag{2.30}$$

For both plane stress and plane strain,

$$\mathbf{E}_i = \frac{E}{(1+\upsilon)(1-2\upsilon)} \begin{bmatrix} 0 & 0 & 0 & 0 & 0 & 0 & 0 & 0 & 0 & 0 & 0 & 0 \\ 0 & 0 & 0 & 0 & 0 & 0 & 0 & 0 & 0 & 0 & 0 & 0 \\ 0 & 0 & 0 & 0 & 0 & 0 & 0 & 0 & 0 & 0 & 0 & 0 \\ 0 & 0 & 0 & 0 & 0 & 0 & 0 & 0 & 0 & 0 & 0 & 0 \\ 0 & 0 & 0 & 0 & 0 & 0 & 0 & 0 & 0 & 0 & 0 & 0 \\ 0 & 0 & 0 & 0 & 0 & 0 & 0 & 0 & 0 & 0 & 0 & 0 \\ 0 & 0 & 0 & 0 & 0 & 0 & 1-\upsilon & \upsilon & \upsilon & 0 & 0 & 0 \\ 0 & 0 & 0 & 0 & 0 & 0 & \upsilon & 1-\upsilon & \upsilon & 0 & 0 & 0 \\ 0 & 0 & 0 & 0 & 0 & 0 & \upsilon & \upsilon & 1-\upsilon & 0 & 0 & 0 \\ 0 & 0 & 0 & 0 & 0 & 0 & 0 & 0 & 0 & \frac{1}{2}-\upsilon & 0 & 0 \\ 0 & 0 & 0 & 0 & 0 & 0 & 0 & 0 & 0 & 0 & \frac{1}{2}-\upsilon & 0 \\ 0 & 0 & 0 & 0 & 0 & 0 & 0 & 0 & 0 & 0 & 0 & \frac{1}{2}-\upsilon \end{bmatrix} \tag{2.31}$$

where E is is Young's modulus and υ is Possion's ratio of block material.

Eq. (2.27) can be represented in terms of the block displacement variables

$$\begin{aligned} \Pi_{\mathrm{e}} &= \iiint_{V_i} \frac{1}{2} \mathbf{D}_i^T \mathbf{E}_i \mathbf{D}_i \mathrm{d}x\mathrm{d}y\mathrm{d}z \\ &= \frac{V_i}{2} \mathbf{D}_i^T \mathbf{E}_i \mathbf{D}_i \end{aligned} \tag{2.32}$$

Minimizing Π_{e} by taking the derivatives, the corresponding 12 × 12 sub-matrices is obtained and added to the global stiffness matrices $\mathbf{K}_{ii}$ in the global equilibrium equation, as shown as below

$$V_i \mathbf{E}_i \rightarrow \mathbf{K}_{ii} \tag{2.33}$$

2.2.3.1.2 SUB-MATRIX OF INITIAL STRESS

In the DDA, the computed stresses of the previous time step will be transferred to the next step as initial stresses. For *Block i* with initial constant stresses,

$$\boldsymbol{\sigma}_0 = \begin{bmatrix} 0 & 0 & 0 & 0 & 0 & 0 & \sigma_x^0 & \sigma_y^0 & \sigma_z^0 & \tau_{xy}^0 & \tau_{yz}^0 & \tau_{zx}^0 \end{bmatrix}^T \tag{2.34}$$

the potential energy can be expressed as:

$$\begin{aligned} \Pi_\sigma &= \iiint_{V_i} \frac{1}{2} \boldsymbol{\varepsilon}^T \boldsymbol{\sigma}_0 \mathrm{d}x\mathrm{d}y\mathrm{d}z \\ &= V_i \mathbf{D}_i^T \boldsymbol{\sigma}_0 \end{aligned} \tag{2.35}$$

Minimizing Π_σ by taking the derivatives, the corresponding 12 × 1 sub-matrices is obtained and added to the global force matrices $\mathbf{F}_i$ in the global equilibrium equation, as shown as below

$$-V_i \boldsymbol{\sigma}_0 \rightarrow \mathbf{F}_i \tag{2.36}$$

2.2.3.1.3 SUB-MATRIX OF POINT LOADING

Assuming the point loading $\left(F_x, F_y, F_z\right)$ acts on any point $\left(x_0, y_0, z_0\right)$ within *Block i*. The potential energy of the point load is

$$\begin{aligned} \Pi_\mathrm{p} &= -\begin{bmatrix} u & v & w \end{bmatrix} \begin{bmatrix} F_x \\ F_y \\ F_z \end{bmatrix} \\ &= \mathbf{D}_i^T \mathbf{T}_i^T \left(x_0, y_0, z_0\right) \begin{bmatrix} F_x \\ F_y \\ F_z \end{bmatrix} \end{aligned} \tag{2.37}$$

Minimizing Π_p by taking the derivatives, the corresponding 12 × 1 sub-matrices is obtained and added to the global force matrices $\mathbf{F}_i$ in the global equilibrium equation, as shown as below

$$\mathbf{T}_i^T \left(x_0, y_0, z_0\right) \begin{bmatrix} F_x \\ F_y \\ F_z \end{bmatrix} \rightarrow \mathbf{F}_i \tag{2.38}$$

2.2.3.1.4 SUB-MATRIX OF BODY FORCE

Self-weight of rock masses is the most common body force. Assuming that $\left(f_x, f_y, f_z \right)$ is the constant body force acting on the entire volume of *Block i*, the potential energy is

$$\begin{aligned} \Pi_{\mathrm{v}} &= -\iiint_{V_i} \begin{bmatrix} u & v & w \end{bmatrix} \begin{bmatrix} f_x \\ f_y \\ f_z \end{bmatrix} \mathrm{d}x\mathrm{d}y\mathrm{d}z \\ &= -\mathbf{D}_i^T \left(\iiint_{V_i} \mathbf{T}_i^T \left(x, y, z \right) \mathrm{d}x\mathrm{d}y\mathrm{d}z \right) \begin{bmatrix} f_x \\ f_y \\ f_z \end{bmatrix} \\ &= -\mathbf{D}_i^T \begin{bmatrix} f_x V_i & f_y V_i & f_z V_i & 0 & 0 & 0 & 0 & 0 & 0 & 0 & 0 & 0 \end{bmatrix}^T \end{aligned} \tag{2.39}$$

Minimizing Π_{v} by taking the derivatives, the corresponding 12 × 1 sub-matrices is obtained and added to the global force matrices $\mathbf{F}_i$ in the global equilibrium equation, as shown as below

$$\begin{bmatrix} f_x V_i & f_y V_i & f_z V_i & 0 & 0 & 0 & 0 & 0 & 0 & 0 & 0 & 0 \end{bmatrix}^T \rightarrow \mathbf{F}_i \tag{2.40}$$

The constant body force is equivalent to a point load on the centroid of gravity.

2.2.3.1.5 SUB-MATRIX OF MEASURED DISPLACEMENTS

As boundary condition, displacement $\left(u_m, v_m, w_m \right)$ are sometimes fixed or pre-determined on any prescribed point $\left(x_0, y_0, z_0 \right)$ within *Block i*. Assuming that the virtual displacement of the point is $\left(u, v, w \right)$, it imposes a stiff spring to force its displacement $\left(u, v, w \right)$ to $\left(u_m, v_m, w_m \right)$. Then, the total strain energy of the spring is

$$\begin{aligned}\Pi_{\mathrm{m}} &= \frac{k}{2}\left[\left(u-u_m\right)^2+\left(v-v_m\right)^2+\left(w-w_m\right)^2\right] \\ &= \frac{k}{2}\mathbf{D}_i^T\mathbf{T}_i^T\left(x_0,y_0,z_0\right)\mathbf{T}_i\left(x_0,y_0,z_0\right)\mathbf{D}_i - k\mathbf{D}_i^T\mathbf{T}_i^T\left(x_0,y_0,z_0\right)\begin{bmatrix}u_m\\v_m\\w_m\end{bmatrix}+\frac{k}{2}\begin{bmatrix}u_m & v_m & w_m\end{bmatrix}\begin{bmatrix}u_m\\v_m\\w_m\end{bmatrix}\end{aligned} \tag{2.41}$$

where k is the stiffness of the spring.

Minimizing Π_{m} by taking the derivatives, the corresponding 12 × 12 sub-matrices and two 12 × 1 sub-matrices are obtained and added to the global stiffness matrices, $\mathbf{K}_{ii}$, and the global force sub-matrices, $\mathbf{F}_i$, in the global equilibrium equation respectively, as shown as below

$$k\mathbf{T}_i^T\left(x_0,y_0,z_0\right)\mathbf{T}_i\left(x_0,y_0,z_0\right)\rightarrow\mathbf{K}_{ii} \tag{2.42}$$

$$k\mathbf{T}_i^T\left(x_0,y_0,z_0\right)\begin{bmatrix}u_m\\v_m\\w_m\end{bmatrix}\rightarrow\mathbf{F}_i \tag{2.43}$$

It should be noted that the stiffness of the springs could not be increased infinitely to lock the fixed points. It is usually set under the order of magnitude arounf 10 ~ 100E_0L_0 to ensure that the whole coefficient matrix will not become ill-conditioned as the introduction of these springs. E_0 is the Young's modulus of the block material and L_0 is the average block "diameter".

2.2.3.1.6 SUB-matrix OF INERTIA FORCE

In DDA, the time steps are chosen such that the maximum displacements in each time step are small and the formulae for small displacements are accurate enough. The time steps are used by both statics and dynamics. The dynamic computation inherits the full velocity at the end of the previous time step. The static computation inherits only a part of the velocity at the end of the previous time step as the initial velocity at the beginning of this time step. For large deformation, the

statics is a stabilized limit case of dynamics after very long time.

Denote $\left(u(t), v(t), w(t)\right)$ as the time dependent displacement of any point (x, y, z) of *Block i* and ρ as the mass per unit volume. The force of inertia per unit volume is

$$\begin{bmatrix} f_x \\ f_y \\ f_z \end{bmatrix} = -\rho \frac{\partial^2}{\partial t^2} \begin{bmatrix} u(t) \\ v(t) \\ w(t) \end{bmatrix} = -\rho \mathbf{T}_i(x, y, z) \frac{\partial^2 \mathbf{D}_i(t)}{\partial t^2} \tag{2.44}$$

The potential energy of inertia force applied on *Block i* is

$$\begin{aligned} \Pi_i &= -\iiint_{V_i} \begin{bmatrix} u & v & w \end{bmatrix} \begin{bmatrix} f_x \\ f_y \\ f_z \end{bmatrix} \mathrm{d}x\mathrm{d}y\mathrm{d}z \\ &= \iiint_{V_i} \rho \mathbf{D}_i^T \mathbf{T}_i^T(x, y, z) \mathbf{T}_i(x, y, z) \frac{\partial^2 \mathbf{D}_i(t)}{\partial t^2} \mathrm{d}x\mathrm{d}y\mathrm{d}z \\ &= \rho \mathbf{D}_i^T \frac{\partial^2 \mathbf{D}_i(t)}{\partial t^2} \iiint_{V_i} \mathbf{T}_i^T(x, y, z) \mathbf{T}_i(x, y, z) \mathrm{d}x\mathrm{d}y\mathrm{d}z \end{aligned} \tag{2.45}$$

Denote Δt as the time interval of the time step, $\mathbf{D}_i$ as the displacement increment during this time step. Assume the acceleration is constant over this entire time step. Then applying the scheme of the average acceleration in Eq. (2.9)

$$\frac{\partial^2 \mathbf{D}_i(t)}{\partial t^2} = \frac{\partial^2 \mathbf{D}_i(t + \Delta t)}{\partial t^2} = \frac{2}{(\Delta t)^2} \mathbf{D}_i - \frac{2}{\Delta t} \mathbf{V}_i(t) \tag{2.46}$$

where

$$\mathbf{V}_i(t) = \frac{\partial \mathbf{D}_i(t)}{\partial t} \tag{2.47}$$

The velocity at the end of this time step is

$$\mathbf{V}_i\left(t+\Delta t\right)=\frac{2}{\Delta t}\mathbf{D}_i-\mathbf{V}_i\left(t\right) \tag{2.48}$$

Then, the potential energy becomes

$$\Pi_{\mathrm{i}}=\rho\mathbf{D}_i^T\iiint_{V_i}\mathbf{T}_i^T\left(x,y,z\right)\mathbf{T}_i\left(x,y,z\right)\mathrm{d}x\mathrm{d}y\mathrm{d}z\cdot\left(\frac{2}{\left(\Delta t\right)^2}\mathbf{D}_i-\frac{2}{\Delta t}\mathbf{V}_i\left(t\right)\right) \tag{2.49}$$

Minimizing Π_{i} by taking the derivatives, the corresponding 12 × 12 sub-matrices and two 12 × 1 sub-matrices are obtained and added to the global stiffness matrices, $\mathbf{K}_{ii}$, and the global force sub-matrices, $\mathbf{F}_i$, in the global equilibrium equation respectively, as shown as below

Mass matrix:

$$\frac{2\rho}{\left(\Delta t\right)^2}\iiint_{V_i}\mathbf{T}_i^T\left(x,y,z\right)\mathbf{T}_i\left(x,y,z\right)\mathrm{d}x\mathrm{d}y\mathrm{d}z\rightarrow\mathbf{K}_{ii} \tag{2.50}$$

Velocity matrix:

$$\frac{2\rho}{\Delta t}\mathbf{V}_i\left(t\right)\iiint_{V_i}\mathbf{T}_i^T\left(x,y,z\right)\mathbf{T}_i\left(x,y,z\right)\mathrm{d}x\mathrm{d}y\mathrm{d}z\rightarrow\mathbf{F}_i \tag{2.51}$$

The integration can be obtained from

$$\iiint_{V_i} \mathbf{T}_i^T(x,y,z)\,\mathbf{T}_i(x,y,z)\,\mathrm{d}x\mathrm{d}y\mathrm{d}z =$$

$$\begin{bmatrix}
S_0 & 0 & 0 & 0 & 0 & 0 & 0 & 0 & 0 & 0 & 0 & 0 \\
0 & S_0 & 0 & 0 & 0 & 0 & 0 & 0 & 0 & 0 & 0 & 0 \\
0 & 0 & S_0 & 0 & 0 & 0 & 0 & 0 & 0 & 0 & 0 & 0 \\
0 & 0 & 0 & S_2+S_3 & -S_4 & -S_5 & 0 & -S_6 & S_6 & \frac{S_2-S_3}{2} & \frac{S_4}{2} & -\frac{S_5}{2} \\
0 & 0 & 0 & -S_4 & S_1+S_3 & -S_6 & S_5 & 0 & -S_5 & -\frac{S_4}{2} & \frac{S_3-S_1}{2} & \frac{S_6}{2} \\
0 & 0 & 0 & -S_5 & -S_6 & S_1+S_2 & -S_4 & S_4 & 0 & \frac{S_5}{2} & -\frac{S_6}{2} & \frac{S_1-S_2}{2} \\
0 & 0 & 0 & 0 & S_5 & -S_4 & S_1 & 0 & 0 & 0 & -\frac{S_6}{2} & \frac{S_4}{2} \\
0 & 0 & 0 & -S_6 & 0 & S_4 & 0 & S_2 & 0 & \frac{S_6}{2} & 0 & \frac{S_4}{2} \\
0 & 0 & 0 & S_6 & -S_5 & 0 & 0 & 0 & S_3 & \frac{S_6}{2} & \frac{S_5}{2} & 0 \\
0 & 0 & 0 & \frac{S_2-S_3}{2} & -\frac{S_4}{2} & \frac{S_5}{2} & 0 & \frac{S_6}{2} & \frac{S_6}{2} & \frac{S_2+S_3}{4} & \frac{S_4}{4} & \frac{S_5}{4} \\
0 & 0 & 0 & \frac{S_4}{2} & \frac{S_3-S_1}{2} & -\frac{S_6}{2} & -\frac{S_6}{2} & 0 & \frac{S_5}{2} & \frac{S_4}{4} & \frac{S_1+S_3}{4} & \frac{S_6}{4} \\
0 & 0 & 0 & -\frac{S_5}{2} & \frac{S_6}{2} & \frac{S_1-S_2}{2} & \frac{S_4}{2} & \frac{S_4}{2} & 0 & \frac{S_5}{4} & \frac{S_6}{4} & \frac{S_1+S_2}{4}
\end{bmatrix} \tag{2.52}$$

where

$$\begin{cases}
S_0 = S_i^1 \\
S_1 = S_i^{x^2} - x_c \cdot S_i^x \\
S_2 = S_i^{y^2} - y_c \cdot S_i^y \\
S_3 = S_i^{z^2} - z_c \cdot S_i^z \\
S_4 = S_i^{xy} - x_c \cdot S_i^y \\
S_5 = S_i^{zx} - z_c \cdot S_i^x \\
S_6 = S_i^{yz} - y_c \cdot S_i^z
\end{cases} \tag{2.53}$$

$$\begin{cases} x_c = \dfrac{S_i^x}{S_i^1} \\ y_c = \dfrac{S_i^y}{S_i^1} \\ z_c = \dfrac{S_i^z}{S_i^1} \end{cases} \tag{2.54}$$

(x_c, y_c, z_c) is the centroid of *Block i* and S_i^1, S_i^x, S_i^y, S_i^z, $S_i^{x^2}$, $S_i^{y^2}$, $S_i^{z^2}$, S_i^{xy}, S_i^{zx} and S_i^{yz} will be given in the 3D Simplex Integration (*Section 2.2.2*).

2.2.2 SIMPLEX INTEGRATION

Shi (1996, 1997a, b) introduced the method of summing up the oriented area to get the area of the 2D block with any shape (**Figure 2.4**). Simplex integrations can compute ordinary integrations on any complex without subdividing mesh. *P* can be the point of anywhere in the 2D domain.

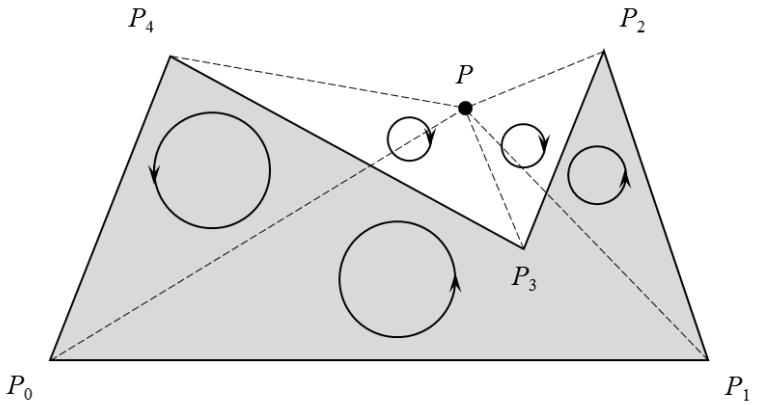

Figure 2. 4 Simplex integration on complex in 2D.

Integration domains of the 3D blocks usually have complex shapes in 3D DDA. Therefore, integrations are more difficult than those of FEM. Integration domains are the major differences between the two methods. The FEM computes the complex functions in simple domains, while DDA computes simple functions in complex domains. The simplex in 2D is a triangle, while it is a tetrahedron in 3D domain, as shown in Figure 2.5.

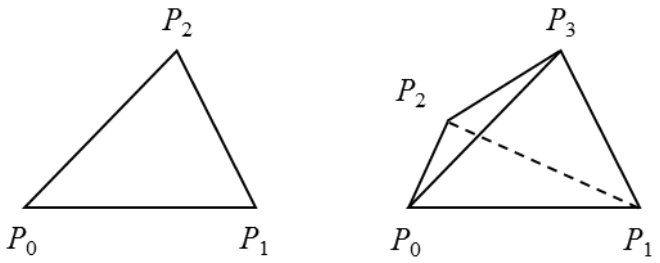

(a) 2D simplex (b) 3D simplex

Figure 2. 5 Simplex in 2D and 3D.

The coordinates of the vertices P_0, P_1, P_2, P_3 on the 3D simplex are supposed as (x_0, y_0, z_0), (x_1, y_1, z_1), (x_2, y_2, z_2) and (x_3, y_3, z_3) respectively. Hence, the 3D simplex volume can be calculated by using Eq. (2.55)

$$V = \frac{1}{6}\begin{vmatrix} 1 & x_0 & y_0 & z_0 \\ 1 & x_1 & y_1 & z_1 \\ 1 & x_2 & y_2 & z_2 \\ 1 & x_3 & y_3 & z_3 \end{vmatrix} \tag{2.55}$$

3D simplex has both positive and negative orientations which are defined as positive and negative volumes respectively. Furthermore, any general block can be divided into simplexes. And the integrations of the general block can be treated as the summation of the oriented subdivided simplexes.

Assume the vertex list of *Polygon j* is

$$P_0^j P_1^j \cdots P_{m(j)-1}^j \tag{2.56}$$

where $m(j)$ is the sum of vertex on *Polygon j*. Define

$$P_0^j = P_{m(j)}^j \tag{2.57}$$

to complete the definition of loops of *Polygon j* by repeating the first vertex on the face. The coordinate of each vertex can be expressed as:

$$P_k^j = \left(x_k^j, y_k^j, z_k^j \right) \tag{2.58}$$

The current block is assumed to be composed by *s* polygons in total and set $P = \left(0,0,0 \right)$. The volume of this block is given by Eq. (2.59). Calculated by simplex integrations integrals for 1, *x*, *y*, *z*, x^2, y^2, z^2, *xy*, *yz*, *zx* are represented by the coordinates of the boundary vertices only.

$$\begin{aligned} S_i^1 &= \iiint_{V_i} 1 \mathrm{d}x\mathrm{d}y\mathrm{d}z \\ &= \sum_{j=1}^{s} \sum_{k=1}^{m(\mathrm{j})-2} \int_{PP_0^j P_k^j P_{k+1}^j} 1 D\left(x, y, z \right) \\ &= \frac{1}{6} \sum_{j=1}^{s} \sum_{k=1}^{m(\mathrm{j})-2} \begin{vmatrix} x_0^j & y_0^j & z_0^j \\ x_k^j & y_k^j & z_k^j \\ x_{k+1}^j & y_{k+1}^j & z_{k+1}^j \end{vmatrix} \end{aligned} \tag{2.59}$$

$$\begin{aligned} S_i^x &= \iiint_{V_i} x \mathrm{d}x\mathrm{d}y\mathrm{d}z \\ &= \sum_{j=1}^{s} \sum_{k=1}^{m(\mathrm{j})-2} \int_{PP_0^j P_k^j P_{k+1}^j} x D\left(x, y, z \right) \\ &= \frac{1}{24} \sum_{j=1}^{s} \sum_{k=1}^{m(\mathrm{j})-2} \begin{vmatrix} x_0^j & y_0^j & z_0^j \\ x_k^j & y_k^j & z_k^j \\ x_{k+1}^j & y_{k+1}^j & z_{k+1}^j \end{vmatrix} \cdot \left(x_0^j + x_k^j + x_{k+1}^j \right) \end{aligned} \tag{2.60}$$

$$\begin{aligned} S_i^y &= \iiint_{V_i} y \mathrm{d}x\mathrm{d}y\mathrm{d}z \\ &= \sum_{j=1}^{s} \sum_{k=1}^{m(\mathrm{j})-2} \int_{PP_0^j P_k^j P_{k+1}^j} y D\left(x, y, z \right) \\ &= \frac{1}{24} \sum_{j=1}^{s} \sum_{k=1}^{m(\mathrm{j})-2} \begin{vmatrix} x_0^j & y_0^j & z_0^j \\ x_k^j & y_k^j & z_k^j \\ x_{k+1}^j & y_{k+1}^j & z_{k+1}^j \end{vmatrix} \cdot \left(y_0^j + y_k^j + y_{k+1}^j \right) \end{aligned} \tag{2.61}$$

$$
\begin{aligned}
S_i^z &= \iiint_{V_i} z\mathrm{d}x\mathrm{d}y\mathrm{d}z \\
&= \sum_{j=1}^{s}\sum_{k=1}^{m(\mathrm{j})-2} \int_{PP_0^jP_k^jP_{k+1}^j} zD(x,y,z) \\
&= \frac{1}{24}\sum_{j=1}^{s}\sum_{k=1}^{m(\mathrm{j})-2} \begin{vmatrix} x_0^j & y_0^j & z_0^j \\ x_k^j & y_k^j & z_k^j \\ x_{k+1}^j & y_{k+1}^j & z_{k+1}^j \end{vmatrix} \cdot \left(z_0^j + z_k^j + z_{k+1}^j\right)
\end{aligned}
\tag{2.62}
$$

$$
\begin{aligned}
S_i^{x^2} &= \iiint_{V_i} x^2\mathrm{d}x\mathrm{d}y\mathrm{d}z \\
&= \sum_{j=1}^{s}\sum_{k=1}^{m(\mathrm{j})-2} \int_{PP_0^jP_k^jP_{k+1}^j} x^2D(x,y,z) \\
&= \frac{1}{60}\sum_{j=1}^{s}\sum_{k=1}^{m(\mathrm{j})-2} \begin{vmatrix} x_0^j & y_0^j & z_0^j \\ x_k^j & y_k^j & z_k^j \\ x_{k+1}^j & y_{k+1}^j & z_{k+1}^j \end{vmatrix} \cdot \left(x_0^jx_0^j + x_0^jx_k^j + x_0^jx_{k+1}^j + x_k^jx_k^j + x_k^jx_{k+1}^j + x_{k+1}^jx_{k+1}^j\right)
\end{aligned}
\tag{2.63}
$$

$$
\begin{aligned}
S_i^{y^2} &= \iiint_{V_i} y^2\mathrm{d}x\mathrm{d}y\mathrm{d}z \\
&= \sum_{j=1}^{s}\sum_{k=1}^{m(\mathrm{j})-2} \int_{PP_0^jP_k^jP_{k+1}^j} y^2D(x,y,z) \\
&= \frac{1}{60}\sum_{j=1}^{s}\sum_{k=1}^{m(\mathrm{j})-2} \begin{vmatrix} x_0^j & y_0^j & z_0^j \\ x_k^j & y_k^j & z_k^j \\ x_{k+1}^j & y_{k+1}^j & z_{k+1}^j \end{vmatrix} \cdot \left(y_0^jy_0^j + y_0^jy_k^j + y_0^jy_{k+1}^j + y_k^jy_k^j + y_k^jy_{k+1}^j + y_{k+1}^jy_{k+1}^j\right)
\end{aligned}
\tag{2.64}
$$

$$
\begin{aligned}
S_i^{z^2} &= \iiint_{V_i} z^2\mathrm{d}x\mathrm{d}y\mathrm{d}z \\
&= \sum_{j=1}^{s}\sum_{k=1}^{m(\mathrm{j})-2} \int_{PP_0^jP_k^jP_{k+1}^j} z^2D(x,y,z) \\
&= \frac{1}{60}\sum_{j=1}^{s}\sum_{k=1}^{m(\mathrm{j})-2} \begin{vmatrix} x_0^j & y_0^j & z_0^j \\ x_k^j & y_k^j & z_k^j \\ x_{k+1}^j & y_{k+1}^j & z_{k+1}^j \end{vmatrix} \cdot \left(z_0^jz_0^j + z_0^jz_k^j + z_0^jz_{k+1}^j + z_k^jz_k^j + z_k^jz_{k+1}^j + z_{k+1}^jz_{k+1}^j\right)
\end{aligned}
\tag{2.65}
$$

$$
\begin{aligned}
S_i^{xy} &= \iiint_{V_i} xy\mathrm{d}x\mathrm{d}y\mathrm{d}z \\
&= \sum_{j=1}^{s}\sum_{k=1}^{m(\mathrm{j})-2} \int_{PP_0^jP_k^jP_{k+1}^j} xyD(x,y,z) \\
&= \frac{1}{60}\sum_{j=1}^{s}\sum_{k=1}^{m(\mathrm{j})-2} \begin{vmatrix} x_0^j & y_0^j & z_0^j \\ x_k^j & y_k^j & z_k^j \\ x_{k+1}^j & y_{k+1}^j & z_{k+1}^j \end{vmatrix} \\
&\quad \cdot\left(2x_0^jy_0^j + x_0^jy_k^j + x_0^jy_{k+1}^j + x_k^jy_0^j + 2x_k^jy_k^j + x_k^jy_{k+1}^j + x_{k+1}^jy_0^j + x_{k+1}^jy_k^j + 2x_{k+1}^jy_{k+1}^j\right)
\end{aligned} \tag{2.66}
$$

$$
\begin{aligned}
S_i^{yz} &= \iiint_{V_i} yz\mathrm{d}x\mathrm{d}y\mathrm{d}z \\
&= \sum_{j=1}^{s}\sum_{k=1}^{m(\mathrm{j})-2} \int_{PP_0^jP_k^jP_{k+1}^j} yzD(x,y,z) \\
&= \frac{1}{60}\sum_{j=1}^{s}\sum_{k=1}^{m(\mathrm{j})-2} \begin{vmatrix} x_0^j & y_0^j & z_0^j \\ x_k^j & y_k^j & z_k^j \\ x_{k+1}^j & y_{k+1}^j & z_{k+1}^j \end{vmatrix} \\
&\quad \cdot\left(2y_0^jz_0^j + y_0^jz_k^j + y_0^jz_{k+1}^j + y_k^jz_0^j + 2y_k^jz_k^j + y_k^jz_{k+1}^j + y_{k+1}^jz_0^j + y_{k+1}^jz_k^j + 2y_{k+1}^jz_{k+1}^j\right)
\end{aligned} \tag{2.67}
$$

$$
\begin{aligned}
S_i^{zx} &= \iiint_{V_i} zx\mathrm{d}x\mathrm{d}y\mathrm{d}z \\
&= \sum_{j=1}^{s}\sum_{k=1}^{m(\mathrm{j})-2} \int_{PP_0^jP_k^jP_{k+1}^j} zxD(x,y,z) \\
&= \frac{1}{60}\sum_{j=1}^{s}\sum_{k=1}^{m(\mathrm{j})-2} \begin{vmatrix} x_0^j & y_0^j & z_0^j \\ x_k^j & y_k^j & z_k^j \\ x_{k+1}^j & y_{k+1}^j & z_{k+1}^j \end{vmatrix} \\
&\quad \cdot\left(2z_0^jx_0^j + z_0^jx_k^j + z_0^jx_{k+1}^j + z_k^jx_0^j + 2z_k^jx_k^j + z_k^jx_{k+1}^j + z_{k+1}^jx_0^j + z_{k+1}^jx_k^j + 2z_{k+1}^jx_{k+1}^j\right)
\end{aligned} \tag{2.68}
$$

2.2.3 CONTACT DETECTION

In 3D DDA, a rigorous contact theory is an essential part because it governs the interaction of the blocks. A comprehensive theory mainly involves contact detection

and contact mechanics (Beyabanaki, Jafari and Yeung, 2010). The former is mainly concerned with the geometric aspects of the method, e.g. the type of contact between two blocks. The latter is mainly concerned with the physical aspects of the method, e.g. the mechanical response of blocks in contact.

2.2.4 CONTACT MECHANICS

DDA uses a penalty-constraint approach in which the contact is assumed to be rigid. As a result, no overlapping or inter-penetration of the blocks is allowed. This is called an impenetrability constraint. Shi (1988) used the penalty method in the original DDA.

In the penalty method, when two blocks overlap, an impenetrability constraint is implemented by applying a numerical penalty function analogous to stiff springs at the contacts in the direction of the penetrating corner to prevent inter-penetration. Numerically, this is done by adding penalty value (usually a large number) to the contact terms in the global equations. In the original DDA program, within each time step, the global equations are solved iteratively by repeatedly adding and removing contact springs (penalty values) until each of the contacts converges to a constant state. This procedure of adding and removing contact springs (penalty values) is known as open-close iterations in the DDA literature. The open-close iterations are continued until there is no penetration at any contact point. If the no-penetration constraint is not satisfied within a specified number of iterations (typically 6-8 iterations), the time step is reduced by one third and the process is repeated with the reduced time step.

The Mohr-Coulomb joint failure criterion is used in DDA to check failure along discontinuities just like Figure 2.6 shows.

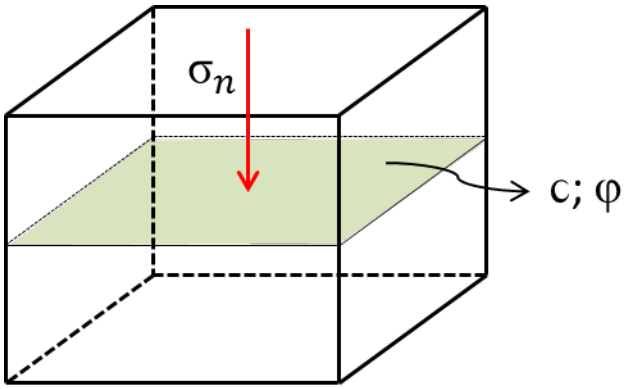

Figure 2.6 The sketch of Mohr-Coulomb law

In the original DDA, the normal component of the contact force, F_n is compressive, i.e.,

$$F_{\mathrm{n}} = -k_{\mathrm{n}} d_{\mathrm{n}} > 0,\ d_{\mathrm{n}} < 0 \tag{2.1}$$

where $d_{\mathrm{n}} < 0$ means penetrations in DDA. The shear component of the contact force satisfies

$$F_{\mathrm{s}} < F_{\mathrm{n}} \tan\phi + cA_{\mathrm{c}} \tag{2.1}$$

where ϕ is the joint friction angle, c is the joint cohesion and A_{c} is contact area of the joint. If the driving shear force, F_{s}, is larger than the Mohr-Coulomb resisting shear force causing sliding, contact is in the "sliding" state. For this contact state, the stiff penalty spring is applied only in the normal direction to prevent inter-penetration between blocks and to allow sliding controlled by the friction law. The sliding force is calculated from the normal contact force of the previous iteration. The contact state can have three basic types, locked, sliding, and open. For the locked contact, both normal and shear spring are applied. For the sliding contact, only the shear spring is applied, but a pair of frictional force is added. There will be no spring and force when the contact is judged as open contact. The locked and sliding contacts are showed in Figure 2.7. Additionally, it should be mentioned that once the contact status changes from locked to sliding, the cohesion will be not taken into consideration.

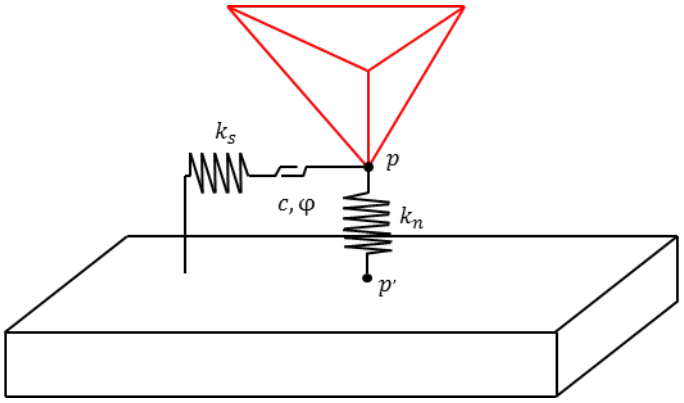

(a)

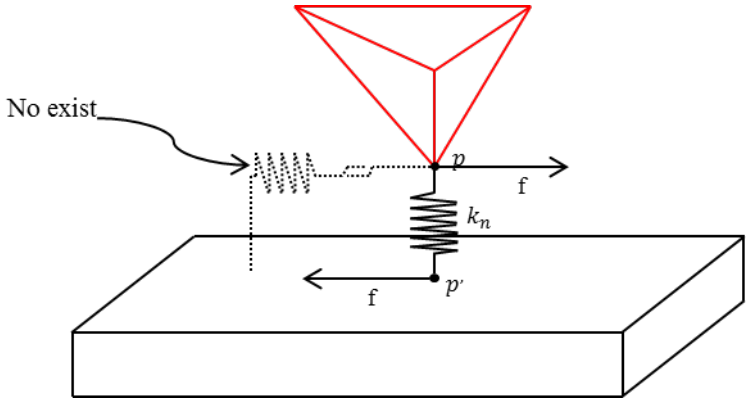

(b)

Figure 2.7 The schema of locked contact (a) and sliding contact (b)

2.3 The 3D DDA program structure

2.3.1 OPEN-CLOSE ITERATION

In the mechanical computation process of 3D DDA, a three-parameter (friction angle, cohesion, tensile strength) Mohr-Coulomb law is applied to determine the contact state (open, sliding, locked) between blocks.

Within each time step, the global equilibrium equations are solved repeatedly while selecting the closed entrance positions. The procedure of adding or removing penalty springs and/or frictional force, which depends on the changes in contact

state, is known as *open-close iteration* (Shi, 1988). Each contact has three possible states: open, locked, and sliding. No springs or frictional forces are applied on an open contact. A normal spring and a pair of frictional forces are applied on a sliding contact. A normal spring and a shear spring are applied on a locked contact.

2.3.2 GENAERAL PROCEDURE FRO 3D DDA PROGRAM

For the general procedure of 3D DDA program, there are several steps for the whole process. For simplicity, it can be summarized as the following steps:

1) Inputting the geometric data (such as the point coordinates, lines and faces constitute elements), the physical parameters (for example, density, Young's modulus, and Poisson's ratio), the computational parameters (such as spring's penalty, simulation time, time step, and maximum allowed displacement ratio) and etc.

2) Initiate the global equilibrium equation and assemble non-contact terms. During this step, the contacts and contact forces will be updated, meanwhile, the sub-matrices of non-contact terms will be assembled and added, which includes the inertia term, fix point or displacement boundary, the stiffness, the initial stress, the point loading, the volume forces and etc.

3) The above mentioned open-close iteration will be performed. Firstly, according to the contact state of each contact point, the addition or remove spring or frictional forces will be executed. Then, the system's equilibrium equation will be solved and each block's position will be updated. However, this is not the end. The verification of the consistency of open-close for each contact before and after the iteration will be performed.

4) Once the consistency is satisfied, the process of open-close iteration can be jumped. Moreover, if the consistency is not satisfied and at the same time, the iteration step is more than six, the time reduction will happen.

5) When the open-close iteration is finished, the maximum displacement ratio will be checked. If it is bigger than the pre-defined maximum displacement ratio, the

time increment will be reduced. If it is under the pre-defined, the result will be outputted and the close contact will be transferred until the final simulation step is achieved.

tion step is achieved.

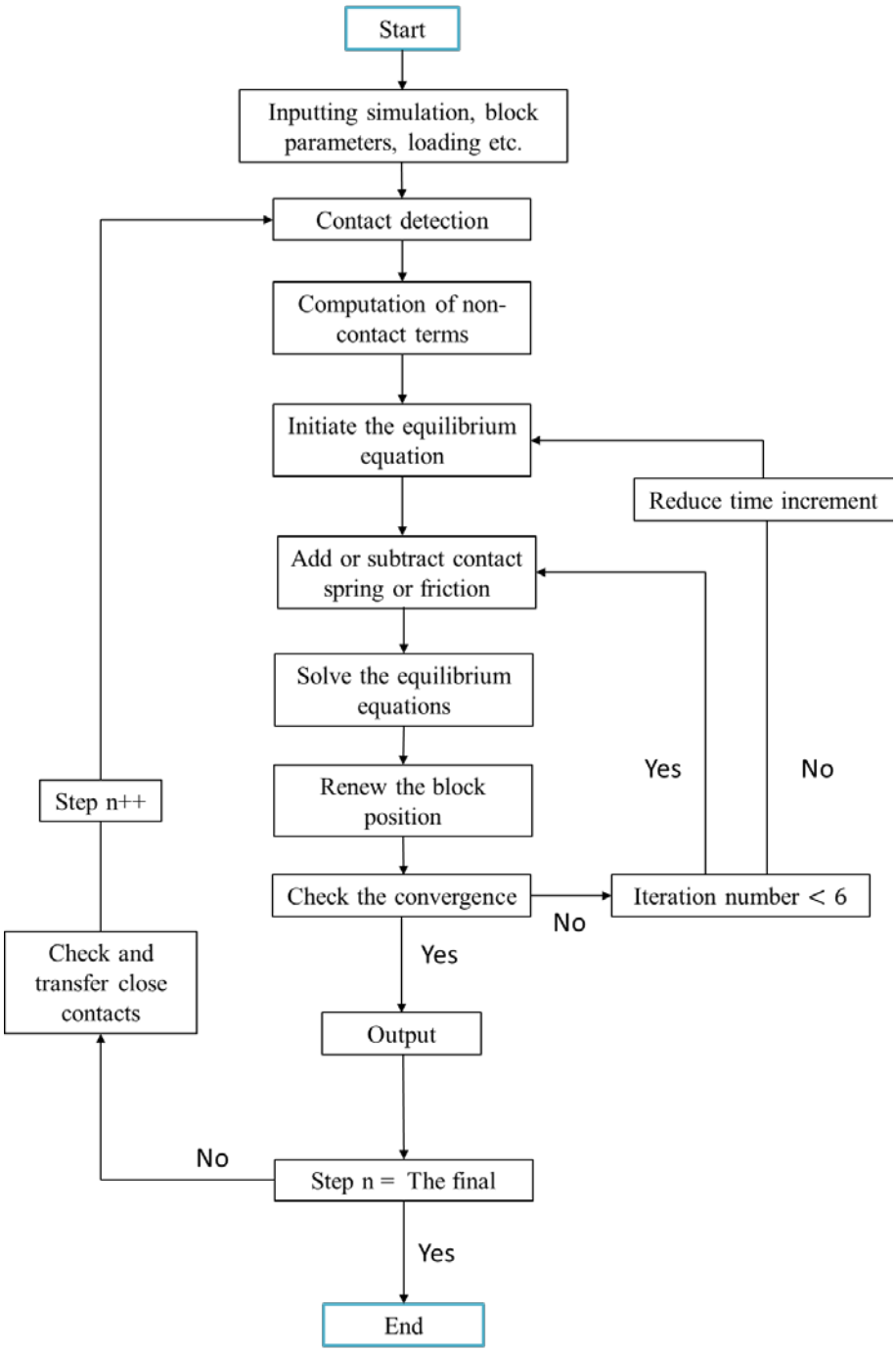

Figure 2.8 General procedure of 3D DDA program.

2.4 UNSOLVED PROBLEMS IN THE EXTISTING 3D DDA PROGRAM

Although there are many achievements has been made on the DDA method, the main research focus on the 2D DDA. For the 2D DDA method, from the basic theory and large-scale application, it has shown its advantages both in accuracy and efficiency. For the 3D DDA method, the research is in a preliminary state. According to the literature review, the research about the 3D DDA is mainly on two aspects: 1) the basic formulations, the contact detection and constraints (Shi 2001, Liu 2004, Jiang and Yeung 2004, Beyabanaki Jafari and Yeung 2010, Beyabanaki, Yeung et al 2010, Chen et al. 2004, Wang et al. 2006, Beyabanaki et al. 2008, Keneti et al. 2008, Ahn and Song 2011, and Mikola and Sitar 2013); 2) the basic verification applications such as the classical wedge model and key block theory were used by Yeung et al. (2003) and Bakun-Mazor (2012) et al. to clarify the availability of the 3D DDA program, and The real 3D rock-fall problems were solved by Chen et al. (2013). The unsolved problems of the existing 3D DDA program which will be discussed in this thesis are listed as followings:

1) Without an effective pre-processor for complex slope model construction. When creating the 3D model for the real slope simulation, there are two major necessary steps 1) the construction of blocky systems that consisting of discontinuities, in which the block formulation and cutting are unavoidable. For the latter, the original pre-processor is not effective and even lost its ability when dealing with complex cutting problems; 2) the accurate construction of real 3D terrain, which play an important role in the 3D DDA simulation such as the stability, run-out analysis if the more accurate result is needed.

2) Unable to perform the stability analysis and runout simulation under a potential earthquake. As we know, the earthquake is one of the major factors that can cause the landslide. Although the seismic loading can be applied in the 2D DDA, the research about the slope under earthquake in the 3D DDA is rare in the literatures especially when take the 3D terrain into consideration. For the stability analysis, how to judge the factor of safety is also a problem in the 3D DDA.

3) Unable to evaluate the preventive effect of using anchor reinforcement. The anchor reinforcement is an important countermeasure for the slide-prone slope. If the slope is judged as unstable when certain earthquake is applied, the anchors can be applied to improve the stability. Although some work has been done on the 2D anchor reinforcement simulation, how to add the anchor function into the 3D DDA program is a problem that exists.

REFERENCES

Ala G, Francomano E, Tortorici A, Toscano E, Viola F, di Ingegneria Elettrica D, e delle Telecomunicazioni E. (2007). A meshfree particle method for transient full-wave simulation. IEEE Trans Magn 43(4):1333-1336

Alia A, Souli M. (2006). High explosive simulation using multimaterial formulations. Appl Therm Eng 26(10):1032-1042

Anghileri M, Castelletti LML, Tirelli M. (2005). Fluid structure interaction of water filled tanks during the impact with the ground. Int J Impact Eng 31(3):235-254

Antoci C, Gallati M, Sibilla S. (2007). Numerical simulation of fluid-structure interaction by SPH. Comput Struct 85(11- 14):879-890

Apfel RE, Tian Y, Jankovsky J, Shi T, Chen X, Holt RG, Trinh E, Croonquist A, Thornton KC, Sacco JA. (1997). Free oscillations and surfactant studies of superdeformed drops in microgravity. Phys Rev Lett 78(10):1912-1915

Benz W. (1988). Applications of smooth particle hydrodynamics (SPH) to astrophysical problems. Comput Phys Commun 48(1):97-105

Benz W, Asphaug E. (1995). Simulations of brittle solids using smooth particle hydrodynamics. Comput Phys Commun 87(1):253-265

Berczik P. (2000). Modeling the star formation in galaxies using the chemo-dynamical SPH code. Astrophys Space Sci 271(2):103-126

Beyabanaki SAR, Ferdosi B and Mohammadi S. (2009). Validation of dynamic block displacement analysis and modification of edge-to-edge contact constraints in 3-D DDA. International Journal of Rock Mechanics and Mining Sciences, 46(7), 1223-1234.

Beyabanaki SAR, Jafari A and Yeung MR. (2010). High-order three-dimensional discontinuous deformation analysis (3-D DDA). International Journal for Numerical Methods in Biomedical Engineering, 26(12), 1522-1547.

Beyabanaki SAR, Jafari A, Biabanaki SOR and Yeung MR. (2009b). Nodal-based three-dimensional discontinuous deformation analysis (3-D DDA). Computers and Geotechnics, 36(3), 359-372.

Beyabanaki SAR, Jafari A, Biabanaki SOR and Yeung MR. (2009a). A coupling model of 3-D discontinuous deformation analysis (3-D DDA) and finite element method. Arabian Journal for Science and Engineering, 34(1B), 108.

Beyabanaki SAR, Mikola RG and Hatami K. (2008). Three-dimensional discontinuous deformation analysis (3-D DDA) using a new contact resolution algorithm. Computers and Geotechnics, 35(3), 346-356.

Beyabanaki SAR, Mikola RG, Biabanaki SOR and Mohammadi S. (2009b). New point-to-face contact algorithm for 3-D contact problems using the augmented Lagrangian method in 3-D DDA. Geomechanics and Geoengineering: An International Journal, 4(3), 221-236.

Beyabanaki SAR, Yeung MR, Mohammadi S and Gao YN. (2010). Contact theory for deformable blocks in three-dimensional discontinuous

deformation analysis (3-D DDA). In 44th U.S. Rock Mechanics Symposium and 5th U.S.-Canada Rock Mechanics Symposium, 27-30 June, Salt Lake City, Utah.

Bicanic N and Stirling C. (2001). DDA analysis of the Couplet/Heyman minimum thickness arch problem. In Proceedings of the Fourth International Conference on Analysis of Discontinuous Deformation, Bi!cani!c N (ed.). University of Glasgow: Glasgow, 2001; 165-170.

Bonet J, Kulasegaram S. (2000). Correction and stabilization of smooth particle hydrodynamics methods with applications in metal forming simulations. Int J Numer Methods Eng 47(6):1189-1214

Borve S, Omang M, Trulsen J (2001) Regularized smoothed particle hydrodynamics: a new approach to simulating magnetohydrodynamic shocks. Astrophys J 561(1):82-93.

Bromm V, Yoshida N, Hernquist L. (2003). The first supernova explosions in the universe. Astrophys J 596(2):L135-L138

Bui HH, Fukagawa R, Sako K. (2006). Smoothed particle hydrodynamics for soil mechanics. Taylor and Francis, London

Bui HH, Fukagawa R, Sako K and Ohno S. (2008). Lagrangian meshfree particles method (SPH) for large deformation and failure flows of geomaterial using elastic-plastic soil constitutive model. Int J Numer Anal Methods 32(12):1537-1570.

Bui HH, Sako K and Fukagawa R. (2007). Numerical simulation of soil-water interaction using smoothed particle hydrodynamics (SPH) method. J Terramech 44(5):339-346.

Bulgarelli UP. (2005). The application of numerical methods for the solution of some problems in free-surface hydrodynamics. J Ship Res

49(4):288-301.

Bursik M, Martinez-Hackert B, Delgado H and Gonzalez-Huesca A. (2003). A smoothed-particle hydrodynamic automaton of landform degradation by overland flow. Geomorphology 53(1-2):25- 44.

Busegnies Y, Francois J and Paulus G. (2007). Unidimensional SPH simulations of reactive shock tubes in an astrophysical perspective. Shock Waves 16(4-5):359-389.

Cleary PW, Prakash M, Ha J (2006) Novel applications of smoothed particle hydrodynamics (SPH) in metal forming. J Mater Process Technol 177(1-3):41-48

Cleary PW, Prakash M, Ha J, Stokes N and Scott C. (2007). Smooth particle hydrodynamics: status and future potential. Prog Comput Fluid Dyn 7(2-4):70-90

Colagrossi A, Landrini M. (2003). Numerical simulation of interfacial flows by smoothed particle hydrodynamics. J Comput Phys 191(2):448-475

Crespo AJC, Gomez-Gesteira M, Carracedo P and Dalrymple RA. (2008). Hybridation of generation propagation models and SPH model to study severe sea states in Galician Coast. J Mar Syst 72(14):135-144.

Crespo AJC, Gomez-Gesteira M and Dalrymple RA. (2007). 3D SPH simulation of large waves mitigation with a dike. J Hydraul Res 45(5):631-642.

Crespo AJC, Gomez-Gesteira M and Dalrymple RA. (2008). Modeling dam break behavior over a wet bed by a SPH technique. J Waterw Port C 134(6):313-320.

Cundall PA. (1988, June). Formulation of a three-dimensional distinct element model—Part I. A scheme to detect and represent contacts in a system composed of many polyhedral blocks. In International Journal of Rock Mechanics and Mining Sciences and Geomechanics Abstracts (Vol. 25, No. 3, pp. 107-116). Pergamon.

Doolin DM. (2005). Unified displacement boundary constraint formulation for discontinuous deformation analysis (DDA). International journal for numerical and analytical methods in geomechanics, 29(12), 1199-1207.

Doolin, D. M and Sitar N. (2001). DDAML—discontinuous deformation analysis markup language. International Journal of Rock Mechanics and Mining Sciences, 38(3), 467-474.

Felippa CA. (1986). Penalty-function iterative procedures for mixed finite element formulations. International journal for numerical methods in engineering, 22(1), 267-279.

Francomano E, Tortorici A, Toscano E, Ala G and Viola F. (2009). On the use of a meshless solver for PDEs governing electromagnetic transients. Appl Math Comput 209(1):42-51.

Frederic AR, James CL. (1999). Smoothed particle hydrodynamics calculations of stellar interactions. J Comput Appl Math 109:213-230

Gomez-Gesteira M and Dalrymple RA. (2004). Using a threedimensional smoothed particle hydrodynamics method for wave impact on a tall structure. J Waterw Port C 130(2):63-69

Guilcher PM, Ducrozet G, Doring M, Alessandrini B and Ferrant P. (2006). Numerical simulation of wave-body interactions using a modified SPH solver. In: Proceedings of the sixteenth international

offshore and polar engineering conference, San Francisco, CA.

Gutfraind R and Savage SB. (1998). Flow of fractured ice through wedge-shaped channels: smoothed particle hydrodynamics and discrete-element simulations. Mech Mater 29(1):1-17.

Hosseini SM andAmanifard N. (2007). Presenting a modified SPH algorithm for numerical studies of fluid-structure interaction problems. IJE Trans B, Appl 20:167-178.

Hsiung SM and Shi GH. (2001, January). Simulation of earthquake effects on underground excavations using discontinuous deformation analysis (DDA). In DC Rocks 2001 The 38th US Symposium on Rock Mechanics (USRMS). American Rock Mechanics Association.

Hsiung SM. (2001, January). Discontinuous deformation analysis (DDA) with nth order polynomial displacement functions. In DC Rocks 2001 The 38th US Symposium on Rock Mechanics (USRMS). American Rock Mechanics Association.

Hu W, Yao LG and Hua ZZ. (2007). Parallel point interpolation method for three-dimensional metal forming simulations. Eng Anal Bound Elem 31(4):326-342

Hu XY and Adams NA. (2006). A multi-phase SPH method for macroscopic and mesoscopic flows. J Comput Phys 213(2):844- 861.

Hu XY and Adams NA. (2007). An incompressible multi-phase SPH method. J Comput Phys 227(1):264-278.

Hu XY and Adams NA. (2009). A constant-density approach for incompressible multi-phase SPH. J Comput Phys 228(6):2082- 2091.

Hui HH, Fukagawa R and Sako K (2006) Smoothed particle

hydrodynamics for soil mechanics. Terramechanics 26:49-53.

Hultman J and Pharayn A. (1999). Hierarchical, dissipative formation of elliptical galaxies: is thermal instability the key mechanism? Hydrodynamic simulations including supernova feedback multiphase gas and metal enrichment in cdm: structure and dynamics of elliptical galaxies. Astron Astrophys 347:769-798.

Iglesias AS, Rojas LP and Rodriguez RZ. (2004). Simulation of antiroll tanks and sloshing type problems with smoothed particle hydrodynamics. Ocean Eng 31(8-9):1169-1192.

Issa R and Violeau D. (2008). Modelling a plunging breaking solitary wave with eddy-viscosity turbulent SPH models. Comput Mater Continua 8(3):151-164

Jiang FM and Sousa ACM. (2006). SPH numerical modeling for ballistic-diffusive heat conduction. Numer Heat Transfer B, Fundam 50(6):499-515.

Jiang Q, Chen Y, Zhou C and Yeung MCR. (2013). Kinetic energy dissipation and convergence criterion of Discontinuous Deformations Analysis (DDA) for geotechnical engineering. Rock mechanics and rock engineering, 46(6), 1443-1460.

Jiang QH and Yeung MR. (2004). A model of point-to-face contact for three-dimensional discontinuous deformation analysis. Rock Mechanics and Rock Engineering, 37(2), 95-116.

Jing L, Ma Y and Fang Z. (2001). Modelingof fluid flow and solid deformation for fractured rocks with discontinuous deformation analysis (DDA) method. International Journal of Rock Mechanics and Mining Sciences, 38(3), 343-355.

Khayyer A, Gotoh H, Shao SD. (2008). Corrected incompressible SPH method for accurate water-surface tracking in breaking waves. Coast Eng 55(3):236-250

Koo CY and Chen S. (1997, August). Development of second order displacement function for DDA and manifold method. In Working Forum on the Manifold Method of Material Analysis, Volume I (p. 183).

Koo CY and Chern JC. (1996, June). The development of DDA with third order displacement function. In Proceedings of the 1st International Forum on Discontinuous Deformation Analysis (DDA) and Simulations of Discontinuous Media.[S. l.]: TSI Press (pp. 342-349).

Koo CY and Chern JC. (1998). Modification of the DDA method for rigid block problems. International Journal of Rock Mechanics and Mining Sciences, 35(6), 683-693.

Kottenstette JT. (1999). DDA analysis of the RCC modification for Pueblo dam. In Proceedings of Third International Conference on Analysis of Discontinuous Deformation-From Theory To Practice, Vail, Co, Jun., 3-4.

Kottenstette JT. (1999). DDA analysis of the RCC modification for Pueblo Dam. In ICADD-3: Third International Conference on Analysis of Discontinuous Deformation From Theory to Practice, Amadei B (ed.). American Rock Mechanics Association, Balkema: Rotterdam, Washington DC, 127-132.

Koyama T, Nishiyama S, Yang M and Ohnishi Y. (2011). Modelingthe interaction between fluid flow and particle movement with discontinuous deformation analysis (DDA) method. International Journal for Numerical and Analytical Methods in Geomechanics, 35(1), 1-20.

Kveldsvik V, Einstein HH, Nilsen B and Blikra LH. (2009). Numerical analysis of the 650,000 m2 Åknes rock slope based on measured displacements and geotechnical data. Rock mechanics and rock engineering, 42(5), 689-728.

Libersky LD and Petschek AG. (1991). Smooth particle hydrodynamics with strength of materials. In: Advances in the free- Lagrange method including contributions on adaptive gridding and the smooth particle hydrodynamics method, proceedings of the next free-Lagrange conference, Jackson Lake Lodge, Moran, WY, USA

Libersky LD, Petschek AG, Carney TC, Hipp JR and Allahdadi FA. (1993). High strain Lagrangian hydrodynamics: a threedimensional SPH code for dynamic material response. J Comput Phys 109(1):67-75

Lin CT, Amadei B, Jung J and Dwyer J. (1996, October). Extensions of discontinuous deformation analysis for jointed rock masses. In International journal of rock mechanics and mining sciences and geomechanics abstracts (Vol. 33, No. 7, pp. 671-694). Pergamon.

Liu GR and Liu MB. (2003). Smoothed particle hydrodynamics: a meshfree particle method. World Scientific.

Liu J, Kong XJ and Lin G. (2004). Formulations of the three-dimensional discontinuous deformation analysis method. Acta Mechanica Sinica, 20(3), 270-282.

Liu J, Koshizuka S, Oka Y. (2005). A hybrid particle-mesh method for viscous, incompressible, multiphase flows. J Comput Phys 202(1):65-93.

Liu J, Nan Z and Yi P. (2012). Validation and application of three-dimensional discontinuous deformation analysis with tetrahedron finite element meshed block. Acta Mechanica Sinica, 28(6), 1602-1616.

Liu MB and Liu GR. (2010). Smoothed particle hydrodynamics (SPH): an overview and recent developments. Archives of computational methods in engineering, 17(1), 25-76.

Liu MB, Liu GR. (2005). Meshfree particle simulation of micro channel flows with surface tension. Comput Mech 35(5):332- 341

Liu MB, Liu GR and Lam KY. (2002). Investigations into water mitigation using a meshless particle method. Shock Waves 12(3):181-195 250. LiuMB, Liu GR (2004) Smoothed particle hydrodynamics: some recent developments in theory and applications. J Beijing Polytech Univ 30:61-71

Liu MB, Liu GR and Lam KY. (2003). Comparative study of the real and artificial detonation models in underwater explosions. Electron Model 25(2):113-124.

Liu MB, Liu GR, Lam KY and Zong Z (2003) Computer simulation of shaped charge detonation using meshless particle method. Fragblast 7(3):181-202.

Liu MB, Liu GR, Lam KY and Zong Z. (2003). Smoothed particle hydrodynamics for numerical simulation of underwater explosion. Comput Mech 30(2): 106-118.

Liu MB, Liu GR, Zong Z and Lam KY. (2003). Computer simulation of high explosive explosion using smoothed particle hydrodynamics methodology. Comput Fluids 32(3):305-322.

LiuMB, Liu GR, Lam KY and Zong Z. (2003). Meshfree particle simulation of the detonation process for high explosives in shaped charge unlined cavity configurations. Shock Waves 12(6):509-520.

Lohner R, Yang C and Onate E. (2006). On the simulation of flows with

violent free surface motion. Comput Methods Appl Mech Eng 195(41-43): 5597-5620.

Lopez H, Sigalotti L and Di G (2006) Oscillation of viscous drops with smoothed particle hydrodynamics. Phys Rev E 73(5): 51201.

Mikola RG and Sitar N. (2013, January). Explicit Three Dimensional Discontinuous Deformation Analysis for Blocky System. In 47th US Rock Mechanics/Geomechanics Symposium. American Rock Mechanics Association.

Monaghan JJ and Kocharyan A. (1995). SPH simulation of multiphase flow. Comput Phys Commun 87:225-235

Monaghan JJ, Kos A and Issa N. (2003). Fluid motion generated by impact. J Waterw Port C 129(6):250-259

Monaghan JJ and Lattanzio JC. (1991). A simulation of the collapse and fragmentation of cooling molecular clouds. Astrophys J 375(1):177-189

Moresi L, Muhlhous H and Dufour F. (2001). An overview of numerical methods for Earth simulations.

Morris JP, Zhu Y and Fox PJ. (1999). Parallel simulations of porescale flow through porous media. Comput Geotech 25(4):227- 246.

Muller M. (2004). Interactive blood simulation for virtual surgery based on smoothed particle hydrodynamics. Technol Health Care 12(1):25-31.

Munjiza A and Andrews KRF. (1998). NBS contact detection algorithm for bodies of similar size. International Journal for Numerical Methods in Engineering, 43(1), 131-149.

Munjiza A and Andrews KRF. (2000). Penalty function method for combined finite-discrete element systems comprising large number of

separate bodies. International Journal for Numerical Methods in Engineering, 49(11), 1377-1396.

Nezami EG, Hashash YMA, Zhao D and Ghaboussi J. (2004). A fast contact detection algorithm for 3-D discrete element method. Computers and Geotechnics, 31(7), 575-587.

Nezami EG, Hashash, YMA, Zhao D and Ghaboussi J. (2006). Shortest link method for contact detection in discrete element method. International Journal for Numerical and Analytical Methods in Geomechanics, 30(8), 783-801.

Ning Y, An X, Yang J and Ma G. (2010). Simulation of blast induced crater in jointed rock mass by discontinuous deformation analysis method. Frontiers of Structural and Civil Engineering, 4(2), 223-232.

Ning Y, Yang J, An X and Ma G. (2011). Modeling rock fracturing and blast-induced rock mass failure via advanced discretisation within the discontinuous deformation analysis framework. Computers and Geotechnics, 38(1), 40-49.

Ning Y, Yang J, Ma G and Chen P. (2011). Modeling rock blasting considering explosion gas penetration using discontinuous deformation analysis. Rock mechanics and rock engineering, 44(4), 483-490.

Nugent S and Posch HA. (2000). Liquid drops and surface tension with smoothed particle applied mechanics. Phys Rev E 62(4):4968-4975

Oger L and Savage SB. (1999). Smoothed particle hydrodynamics for cohesive grains. Comput Methods Appl Mech Eng 180(1):169-183

Perkins E and Williams JR. (2001). A fast contact detection algorithm insensitive to object sizes. Engineering Computations, 18(1/2), 48-62.

Pimenta LCA, Mendes ML, Mesquita RC and Pereira GAS (2007) Fluids in electrostatic fields: an analogy for multirobot control. IEEE Trans Magn 43(4):1765-1768

Prakash M, Cleary PW, Grandfield J, Rohan P and Nguyen V (2007) Optimisation of ingot casting wheel design using SPH simulations. Prog Comput Fluid Dyn 7(2-4):101-110

Prakash M, Cleary PW, Ha J, Noui-Mehidi MN, Blackburn H and Brooks G. (2007). Simulation of suspension of solids in a liquid in a mixing tank using SPH and comparison with physical modeling experiments. Prog Comput Fluid Dyn 7(2):91-100.

Price DJ and Monaghan JJ. (2004). Smoothed particle magnetohydrodynamics, I: algorithm and tests in one dimension. Mon Not R Astron Soc 348(1):123-138.

Price DJ and Monaghan JJ. (2004). Smoothed particle magnetohydrodynamics, II: variational principles and variable smoothinglength terms. Mon Not R Astron Soc 348(1):139-152.

Price DJ and Monaghan JJ. (2004). Smoothed particle magnetohydrodynamics: some shocking results. Astrophys Space Sci 292(1):279-283.

Qiu LC. (2008). Two-dimensional SPH simulations of landslidegenerated water waves. J Hydraul Eng ASCE 134(5):668-671.

Rizzi E, Rusconi F and Cocchetti G. (2014). Analytical and numerical DDA analysis on the collapse mode of circular masonry arches. Engineering structures, 60, 241-257.

Rogers BD and Dalrymple RA. (2005). SPH modeling of breaking waves. In: Proceedings of the 29th international conference on coastal

engineering 2004, Lisbon, Portugal

Rook R, Yildiz M and Dost S. (2007). Modeling transient heat transfer using SPH and implicit time integration. Numer Heat Transfer B, Fundam 51(1):1-23

Rosswog S and Wagner P. (2002). Towards a macroscopic modeling of the complexity in traffic flow. Phys Rev E 65(3):36106.

Rouainia M, Lewis H, Pearce C, Bicanic N, Couples GD and Reynolds MA. (2006). Hydro-geomechanical modeling of seal behavior in overpressured basins using discontinuous deformation analysis. Engineering geology, 82(4), 222-233.

Shao SD and Gotoh H. (2004). Simulating coupled motion of progressive wave and floating curtain wall by SPH-LES model. Coast Eng J 46(2):171-202.

Shao SD, Ji CM, Graham DI, Reeve DE, James PW and Chadwick AJ. (2006). Simulation of wave overtopping by an incompressible SPH model. Coast Eng 53(9):723-735.

Shen HT, Su JS and Liu LW. (2000). SPH simulation of river ice dynamics. J Comput Phys 165(2):752-770.

Shi GH. (1988). Discontinuous deformation analysis: a new numerical model for the statics and dynamics of block systems (Doctoral dissertation, University of California, Berkeley).

Shi GH. (2001, January). Three dimensional discontinuous deformation analyses. In DC Rocks 2001 The 38th US Symposium on Rock Mechanics (USRMS). American Rock Mechanics Association.

Shi GH. (1996). Simplex Integration for Manifold Method, FEM DDA and

Analytical Analysis. Discontinuous Deformation Analysis (DDA) and Simulations of Discontinuous Media, Salami, M. R. and Don Banks (Eds.), TSI Press, 205-262.

Shi GH. (1997a). Working forum on Manifold Method of material analysis. Vol. 2 the numerical manifold method and simplex integration, U.S. Army Corps of Engineers.

Shi GH. (1997b). Numerical Manifold Method and Discontinuous Deformation Analysis. Beijing, Tsinghua University Press.

Shi GH. (2009). Applications of discontinuous deformation analysis (DDA) to rock engineering. In Computational Mechanics (pp. 136-147). Springer Berlin Heidelberg.

Shi GH. (2014). Application of discontinuous deformation analysis on stability analysis of slopes and underground power houses. Geomechanics and Geoengineering, 9(2), 80-96.

Sigalotti LDG and Lopez H. (2008). Adaptive kernel estimation and SPH tensile instability. Comput Math Appl 55(1):23-50.

Sitar N and MacLaughlin MM. (1997, November). Kinematics and discontinuous deformation analysis of landslide movement. In 2nd Panamerican Symp. on Landslides, Rio de Janeiro.

Sitar N, MacLaughlin MM and Doolin DM. (2005). Influence of kinematics on landslide mobility and failure mode. Journal of geotechnical and geoenvironmental engineering, 131(6), 716-728.

Sousa ACM, Jiang FM (2007) SPH as an inverse numerical tool for the prediction of diffusive properties in porous media. Diffus Solids Liq Heat Transfer, Microstruct Prop 553:171-189

Souto-Iglesias A, Delorme L, Perez-Rojas L and Abril-Perez S. (2006). Liquid moment amplitude assessment in sloshing type problems with smooth particle hydrodynamics. Ocean Eng 33(11-12):1462-1484.

Swegle JW (1992) Report at Sandia National Laboratories.

Swegle JW, Attaway SW. (1995). On the feasibility of using smoothed particle hydrodynamics for underwater explosion calculations. Comput Mech 17(3):151-168.

Tanaka N, and Takano T. (2005). Microscopic-scale simulation of blood flow using SPH method. Int J Comput Methods 2(4):555- 568.

Tartakovsky A and Meakin P. (2005). Modeling of surface tension and contact angles with smoothed particle hydrodynamics. Phys Rev E 72(2):26301.

Tartakovsky AM and Meakin P. (2005). Simulation of unsaturated flow in complex fractures using smoothed particle hydrodynamics. Vadose Zone J 4(3):848-855.

Tartakovsky AM and Meakin P. (2006). Pore scale modeling of immiscible and miscible fluid flows using smoothed particle hydrodynamics. Adv Water Resour 29(10):1464-1478.

Thacker RJ and Couchman HMP. (2001). Star formation, supernova feedback, and the angular momentum problem in numerical cold dark matter cosmogony: halfway there. Astrophys J 555(1):L17- L20.

Thomas PA and Bray JD. (1999). Capturing nonspherical shape of granular media with disk clusters. Journal of Geotechnical and Geoenvironmental Engineering, 125(3), 169-178.

Tsesarsky M and Hatzor YH. (2006). Tunnel roof deflection in blocky rock

masses as a function of joint spacing and friction-A parametric study using discontinuous deformation analysis (DDA). Tunnelling and Underground Space Technology, 21(1), 29-45.

Tsubota K, Wada S, Yamaguchi T. (2006). Simulation study on effects of hematocrit on blood flow properties using particle method. J Biomech Sci Eng 1(1):159-170

Violeau D, Buvat C, Abed-Meraim K, de Nanteuil E. (2007). Numerical modelling of boom and oil spill with SPH. Coast Eng 54(12):895-913.

Wang J, Lin G and Liu J. (2006). Static and dynamic stability analysis using 3D-DDA with incision body scheme. Earthquake Engineering and Engineering Vibration, 5, 273-283.

Wang LZ, Jiang HY, Yang ZX, Xu YC and Zhu XB. (2013). Development of discontinuous deformation analysis with displacement-dependent interface shear strength. Computers and Geotechnics, 47, 91-101.

Wang RX, Ji SY, Shen HT, Yue QJ. (2005). Modified PIC method for sea ice dynamics. China Ocean Eng 19(3):457-468.

Wang W, Huang Y, Grujicic M and Chrisey DB. (2008). Study of impact-induced mechanical effects in cell direct writing using smooth particle hydrodynamic method. J Manuf Sci E, Trans ASME 130(2).

Wu JH and Chen CH. (2011). Application of DDA to simulate characteristics of the Tsaoling landslide. Computers and Geotechnics, 38(5), 741-750.

Wu JH, Juang CH and Lin HM. (2005). Vertex-to-face contact searching algorithm for three-dimensional frictionless contact problems. International journal for numerical methods in engineering, 63(6), 876-897.

Wu JH, Lin JS and Chen CS. (2009). Dynamic discrete analysis of an earthquake-induced large-scale landslide. International Journal of Rock Mechanics and Mining Sciences, 46(2), 397-407.

Wu JH, Ohnishi Y and Nishiyama S. (2004). Simulation of the mechanical behavior of inclined jointed rock masses during tunnel construction using discontinuous deformation analysis (DDA). International journal of rock mechanics and mining sciences, 41(5), 731-743.

Wu JH, Ohnishi Y and Nishiyama S. (2005). A development of the discontinuous deformation analysis for rock fall analysis. International journal for numerical and analytical methods in geomechanics, 29(10), 971-988.

Wu JH. (2007). Applying discontinuous deformation analysis to assess the constrained area of the unstable Chiu-fen-erh-shan landslide slope. International journal for numerical and analytical methods in geomechanics, 31(5), 649-666.

Wu JH. (2008). New edge-to-edge contact calculating algorithm in three-dimensional discrete numerical analysis. Advances in Engineering Software, 39(1), 15-24.

Wu JH. (2010). Seismic landslide simulations in discontinuous deformation analysis. Computers and Geotechnics, 37(5), 594-601.

Wu W, Zhu H, Zhuang X, Ma G and Cai Y. (2014). A multi-shell cover algorithm for contact detection in the three dimensional discontinuous deformation analysis. Theoretical and Applied Fracture Mechanics.

Yeung MR and Leong LL. (1997). Effects of joint attributes on tunnel stability. International Journal of Rock Mechanics and Mining Sciences, 34(3), 348-e1.

Yeung MR, Jiang QH and Sun N. (2003). Validation of block theory and three-dimensional discontinuous deformation analysis as wedge stability analysis methods. International Journal of Rock Mechanics and Mining Sciences, 40(2), 265-275.

Yeung MR, Jiang QH and Sun N. (2007). A model of edge-to-edge contact for three-dimensional discontinuous deformation analysis. Computers and Geotechnics, 34(3), 175-186.

Yeung MR. (1993, December). Analysis of a mine roof using the DDA method. In International journal of rock mechanics and mining sciences and geomechanics abstracts Pergamon, 30(7), 1411-1417.

Yim SC, Yuk D, Panizzo A, Di Risio M and Liu PLF (2008) Numerical simulations of wave generation by a vertical plunger using RANS and SPH models. J Waterw Port C 134(3):143-159.

Zhang MY, Zhang H and Zheng LL. (2007). Application of smoothed particle hydrodynamics method to free surface and solidification problems. Numer Heat Transfer A, Appl 52(4):299-314

Zhang MY, Zhang H and Zheng LL. (2008). Simulation of droplet spreading, splashing and solidification using smoothed particle hydrodynamics method. Int J Heat Mass Transfer 51(13-14):3410-3419.

Zhang MY, Zhang H and Zheng LL (2009) Numerical investigation of substrate melting and deformation during thermal spray coating by SPH method. Plasma Chem Plasma Process 29(1):55-68.

Zhang Y, Chen G, Zheng L, Li Y and Wu J. (2013). Effects of near-fault seismic loadings on run-out of large-scale landslide: A case study. Engineering Geology, 166, 216-236.

Zhang Y, Fu X and Sheng Q. (2014). Modification of the discontinuous

deformation analysis method and its application to seismic response analysis of large underground caverns. Tunnelling and Underground Space Technology, 40, 241-250.

Zhang Y, Xu Q, Chen G, Zhao JX and Zheng L. (2014). Extension of discontinuous deformation analysis and application in cohesive-frictional slope analysis. International Journal of Rock Mechanics and Mining Sciences, 70, 533-545.

Zhao S. (2000). Development of three-dimensional spherical discontinuous deformation analysis for granular materials. Ph.D thesis, North Carolina State University, Carolina.

Zhou CE, Liu GR and Ky Lou (2007) Three-dimensional penetration simulation using smoothed particle hydrodynamics. Int J Comput Methods 4(4):671-691.

Zhou GZ, Ge W and Li JH (2008) A revised surface tension model for macro-scale particle methods. Powder Technol 183(1):21-26.

Zhu Y and Fox PJ (2002) Simulation of pore-scale dispersion in periodic porous media using smoothed particle hydrodynamics. J Comput Phys 182(2):622-645.

Zhu Y, Fox PJ and Morris JP (1999) A pore-scale numerical model for flow through porous media. Int J Numer Anal Methods 23(9):881-904.

Zou S and Dalrymple RA. (2005). Sediment suspension modeling by smoothed particle hydrodynamics. In: Proceedings of the 29th international conference on coastal engineering 2004, Lisbon, Portugal.

CHAPTER 3

COMPARISON BETWEEN 2D AND 3D DDA

3.1 INTRODUCTION

The 2D DDA has been developed maturely not only in theory but also in the practical engineering usage. The very useful user-friendly pre-processor and post-processor has been developed (Chen et al, 1996; Doolin and Sitar, 2001), which makes it convenient for the deep research and more widely used in the practical engineering problems. The practical usages of the 2D DDA is widely such as rock-fall, landslide, underground openings and etc.

Since most geotechnical engineering problems are three dimensional, however, a two-dimensional representation is, at best, a crude approximation. In the case of slopes and tunnels, the orientation and geometry of discontinuities are unlikely to be suitable for two-dimensional idealization, even though the dimension perpendicular to the plane of analysis may be large. To simulate the behavior of rock masses with discontinuities more precisely, the numerical method is required to consider the effects of the distributions of discontinuities, the terrains, the contacts among blocks, and the large displacements in three dimensions.

For the slope analysis, there are two key points: 1) the stability analysis before the slope failure such as the determination of the factor of safety; 2) the run-out analysis after the failure of the slope. These two points are very meaningful for the slope research not only in theory but more the practical meaning. Because for the

former, the landslide-prone slopes can be recognized and for the latter, the dangerous area can judged accordingly.

In order to realize definitely the difference between the 2D DDA and 3D DDA when dealing with the slope stability and runout analysis, the simplified wedge model is used for the simulation in 3D DDA and different section resulting for the 3D model are adopt for the 2D DDA simulation. The reason of using the wedge model is it not only exists in the nature (Figure3.1) but also owns the theoretical solution for the safety factor.

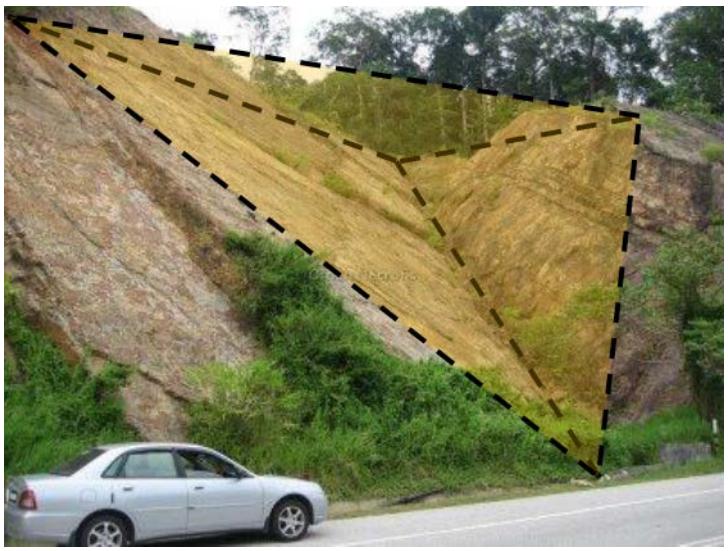

Figure3.1 The failure wedge by the road.

3.2 THE STABILITY ANALYSIS

The stability analysis is of great importance in the slope analysis. The factor of safety is the most generally used value that can evaluate the stability of the slope. However, for the geotechnical engineering, it is very difficult to get the theoretical solution of the factor of safety (FOS). Even if some numerical method can get the FOS, if there is no theoretical solution as standard, the result is more or less questionable.

The wedge, as it owns the theoretical solution and exists in nature, is always been used as the typical model in the verification of the accuracy of numerical

methods. For the 3D DDA, there is no direct way to get the FOS when the slope mode is used for analysis because of the nature of the program. The strength reduction method is an easy and typical method to get the FOS in the slope analysis. By introducing the strength reduction method to the 3D DDA method, the FOS can be got. In the following two sections, the wedge's theoretical solution and the strength reduction method are illustrated in detail separately.

3.2.1 THE THEORETICAL SOLUTION

The factor of safety of the wedge model can be got by the limit equilibrium method, which was proposed by Kovari and Fritz (1975). The illustration of the wedge slope mode can be found in Figure 3.2.

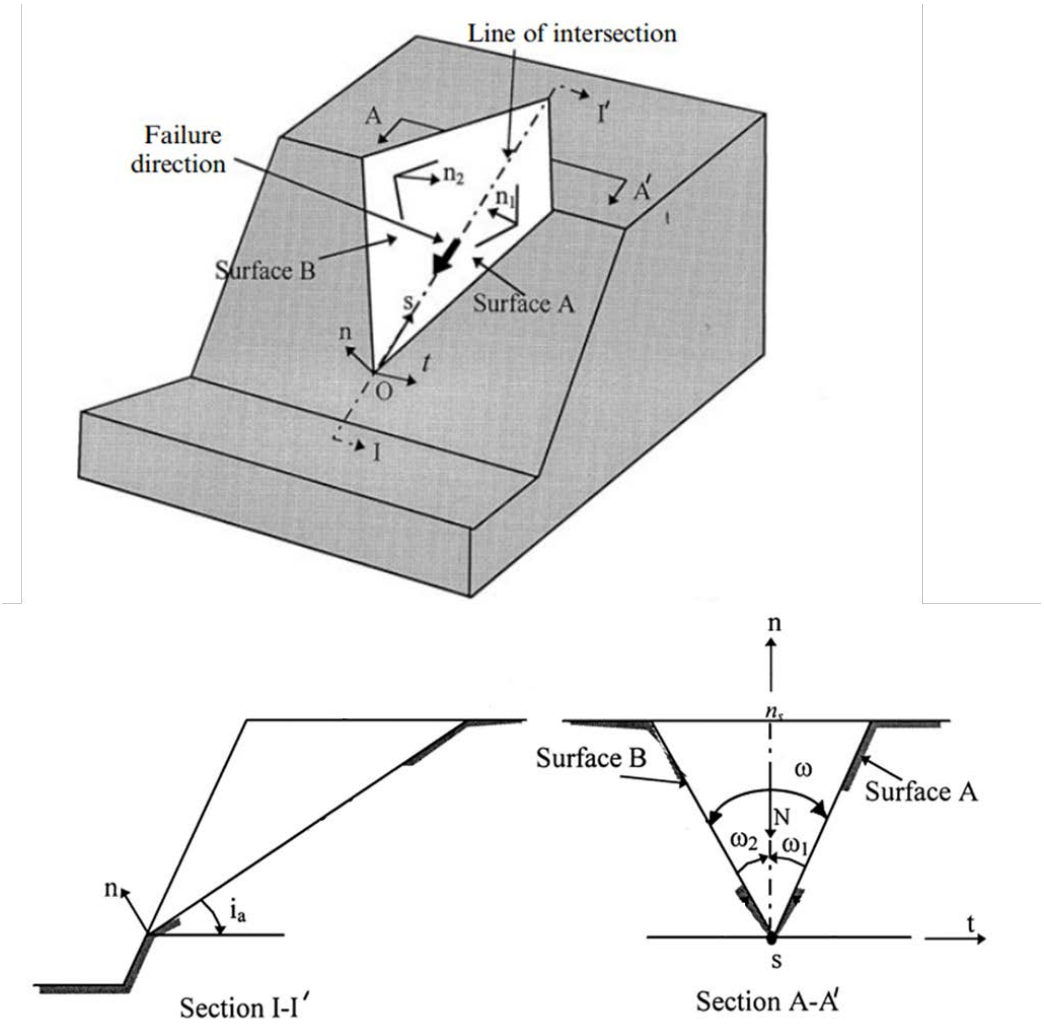

Figure 3.2 The illustration of the geometry wedge slope model

In the Figure 3.2, the i_a is the plunge of the intersection for the section I-I', and the ω_1 is the angle between surface A and the vertical and ω_2 is the angle for the surface B and the vertical direction as shown in the section A-A'. If we assume that the failure of the wedge block obeying the Mohr-coulomb criterion and according to the limit equilibrium method, the factor of safety (SF) can be obtained in the following form:

$$SF = \frac{\lambda w \cos i_a + c(A_1 + A_2)}{w \sin i_a} \tag{3.1}$$

Where, the *w* is the weight of the wedge, and the *c* represents the cohesion strength of the surface. The A_1 and A_2 are the lateral surface area of surface A and surface B separately. The factor λ is called the wedge factor (Kovari and Fritz, 1975), which is the defined as:

$$\lambda = \frac{\cos \omega_1 + \cos \omega_2}{\sin(\omega_1 + \omega_2)} \tag{3.2}$$

The meaning of ω_1 and ω_2 have been illustrated before.

Therefore, for the certain wedge model, if the geometry and physical parameters are known, the factor of safety can be easily obtained. For the DDA analysis, because of no failure mode is preliminarily defined, the strength reduction method is recommended for the calculation of factor of safety.

3.2.2 THE STRENGTH REDUCTION METHOD

In the DDA method, the Mohr-coulomb criterion is used for judge whether the contact(s) state is in the failure state. However, for different kind of cohesion and frictional angle, we just know its state and the factor of safety can not to be got. In order to get the exact value of safety, the theory of shear strength is introduced into the DDA method. Defining SRF as shear reduction factor, the basic formulation this

method is:

$$\frac{\tau}{SRF} = \frac{c}{SRF} + \sigma_n \frac{\tan\varphi}{SRF} \tag{3.3}$$

The other form of this formulation is:

$$\frac{\tau}{SRF} = c' + \sigma_n \tan\varphi' \tag{3.4}$$

$$c' = \frac{\tau}{SRF} \tag{3.5}$$

$$\varphi' = \tan^{-1}(\frac{\tan\varphi}{SRF}) \tag{3.6}$$

In which, the c and φ are the cohesion strength and frictional angle separately. The c' and φ' are the value of these two parameters after reduction.

Through the reduction of cohesion and frictional angle at the same time, the limit state can be determined. The SRF value that locates at the limit state is used as the FOS (Factor of Safety) in the DDA's stability analysis. What is needed to be mentioned is that the choosing of the initial strength values is important for obtaining a reasonable FOS. The initial strength values (cohesion and frictional angle) can be got from the experience, or more recommend from the real laboratory data when the real slope site is chosen for study. During shear strength reduction, it has two kinds of conditions: 1) if the initial strength parameters are large enough to make it stable, the SRF should be improved more than one for the next time's calculation, which will lead to a FOS more than one; 2) if the initial shear parameters is small that can make it unstable, the SRF will be reduced bellow than one for the next turn's simulation, which will result in a FOS bellow than one.

3.3 THE SLOPE MODEL FOR 3D AND 2D DDA

The slope mode that is used for the analysis is the typical wedge model. The reason of using this kind of model is: 1) the wedge-shape slope is a typical common slope type in the engineering, using the simplified wedge mode is of practical meaning; 2) the theoretical solution for the wedge's factor of safety can be easily got, which can be used to verify the accuracy of DDA method.

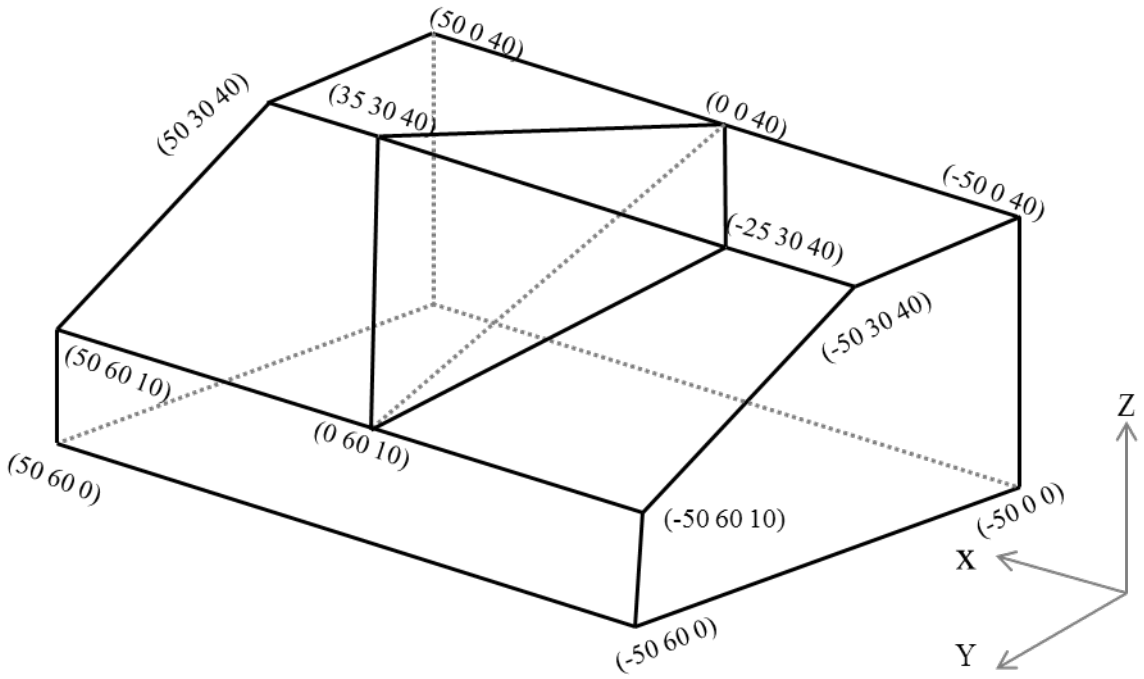

Figure 3.3 The 3D slope model for 3D DDA

The detail coordinates of the slope's model can be found in Fig3.3. As the sliding part should not be one big block, it is divided into many some blocks in the 3D DDA analysis. There are three types of 3D DDA model according to slide part's division: 6 blocks, 12 blocks, and 24 blocks like figure 3.4-3.6 shows. Moreover, the influence of the 3D block number on the runout distance and maximum velocity can be preliminarily evaluated by the 3D DDA methods

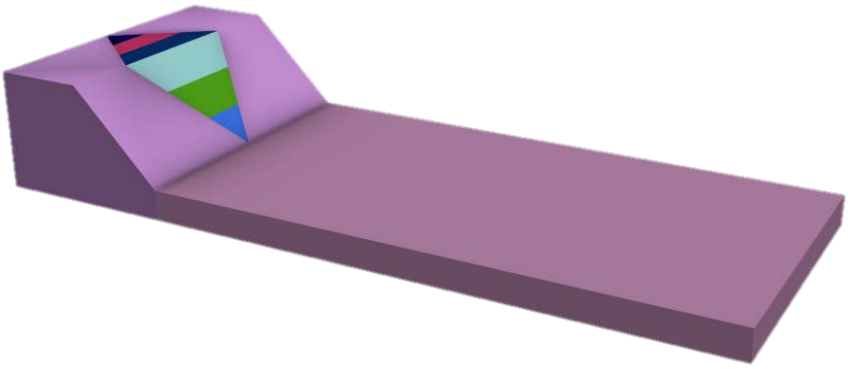

Figure 3.4 The 3D model of 6blocks

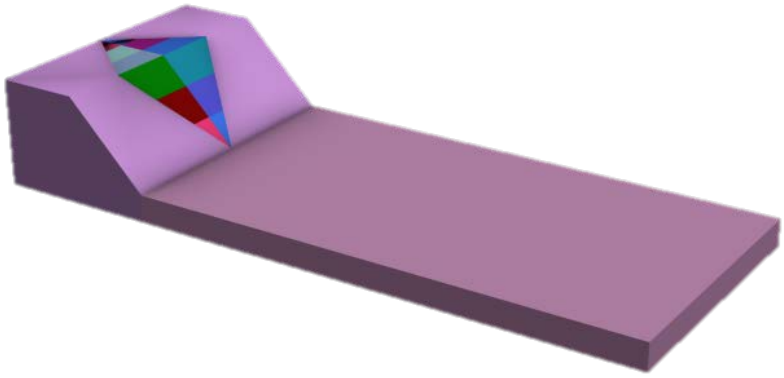

Figure 3.5(a) The 3D model for of 12 blocks

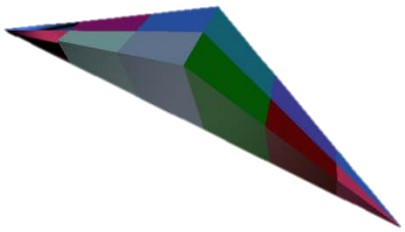

Figure 3.5(b) The 3D model of the sliding part with 12 blocks

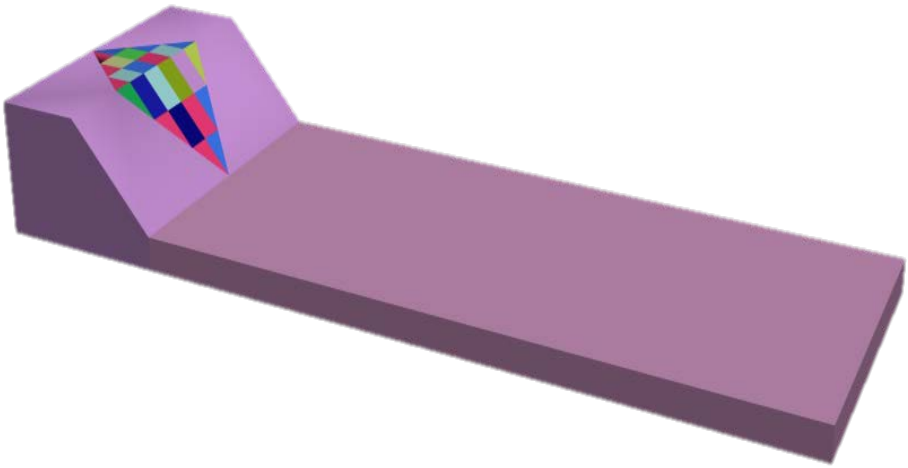

Figure 3.6 (a) The 3D model of 24 blocks

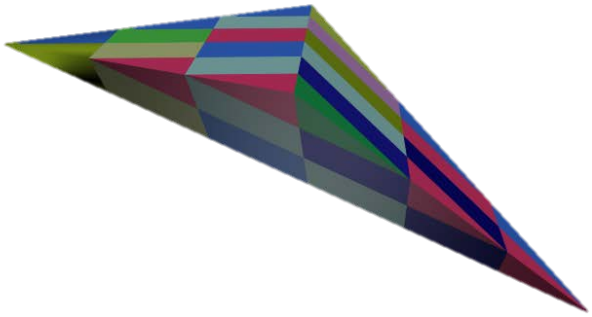

Figure 3.6(b) The 3D model of the sliding part with 24 blocks

For the 2D DDA stability analysis, different sections are used as Figure 3.7 shows. Because of the asymmetry of the 3D model, there are total five section model are used, with interval between each sections are 5 meters as shown in Figure 3.7.The section 3 located at the position that is mostly close to the axis, the 2D model of which is shown as figure 3.8.

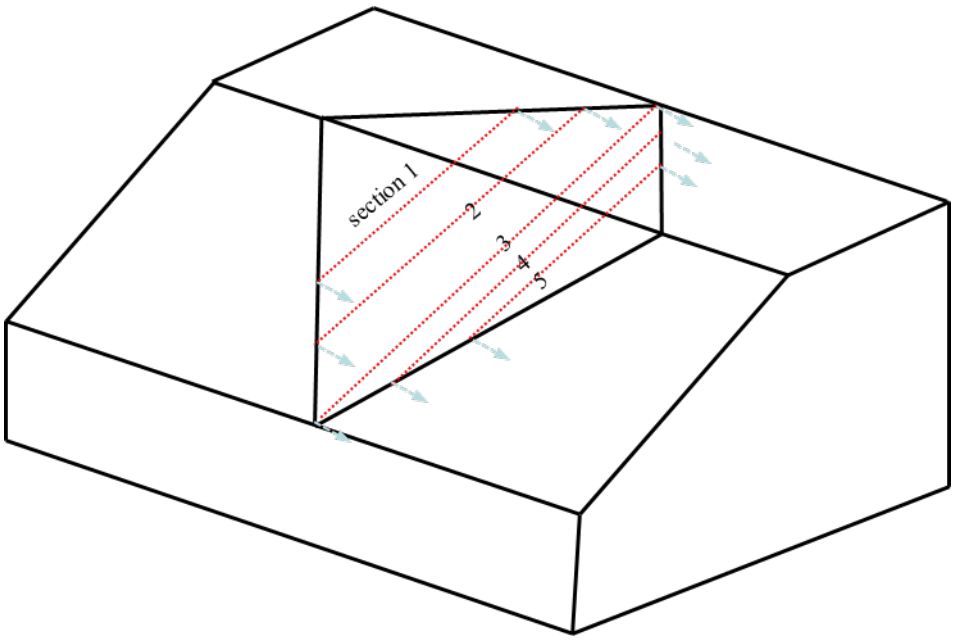

Figure 3.7 Five sections used for the 2D simulation.

Figure 3.8 The model of section 3 for 2D analysis.

In order to make the comparison results are available, the simulation parameters that are used for the 2D and 3D DDA are kept consistent. The simulation parameters that are used for the DDA are listed in Table 3.1.

Table3. 1 Mechanical properties and computational parameters for DDA

Parameters	Value
Density ρ (kg/m^3)	2000
Young's modulus E (GPa)	1
Poisson's ratio υ	0.3
Gravity acceleration (m/s^2)	9.8
Penalty spring stiffness k	15 E
Friction angle ϕ (°)	15(for runout analysis)
Max. allowed displacement ratio	0.001
Time interval (s)	0.001
Total time steps	15000

SOR factor	1.3

3.4 COMPARISON ON THE STABILITY ANALYSIS

In this section the stability analysis will be performed. For the theoretical solution, the method mentioned in Section 3.2.1 will be used, and for the 2D and 3D solution, the strength reduction method mentioned in Section 3.2.2 will be used. A comprehensive comparison between the 2D and 3D solution related to FOS (Factor of Safety) will be performed.

Firstly, the influence of cohesion and frictional angle on the FOS is determined. When the 2D DDA analysis is performed, the profile section 3 is used.

When to evaluate the influence of cohesion strength, the frictional angle should be fixed, in this part, it is fixed as 20 degree. It can be found from Figure 3.9 that, the 3D DDA can obtain a more accurate FOS, while the 2D DDA underestimate the FOS apparently especially when the cohesion strength is greatly increased.

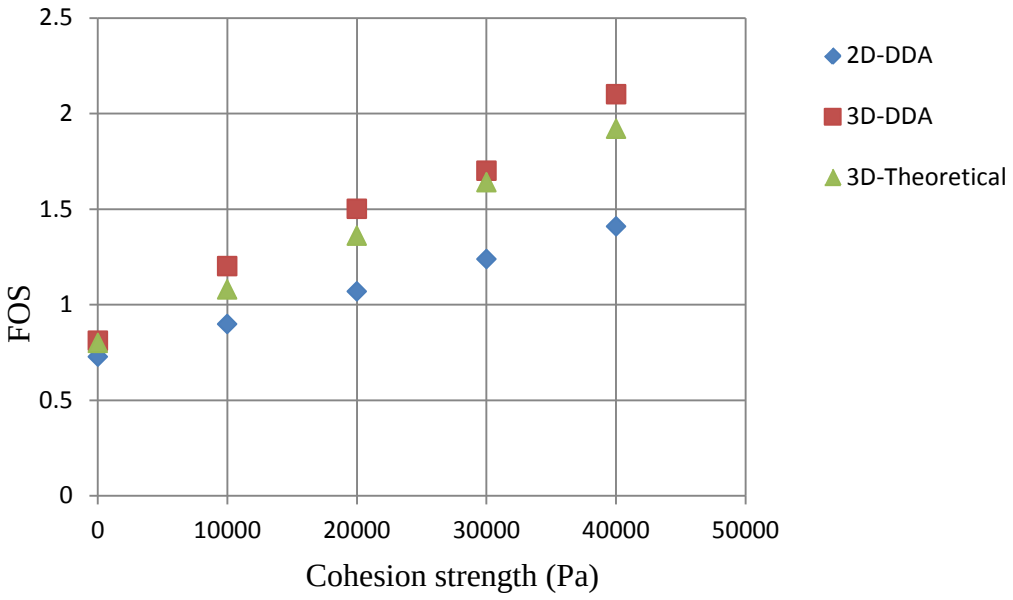

Figure 3.9 The relation between the cohesion strength and FOS

When to evaluate the influence of frictional angle, the cohesion strength should be fixed, in this part, it is fixed as 20 kPa. Similarly, the FOS from the 3D DDA is more close to the theoretical solution. The difference between the 2D DDA solution and the theoretical is increasing slightly when the frictional angle is improved.

It can be conclude that the 3D DDA is more accurate for the slope stability analysis, especially when the strength is get larger. For the 2D DDA, it underestimates the FOS for a certain degree, this is more obvious when the shear strength is much larger, and in this case, the 2D may lose its value.

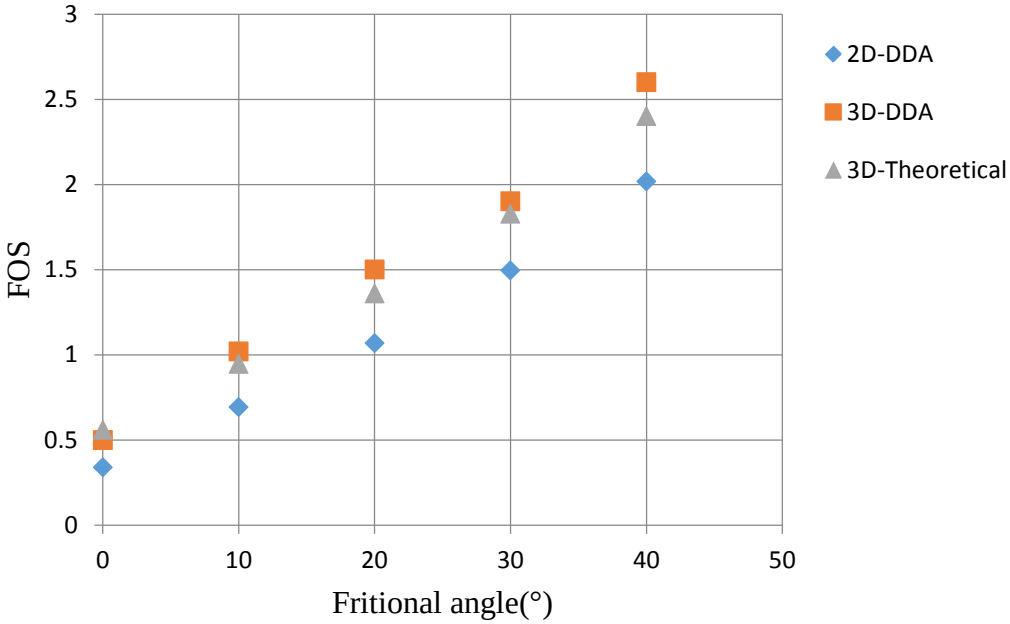

Figure 3.10 The relation between the friction angle and FOS.

Secondly, a comparison between different profiles section (section 1- section 5 illustrated in 3.2) with the 3D DDA solution is made. For this part, the initial strength is chosen as cohesion 20kPa and frictional angle 20 degree. For the convenience, the 3D solution is assumed as section 0.

Figure 3.11 shows the change of FOS when different section is chosen for the 2D DDA analysis, and the red bar is the 3D DDA solution. If takes the 3D solution as the correct solution, as showed before, it is very close to the theoretical solution, the

relative error between the 2D solution and it can be seen in Figure 10. It can be found from the Fig.3.11 and Fig.3.12 that, for most of the 2D DDA solution, it will underestimate the FOS around 20%. The reason is that in the 2D simulation, the lateral friction cannot be taken into consideration. Moreover, the chosen of different section has an influence on the final result, as the result of section one, which is because of the asymmetry of the 3D model.

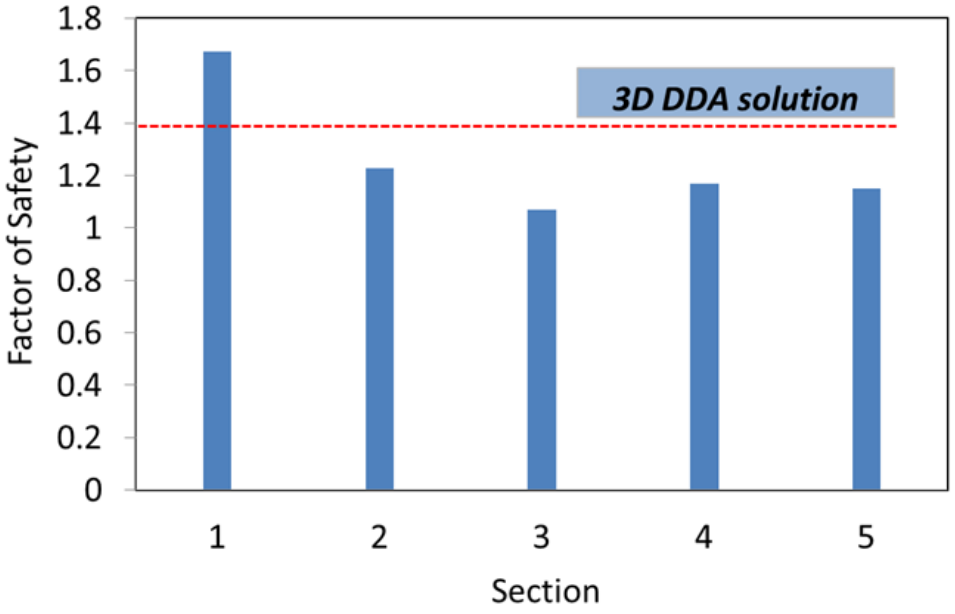

Figure 3.11 The varies of FOS with different profile sections.

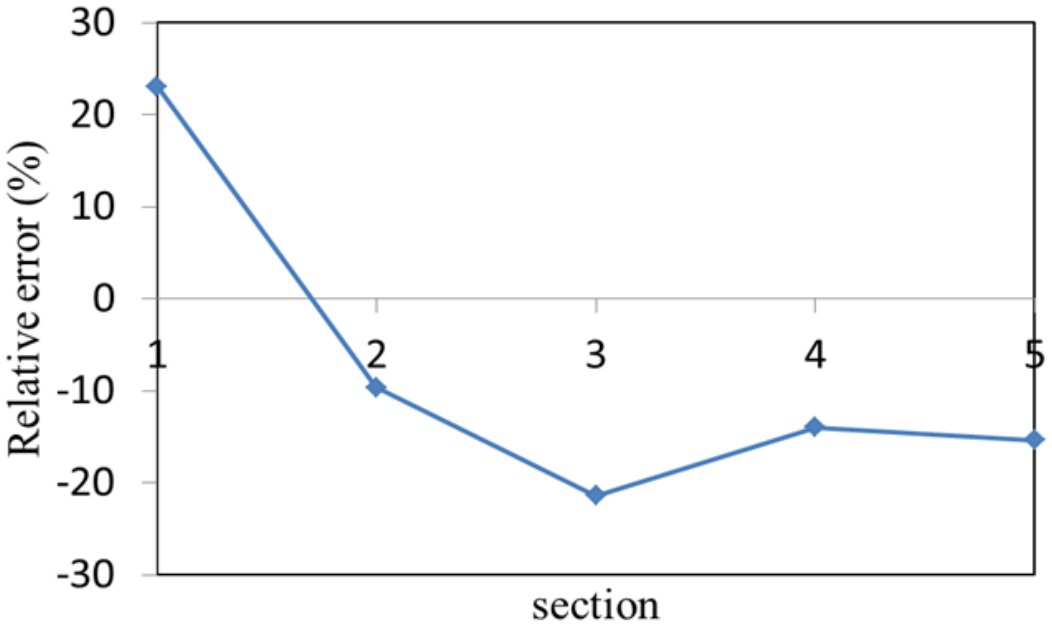

Figure 3.12 The change of relative error with different profile sections.

3.5 COMPARISON ON THE RUNOUT ANALYSIS

In order to realize definitely the difference between the 2D and 3D when dealing with the runout analysis, this section performs the relevant simulation about this issue. Because of no theoretical solution for the runout analysis, just the results from the 2D and 3D simulation are used to illustrate the problem. For the 2D DDA simulation, the profile section 3, which is just located at the failure direction, is used. For the 3D DDA simulation, similar to the stability analysis, three kinds of model, owing sliding parts of 6, 12, and 24 blocks are used. For both the 2D and 3D, the physical parameters are the same as Table 3.1. The study focuses on the runout distance, velocity on the failure direction, and the lateral spread. These three patterns are of practical meaning for safety evaluation and alert area determination.

The failure process in the 2D DDA is shown in Figure 3.13.

(a) 2D DDA, simulation time=0

(b) 2D DDA, simulation time=3s

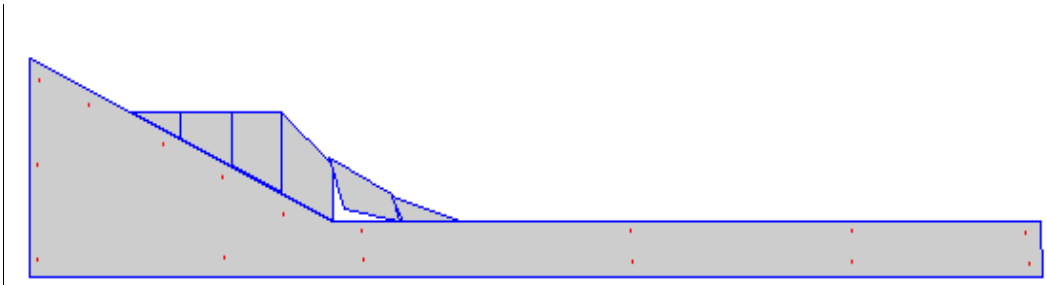

(c) 2D DDA, simulation time=6s

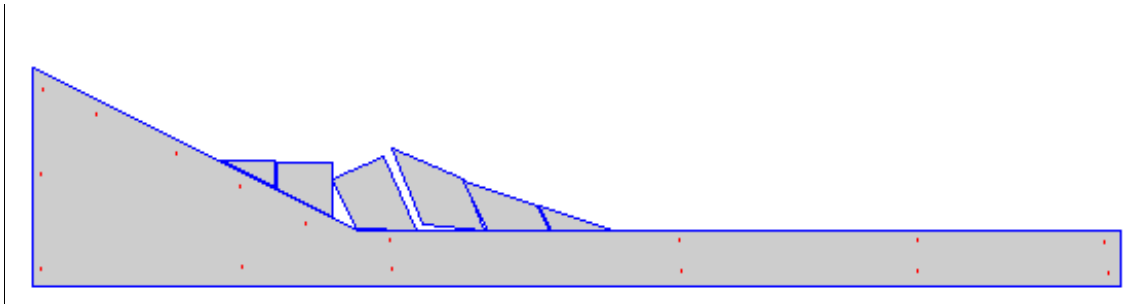

(d) 2D DDA, simulation time=9s

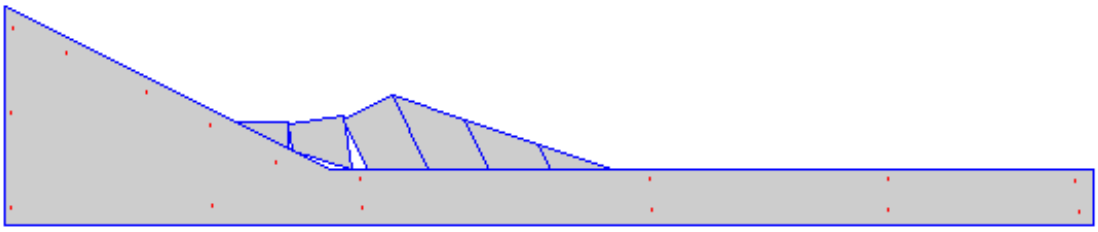

(e) 2D DDA, simulation time=12s

Figure 3.13 The runout process in 2D DDA simulation

The 3D DDA simulation process for the runout analysis is illustrated by Figure 3.14, Figure 3.15 and Figure 3.16.

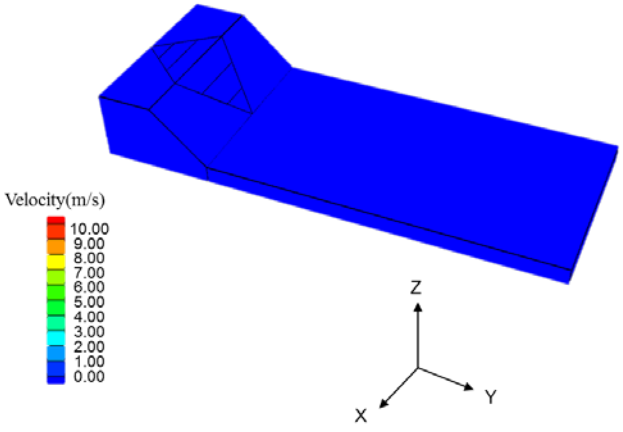

(a) 6blocks, time=0

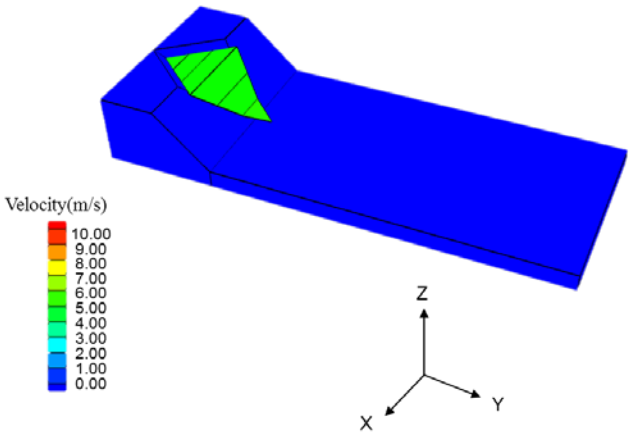

(b) 6blocks, time=3s

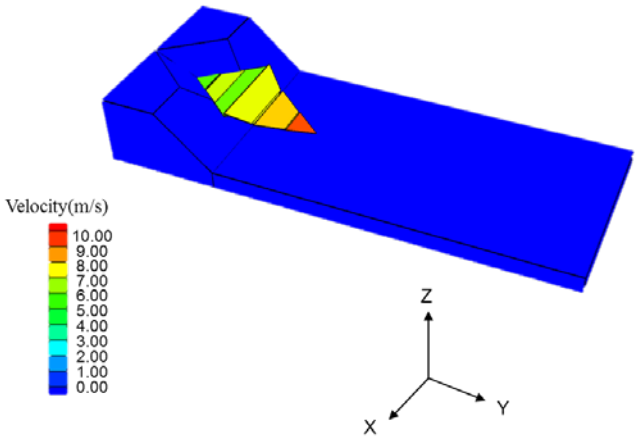

(c) 6blocks, time=6s

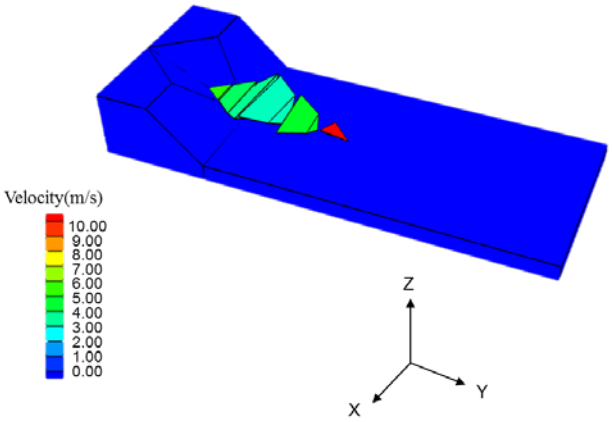

(d) 6blocks, time=9s

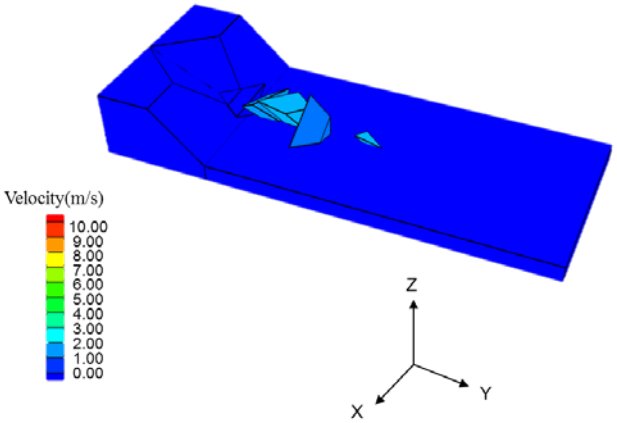

(e) 6blocks, time=12s

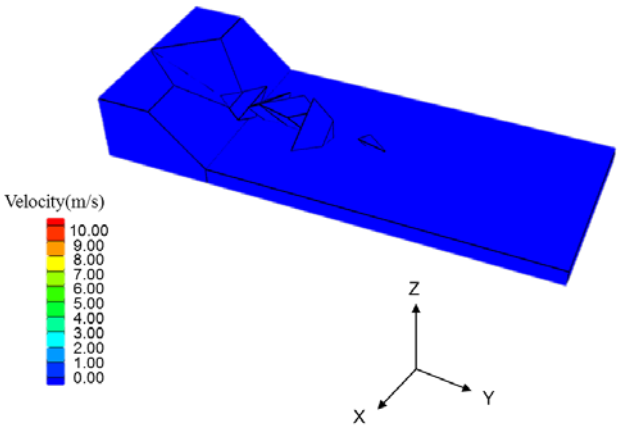

(f) 6blocks, time=15s

Figure 3.14 The runout process for 6 blocks' sliding parts

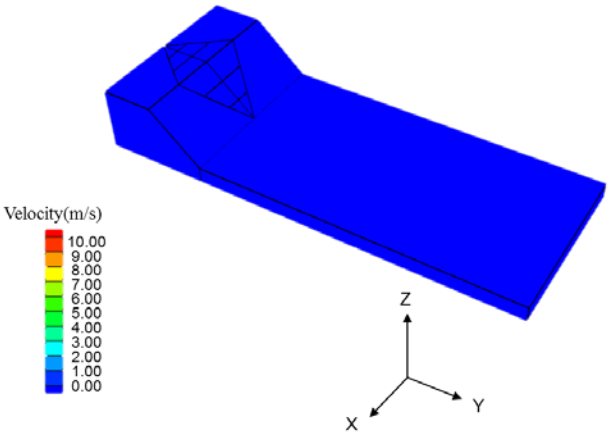

(a) 12blocks, time=0

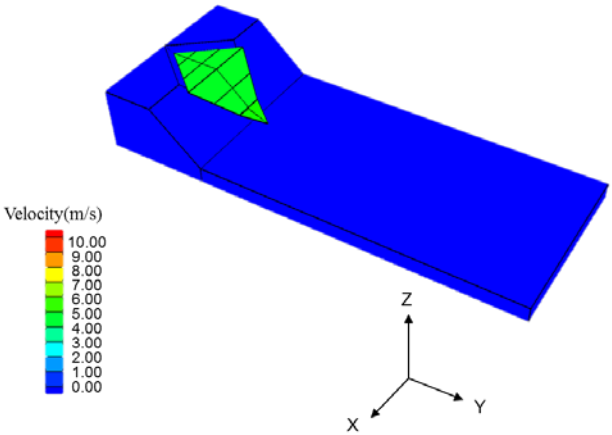

(b) 12blocks, time=3s

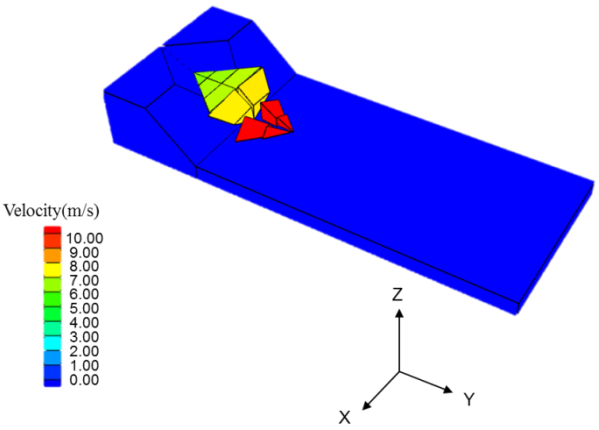

(c) 12blocks, time=6s

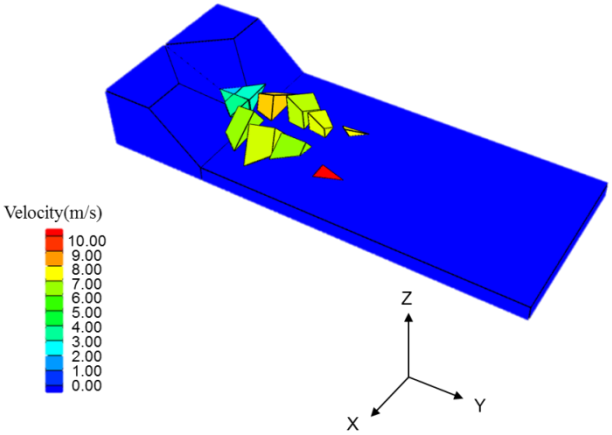

(d) 12blocks, time=9s

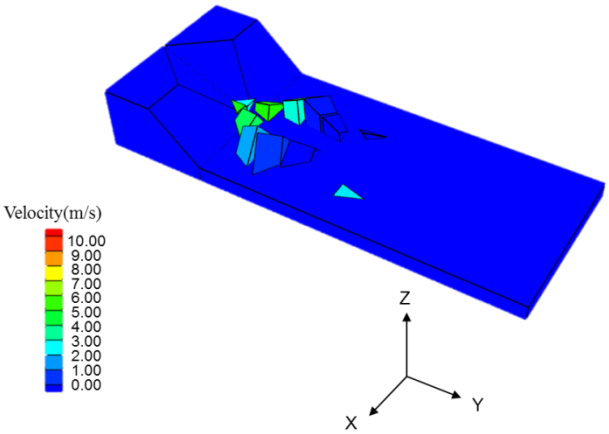

(e) 12blocks, time=12s

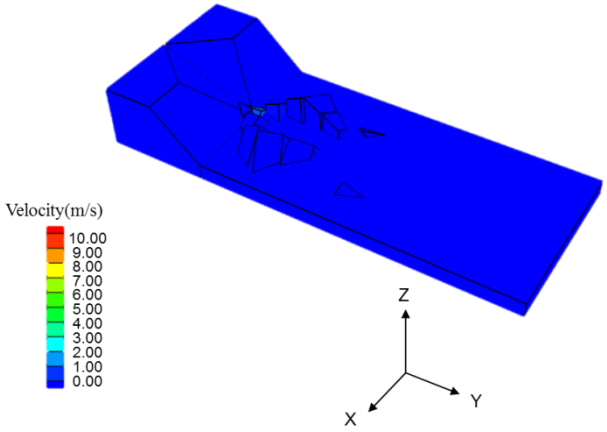

(f) 12blocks, time=15s

Figure 3.15 The runout process for 12 blocks' sliding parts

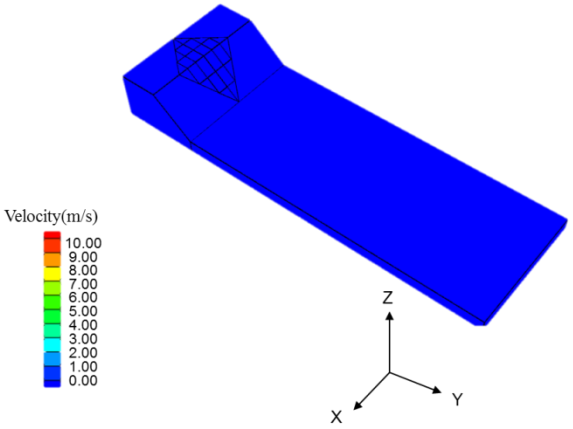

(a) 24blocks, time=0

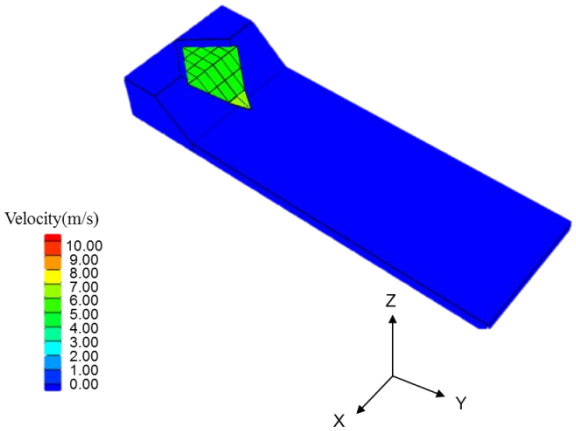

(b) 24blocks, time=3s

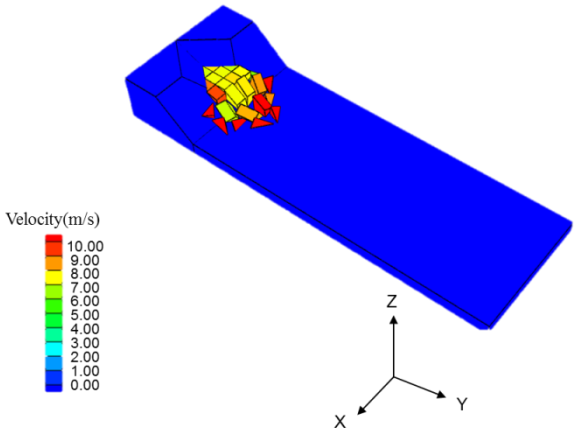

(c) 24blocks, time=6s

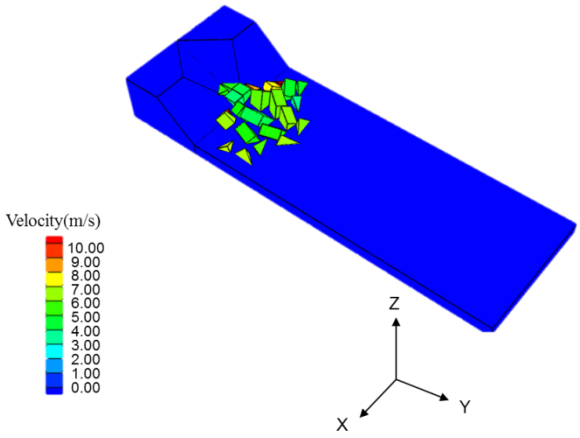

(d) 24blocks, time=9s

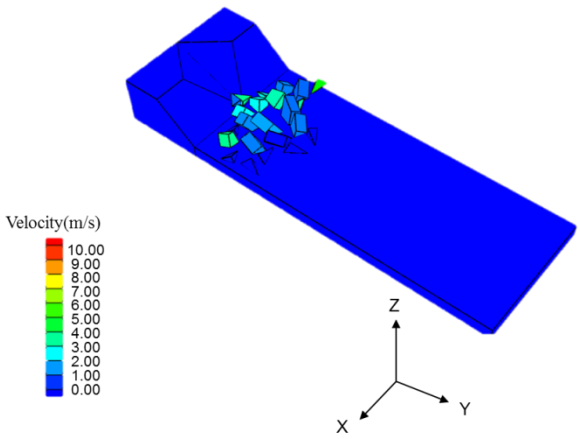

(e) 24blocks, time=12s

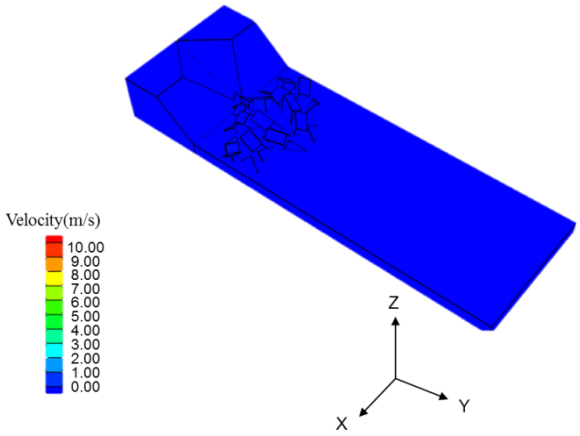

(f) 24blocks, time=15s

Figure 3.16 The runout process for 24 blocks' sliding parts

It can be found that the runout process can be simulated by the 3D DDA method from the start of failure and the final deposit.

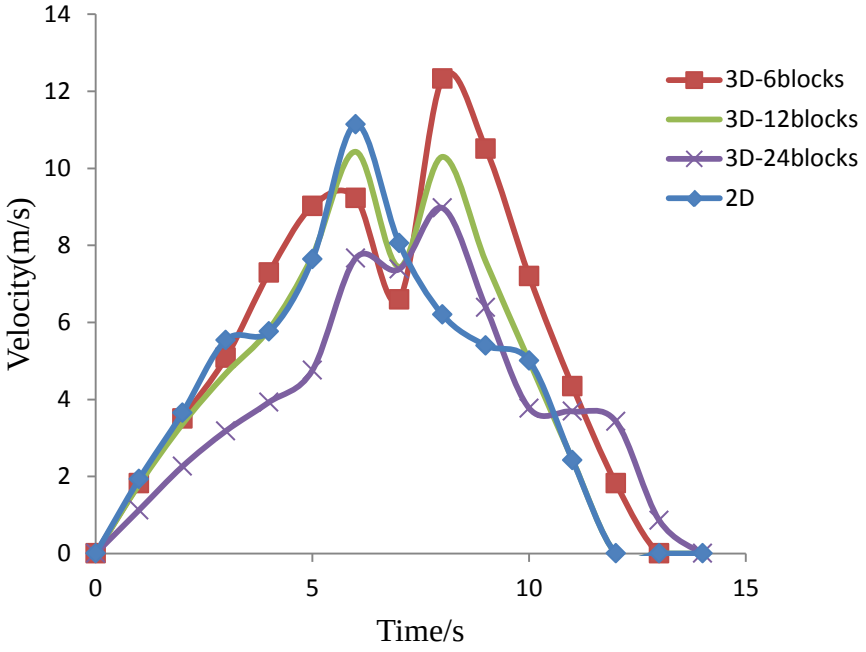

Figure 3.17 The comparison between the 2D and different 3D DDA model on the toe block's velocity pattern

The toe development of toe block's velocity changing with the time is monitored as Figure 17 shows. It can be found that: 1) for the 3D DDA simulation,

no matter how many blocks the sliding part is comprised of, the velocity shows two peak points. The reason is, for this wedge model, the blocks in the central parts are accelerated by the compact from the lateral blocks; 2) the maximum velocity of the toe block in the is generally bigger than that in the 3D DDA simulation, if just the 12 blocks and 14 blocks' models are taken into consideration., as there is no lateral restriction.

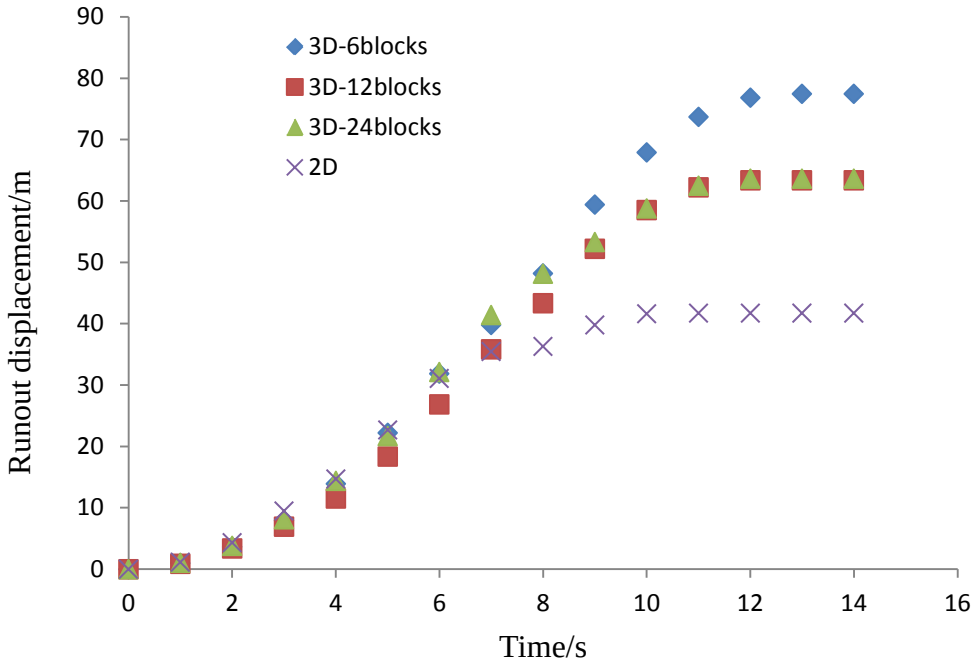

Figure 3.18 The comparison between the 2D and different 3D DDA model on the toe block's runout distance pattern.

The Figure 3.18 shows the pattern of toe block's runout distance development. It can be found that: 1) the difference between the 2D and 3D on the runout displacement analysis is huge. In this case, the runout distance in 2D DDA analysis is much smaller than that in 3D DDA. We cannot conclude this is a common conclusion, because the special wedge mode that make the toe block obtain the twice acceleration from the lateral blocks just like its velocity pattern if the sliding parts are increased from 12 blocks to 24 blocks, the runout displacement pattern tend to be

consistent, which shows that for the runout displacement analysis in the 3D DDA method, a certain number of blocks is enough to get the reasonable results.

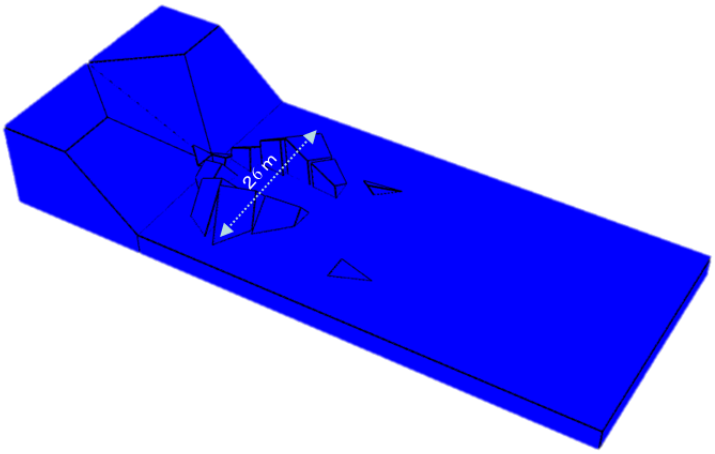

(a) The lateral distribution for 12 blocks' model

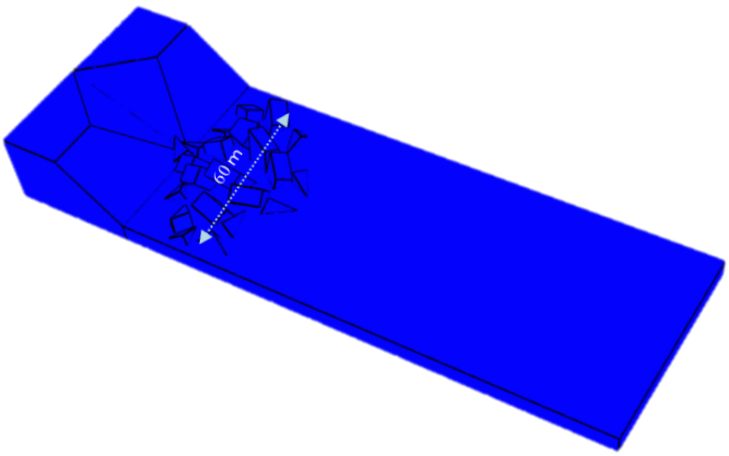

(b) The lateral distribution for 24 blocks' model

Figure 3.19 The lateral distribution characteristics of sliding part with 12 blocks and 24 blocks

The Figure 3.19 shows the lateral distribution patterns of the 12 blocks and 24 blocks' model. Because of there is almost no lateral spread for the 6 blocks' model, its pattern are not shown. For sure, it is a common sense that there is no lateral spread in the 2D analysis. Form figure 3.19, we can find that for the 3D simulation, the lateral spread is obvious. When the sliding block number increases the spread distance may increase. If we calculate this spread distance from the symmetry line, for this certain case, the spread distance will increase from 13 meters to 30 meters when the sliding block number varies from 12 to 24.

3.6 CONCLUSIONS

In this section, in order to show the limitation of 2D analysis and the advantage of 3D DDA, a close comparison between the 2D and 3D DDA on the certain slope model is made. The focus is mainly on two aspects the stability analysis and run-out simulation. The main conclusions are listed as follows:

1) For the stability analysis, the factor of safety is different from section to section. The 2D analysis underestimates the factor of safety around 20% as the lateral friction cannot be considered, and the relative error may increase when the strength parameters increases.

2) When the run-out analysis is compared it can be concluded that run-out distance of the 2D DDA analysis is greatly different from the 3D DDA solution, and the run-out distance is different from section to section. Moreover, the lateral spread can be considered in the 3D DDA method, a lateral spread of 30 meters can be found, which is of practical meaning for the disaster mitigation.

3) The FOS from the 3D DDA is in good agreement with the theoretical solution. Therefore, it is more meaningful and accurate to use the 3D analysis than the 2D.

REFERENCES

Benz W. (1988). Applications of smooth particle hydrodynamics (SPH) to astrophysical problems. Comput Phys Commun 48(1):97-105

Benz W, Asphaug E. (1995). Simulations of brittle solids using smooth particle hydrodynamics. Comput Phys Commun 87(1):253-265

Berczik P. (2000). Modeling the star formation in galaxies using the chemo-dynamical SPH code. Astrophys Space Sci 271(2):103-126

Beyabanaki SAR, Ferdosi B and Mohammadi S. (2009). Validation of dynamic block displacement analysis and modification of edge-to-edge

contact constraints in 3-D DDA. International Journal of Rock Mechanics and Mining Sciences, 46(7), 1223-1234.

Dong X, Wu A and Ren F. (1996). A preliminary application of discontinuous deformation analysis (DDA) to the Three Gorges Dam project. In: MR S, D B, editors. The first international Forumon discontinuous deformation analysis (DDA) and simulations of discontinuous media. Berkeley, CA: TSI Press: Albuquerque, NM; 1996, 310-317.

Dong X, Wu A and Ren F. (1996). A preliminary application of discontinuous deformation analysis (DDA) to the Three Gorges Dam project. In Proceedings of the First International Forum on Discontinuous Deformation Analysis (DDA) and Simulations of Discontinuous Media, Berkeley, CA, Salami MR, Banks D (eds). TSI Press: Albuquerque, NM, 310-317.

Doolin DM and Sitar N. (2004). Time integration in discontinuous deformation analysis. Journal of engineering mechanics, 130(3), 249-258.

Gotoh H, Sakai T (2006) Key issues in the particle method for computation of wave breaking. Coast Eng 53(2-3):171-179

Gotoh H, Shao SD and Memita T. (2004). SPH-LES model for numerical investigation of wave interaction with partially immersed breakwater. Coast Eng 46(1):39-63.

Grayeli R and Hatami K. (2008). Implementation of the finite element method in the three-dimensional discontinuous deformation analysis (3D-DDA). International journal for numerical and analytical methods in geomechanics, 32(15), 1883-1902.

Kim Y. (2007). Experimental and numerical analyses of sloshing flows. J Eng Math 58(1-4):191-210.

Kim YI, Amadei B and Pan E. (1999). Modelingthe effect of water, excavation sequence and rock reinforcement with discontinuous deformation analysis. International Journal of Rock Mechanics and Mining Sciences, 36(7), 949-970.

Kipfer P and Westermann R. (2006). Realistic and interactive simulation of rivers. In: Graphics interface 2006, Quebec, Canada.

Monaghan JJ. (1990). Modelling the universe. Astron Soc Aust Proc 8(3):233-237.

Monaghan JJ. (1992). Smooth particle hydrodynamics. Annu Rev Astron Astrophys 30:543-574.

Monaghan JJ. (1994). Simulating free surface flows with SPH. J Comput Phys 110(2):399-406.

CHAPTER 4

DEVELOPMENT OF A PRACTICAL 3D DDA PRE-PROCESSOR

4.1 INTRODUCTION

The model construction is the first and the indispensable step for the numerical simulation. The 3D model construction is still a challenge for the 3D DDA simulation just like the benchmark paper Gony (2016) published recently pointed: “Modeling three dimensional multi-block structures in 3D-DDA is an elaborate and challenging task”. Although the original task has been developed, it has the following drawbacks:

1) It is not suitable for construct a blocky system with multi-blocks. It does not allow the whole block input as its data element is the triangle face. If the rectangular face of one block is needed, it is avoidable to input two triangles both of which owning three points. It can be acceptable if there are just a few block is needed. However, if a blocky system consisting of many blocks is needed, this process is exhausting and un-tolerable.

2) The block cutting function is insufficient. The block cutting contains two aspects, the block(s) cutting by the cutting plane(s) and cutting between blocks. As mentioned before, the 3D blocky system may contain many blocks interfacing by joints and discontinuities, so it is unavoidable to use the cutting plane(s) to cut the block(s) during the model construction. The Figure 4.1 shows one block is cut by two planes forming four blocks just like the shear joint in nature. Moreover,

sometimes, the cutting between blocks is needed. For example, to build the 3D tunnel model, it is more convenient to use one block to cut the other to form the internal space of the tunnel as Figure 4.2 shows.

Figure 4.1 One block cut by a pair of planes

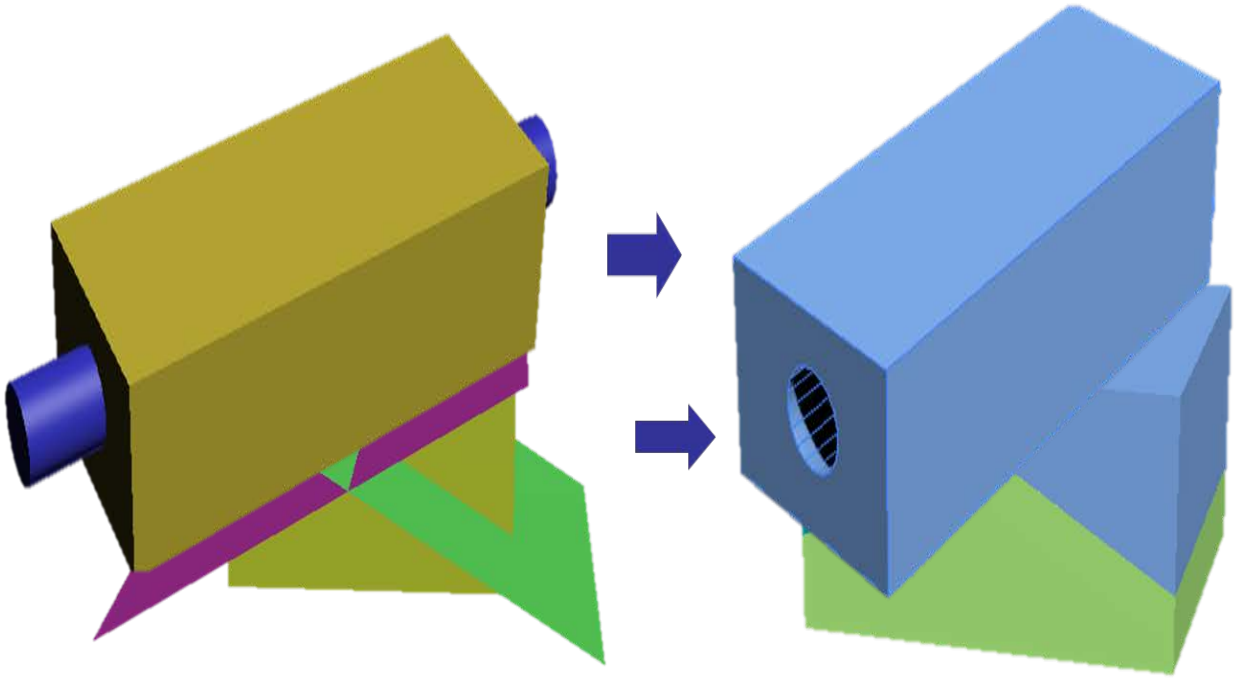

Figure 4.2 One block cut by the other block

3) No user-friendly graphic interface. The modification of the model is based on the point data edit and modification of the model is not by the direct operation on the 3D interface which resulting an exhausting operation if the model is slightly complicated.

4) Cannot handle the real 3D terrain data. Up to now, the 3D DDA is just on the level of basic verification and simple application owing a few of blocks. For the real

3D simulation, such as rockfall and landslide, it is unavoidable to use the real 3D terrain.

Therefore, for the 3D model construction in 3D DDA method, there are two major issues needed to be solved: 1) how to build a blocky system with multiply blocks; 2) how to create the real 3D terrain.

For the multi-blocks construction, the mature commercial soft 3ds Max (Derakhshani, 2014) is always used because of its user-friendly operation. If its output data format can be transferred to the one that 3D DDA used, to build the 3D multi-blocks is not a problem for 3D DDA. The practical pre-processor proposed in this thesis uses the advantages of the 3d Max and the built model data can be transferred to the one that the 3D DDA can be used.

For the 3D terrain, normally, the ArcGIS (ESRI, Arc GIS 10) is normally used to store and emerge the data. If the 3D terrain data in ArcGIS can be transferred to the data format in 3D DDA, the construction of 3D terrain in the 3D DDA will not be a problem.

The developed practical pre-processor takes the advantage of both the commercial software 3ds MAX and Arc GIS to solve the problems of building multi-blocky system and real 3D terrain resulting in the model construction for 3D DDA comes to an more easy issue, which will benefit the development of 3D DDA on the practical issues.

4.2 THE DATA FORMAT IN 3D MAX AND 3D DDA

The output data from the 3ds MAX cannot be read directly by the 3D DDA because of the inconsistency data format. There are many output data format for 3ds MAX, of which the most common and general is the one with suffix “obj” and hereinafter called obj file. For the 3D DDA method, the input geometrical data is with suffix “blk” and hereinafter called blk file. The developed pre-processor can transfer the obj file from the 3ds MAX to the blk file. The data format of the obj flie and the blk file are illustrated in this section.

To illustrate the data structure of the output file- obj file in the 3ds MAX, a cubic block is built with the side length of 5 meters as Figure 4.3 shows.

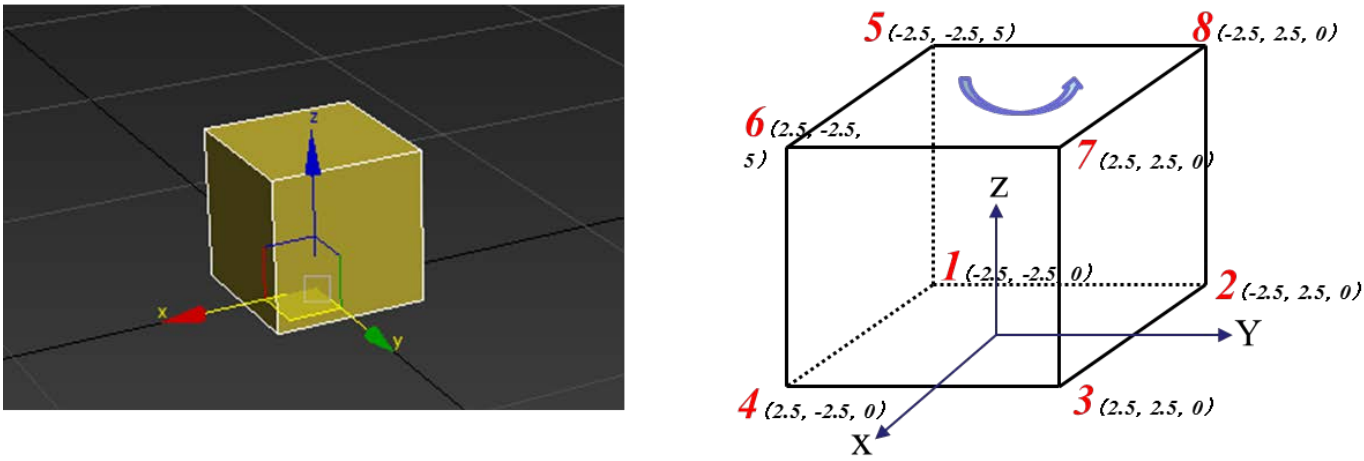

Figure 4.3 The cubic model in the 3ds MAX

The origin of coordinate is on the center of the lower surface. The output “obj” file is as Figure 4.4 shows. The output data owns 8 vertices and 6 polygons and the “V” and “f” represent the vertices and faces respectively. The data structure owns the following patterns: 1) the vertices are ranked from the top to the bottom from 1 to 8; 2) each polygon is formed based on the vertices that following the right-hand low, such as the top polygon in Figure 4.4 is formed by the vertices from 5 to 8.

```
#
# object Box001
#

v  -2.500000000000 -2.500000000000 0.000000000000
v  -2.500000000000 2.500000000000 0.000000000000
v  2.500000000000 2.500000000000 0.000000000000
v  2.500000000000 -2.500000000000 0.000000000000
v  -2.500000000000 -2.500000000000 5.000000000000
v  2.500000000000 -2.500000000000 5.000000000000
v  2.500000000000 2.500000000000 5.000000000000
v  -2.500000000000 2.500000000000 5.000000000000
# 8 vertices

g Box001
f 1 2 3 4
f 5 6 7 8
f 1 4 6 5
f 4 3 7 6
f 3 2 8 7
f 2 1 5 8
# 6 polygons
```

Figure 4.4 The data structure of the obj file for the cubic

The data structure of the blk file- the needed geometrical input file for the 3D DDA is in the form as Figure 4.5 illustrates. It should be mentioned that its material ID and joint ID are arranged from the number zero. From the first line to the last the data are illustrated as following: 1) the number of fixed points, load points and measure points, in the example, there are 4 fixed point and the coordinates of them are listed at the end the file; 2) the second and third line demonstrates the vertex index and the material ID, in the example, the vertex index is from 1 to 7 and the material ID is zero(the material type can be more than one, the ID zero is just an example of one kind of material type); 3) the eight lines of number is the vertex coordinates; 4) then the facet index and joint ID are needed, for the cubic, there are six facet indexed from 0 to 5 and for each facet the joint ID is set to be zero(the joint type can be various and the zero is just an example of one kind of joint type); 5) after that, the six lines show the facet orders, which is similar like that in the blk file, while its index starts from the zero; 6) at the end of the file is the 4 fixed coordinates and if the load and measure points are exist, the relevant coordinates should be listed.

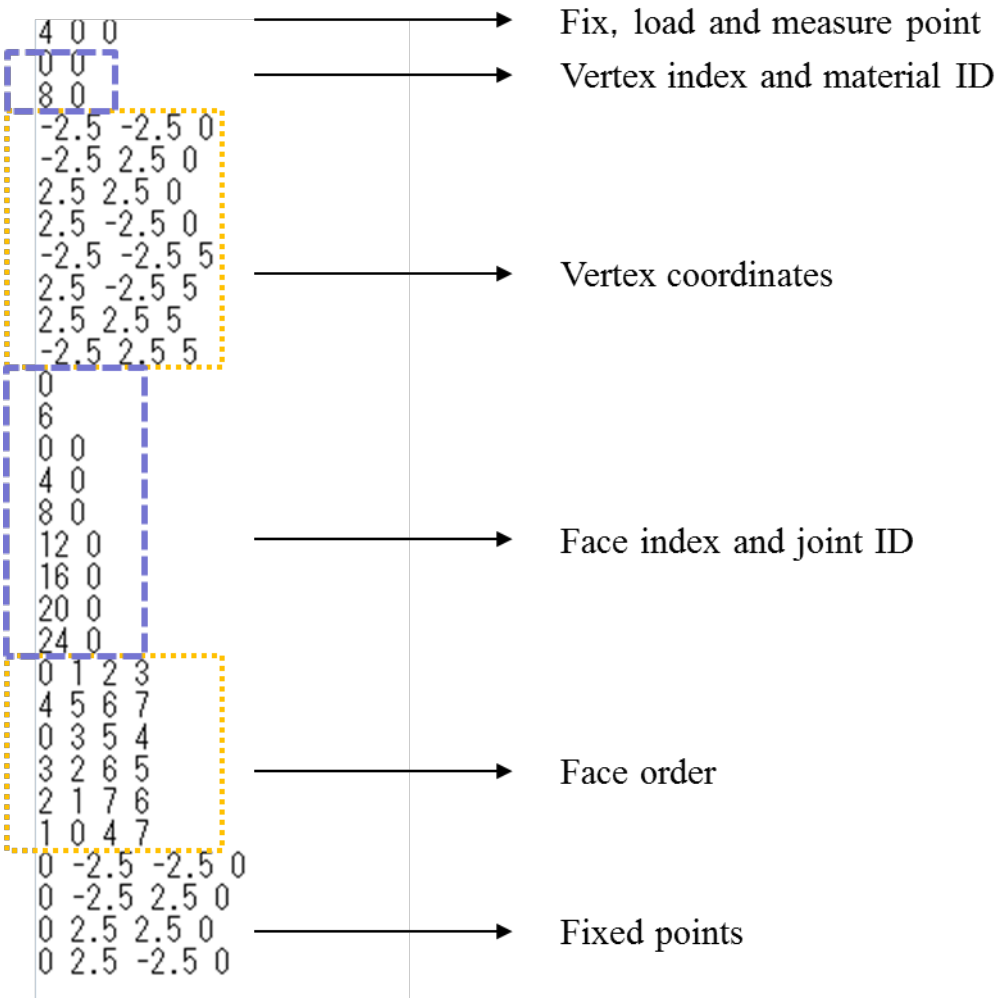

Figure 4.5 The data structure of the blk file for the cubic

4.3 THE PROCEDURE OF THE NEW PRE-PROCESSOR

As illustrated before, the new practical pre-processor for the 3D DDA model construction take advantage of the commercial software 3ds MAX and ArcGIS, the main procedure of its model construction is illustrated as Figure 4.6. Using new pre-processor, the 3D DDA model can be easily constructed containing not only sliding parts which are created original from the 3ds MAX but also the 3D terrain base part. The main procedure includes the following three steps in order:

1) Creating the 3D blocks from 3ds MAX. During this step, the 3D blocks can be constructed by the 3d MAX using the function of either direct block construction or block cutting function. After this, the output file that is from the 3ds MAX will be

transferred to the blk file by the pre-processor, which can be used for the 3D DDA program;

2) Creating the 3D terrain original from ArcGIS. In this process, the real terrain data in the ArcGIS platform no matter in the counter map or the DEM form can be used and transferred to the blk file that the 3D DDA can be used;

3) Combination of the two above blk files together to form the complete blk file which contains both the 3D sliding blocks and the 3D terrain base.

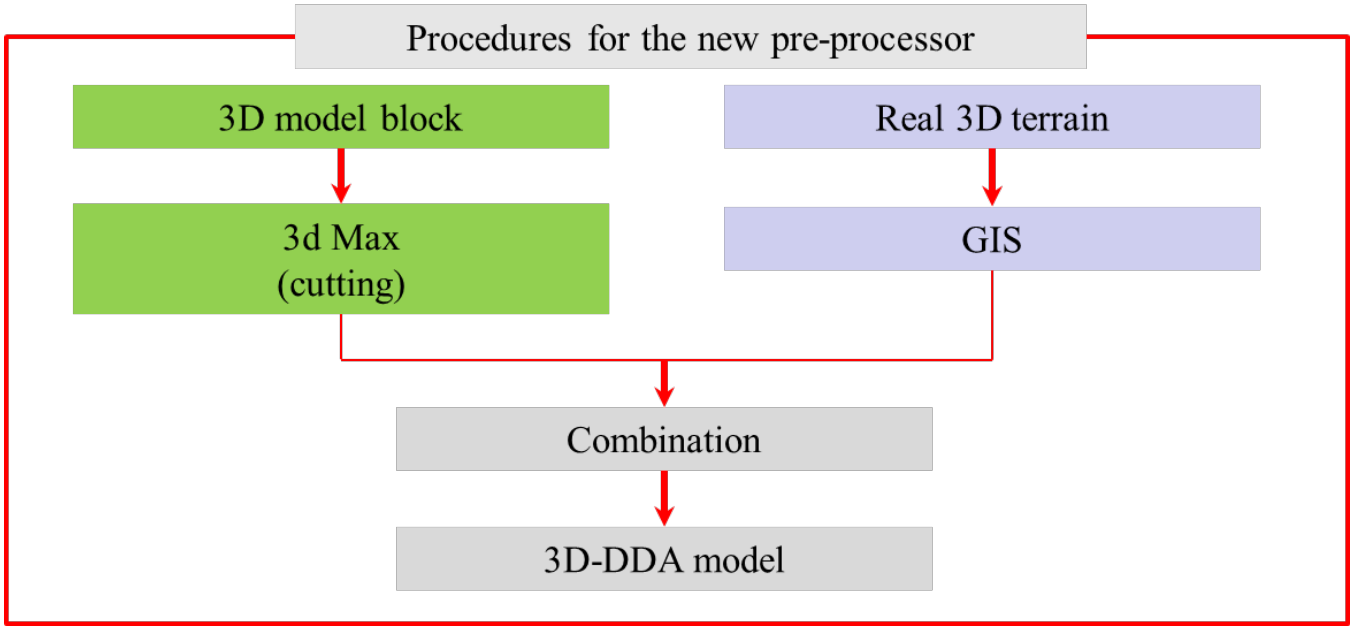

Figure 4.6 The main process of the new pre-processor

There are two important steps in the new pre-processor as mentioned before the 3D model construction and the 3D real terrain, which are the cores of this new pre-processor and will be illustrated in detail at the following sections.

4.4 3D BLOCK CONSTRUCTION USING 3D MAX

The construction of the 3D block is one necessary and important step for the numerical simulation. In order to construct the 3D model conveniently, the pre-processor is developed taking advantage of the commercial software 3d MAX. The

main process of 3D block mode construction is shown as Figure 4.7.

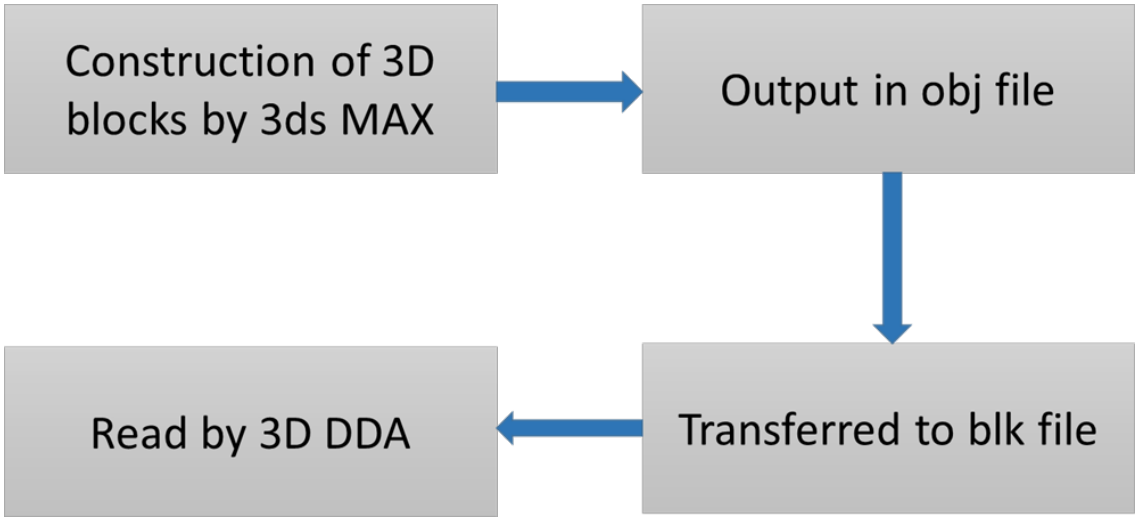

Figure 4.7 The process of 3D model construction

This process contains mainly two major steps: firstly, the 3D model is constructed by the 3dMAX and is output in the data format of obj; then, the obj file is transferred to the blk file which can be read by the 3D DDA as the geometrical input data.

The 3D model construction in the 3dMAX can be performed by

1) Direct model construction; the 3dMAX platform provides many object types which can be selected and constructed by the user easily, as Figure 4.8 shows, such as the box, sphere and etc., which are listed in the option “ standard primitives”.

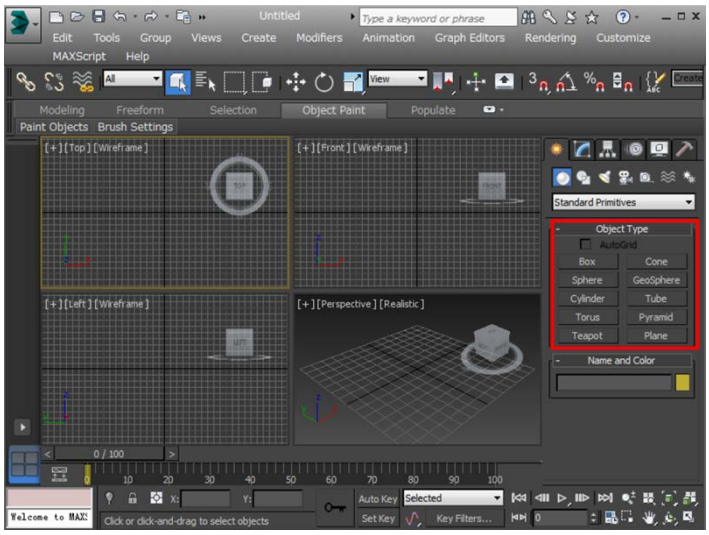

Figure 4.8 The options of object type in the 3dMAX interface.

2) Cutting function; the cutting function in the 3dMAX is in two forms: the normal cutting of the object (s) by the cutting faces and the blocks cutting each other. The Figure 4.8 illustrate one yellow block is cut to six small blocks by three cutting planes using the function of “ProCutter” provided by the 3dsMAX

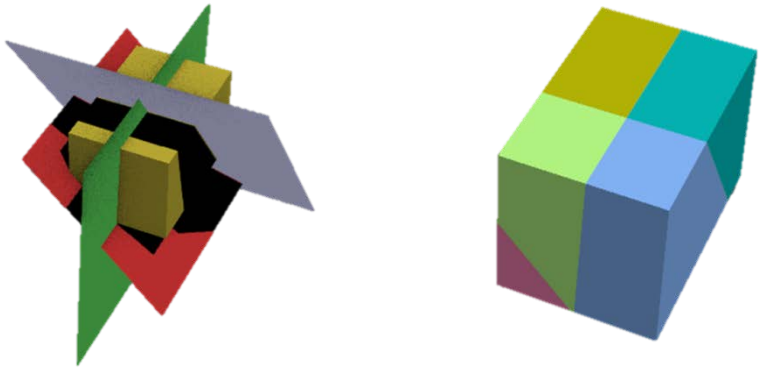

Figure 4.8 The example of “Procutter” function in 3dsMAX.

The “ProCuttter” function is listed in the option of “Compound Objects” as in the Figure 4.9. The operation of the “ Procutter” should be cautious: 1) The cutter objects should be the cutting faces and the stock objects are the ones that needed to be cut; 2) the cutter tool mode must auto extract mesh and explode by elements; 3) the cutter parameters must stock outside cutter and stock inside cutter. Moreover,

after the operation of “ProCutter” the cutting planes should be deleted because they are not useful anymore.

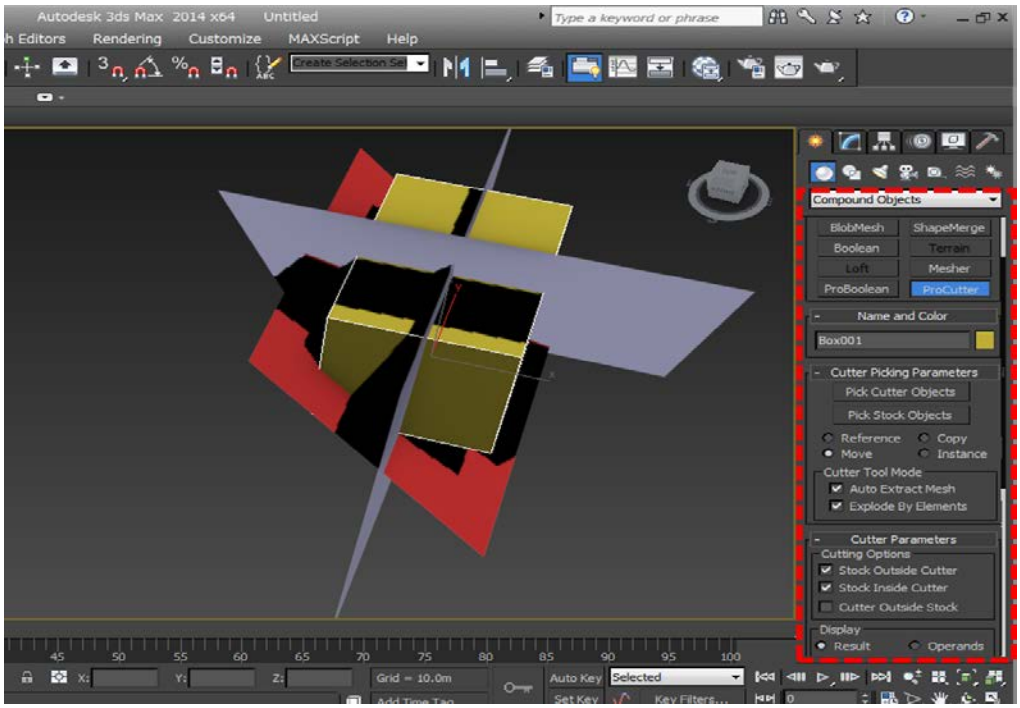

Figure 4.9 The selection of sub-options in the “Procutter”.

4.5 3D TERRAIN USING ARCGIS

In order to make sure the accuracy of the simulation, the real 3D terrain is very necessary, for example, the runout of the landslide and the rock-fall, in which the 3D terrain influences the result a lot. For the 3D DDA method, to capture and reproduce the 3D terrain is a big challenge. In this section, an approach is proposed in the new pre-processor taking advantage of the ArcGIS as in Figure 4.10.

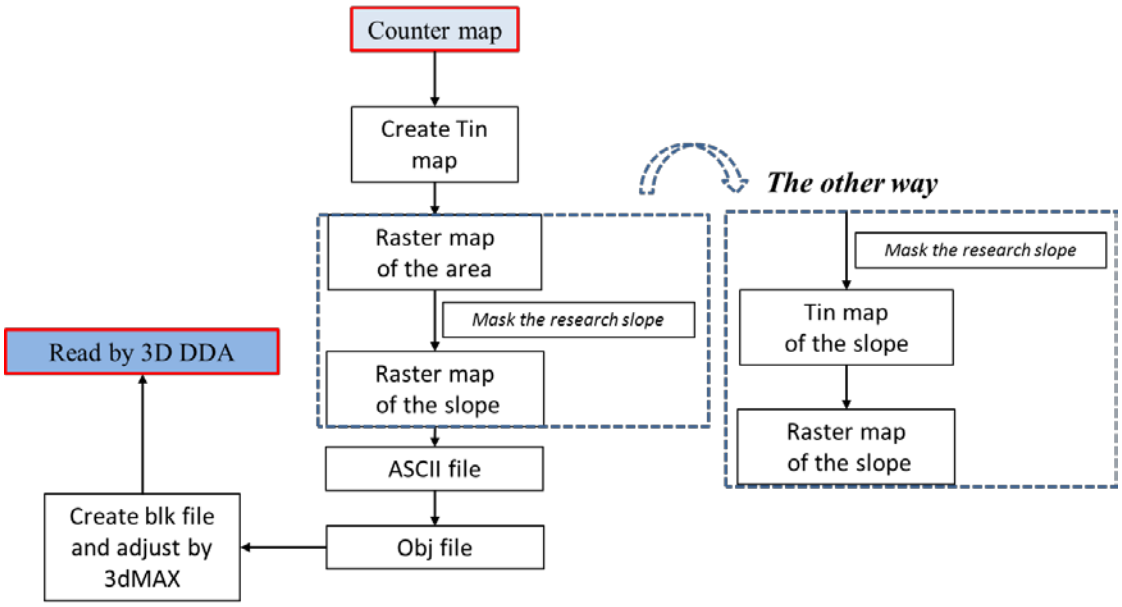

Figure 4.10 The main process of creating 3D terrain

The process of the 3D real terrain construction by the developed pre-processor includes the following two main steps: 1) creating the ASCII file by the ArcGIS; during this step, the counter map of this area should be transferred to the raster map firstly, then the relevant research slope need to be masked to form the ASCII file of it; 2) The ASCII file of the research slope is transferred into the obj file, which can be read and adjusted by the 3dMAX conveniently. After this, the operation is just like the construction of 3D block as illustrated before. It should be mentioned that “the other way” in the Figure 4.10 means a parallel way to extract the research slope from the whole area data, which “mask” the Tin map of the relevant slope directly from the Tin map of the whole area, while the method in the flow chart doing this after the formation of the whole area’s Raster map. The “mask” means to use the polygon shape file to target the research slope from the whole data of the area. The process of the operation is illustrated in the Figure 4.11.

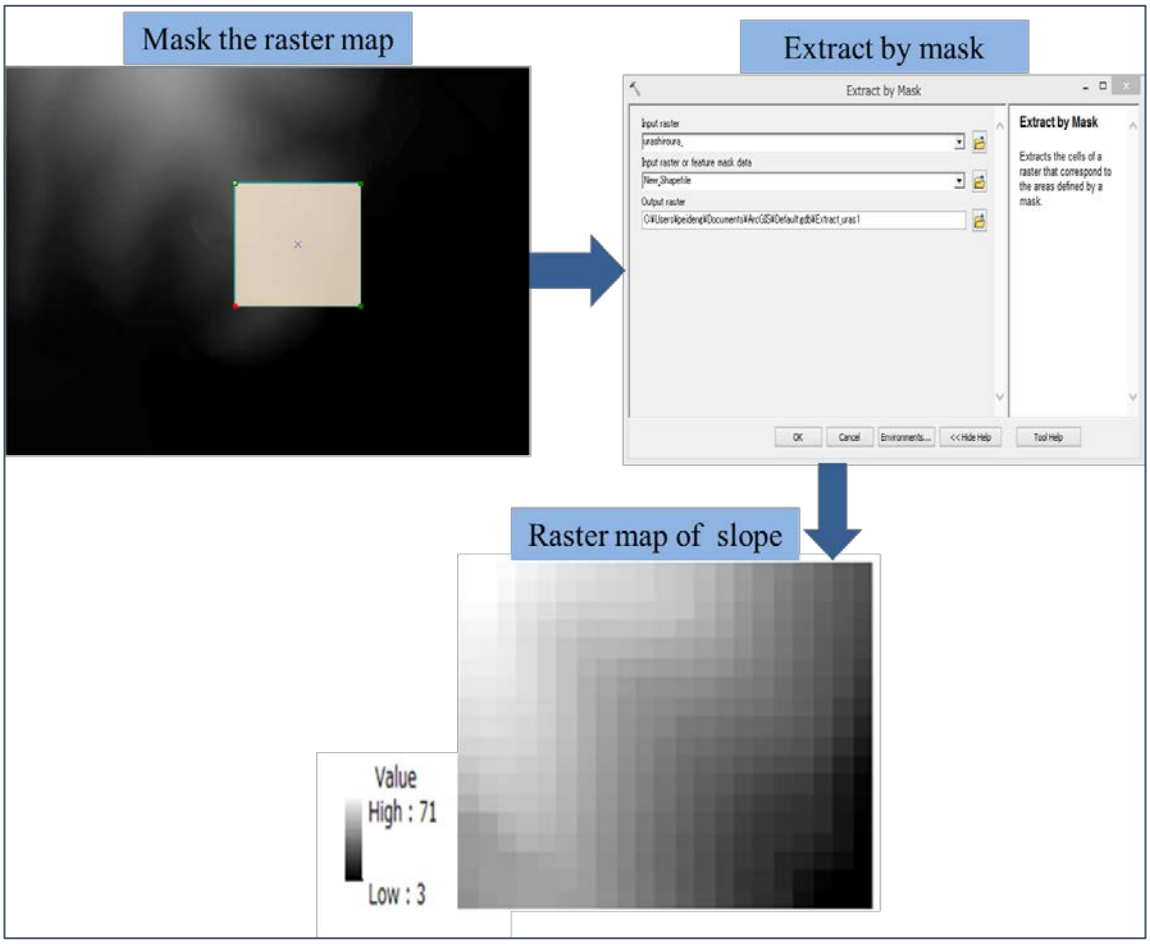

Figure4.11 The operation of forming raster map by “Extract by mask”

The operation of the “mask” is necessary because we need to extract the relevant research slope from whole area’s map. As we can find from Figure 4.11, the raster map of the whole area is masked by a polygon, which locks the research slope. Then by using the function “Extract by mask” provided in the ArcGIS, the raster map of the slope can be extracted easily.

When the Tin map is transferred to the Rater map as illustrated in Figure 4.12, it should be very cautious that the “cell size” needs to be proper. The cell size in the Figure 4.12 is in the unit of meter. Its value is neither too big nor too small. If it is too big, the precision is not enough, while if too small, despite it is accurate enough, its data size is so large that the computational efficiency is greatly influenced.

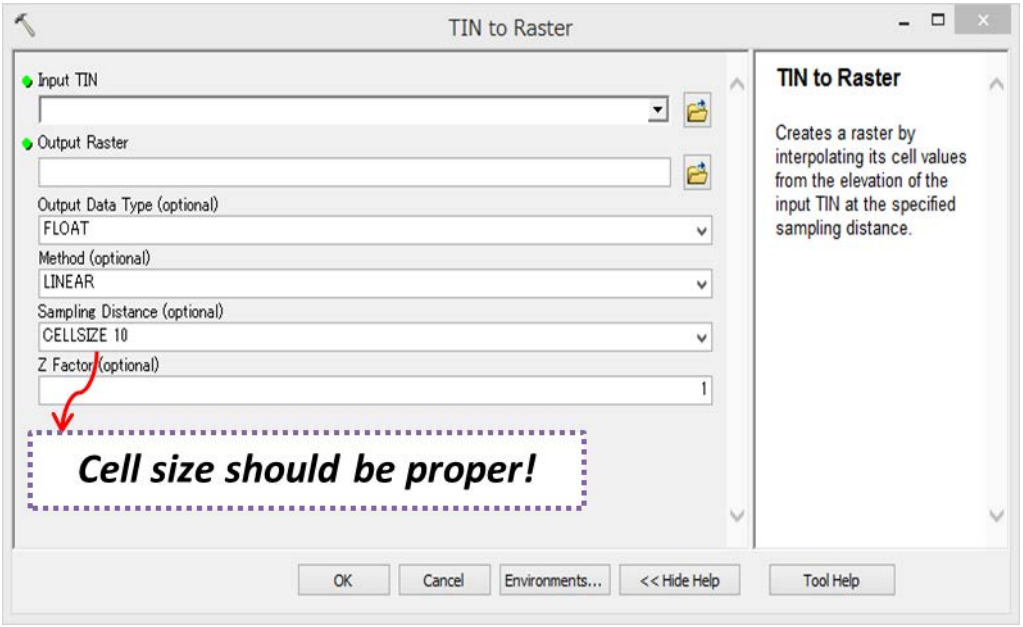

Figure 4.12 The operation of transferring Tin to Raster

The operation of the “Raster to ASCII” by the ArcGIS is shown in Figure 4.13

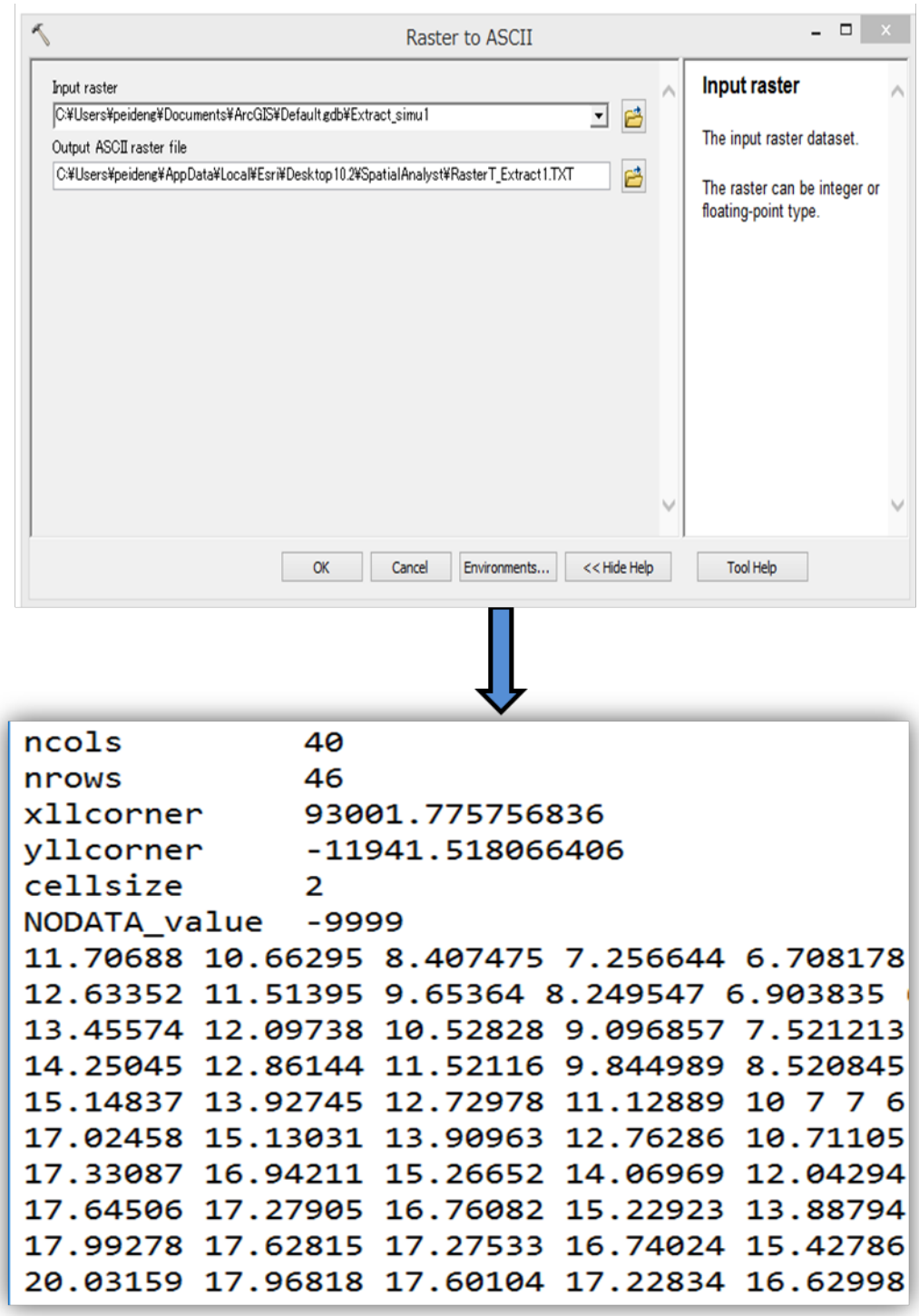

Figure 4.13 The " Raster to ASCII" by ArcGIS.

4.6 THE EXAMPLE OF THE PRE-PROCESSOR IN THE DAIGANJI SLOPE

The Daiganji slope located at the Oita prefecture in Japan. The field

investigation has been performed and the slope area and slide surface can be roughly estimated. Besides, the relatively accurate counter map can be acquired. Therefore, the condition is mature for building the 3D slope model.

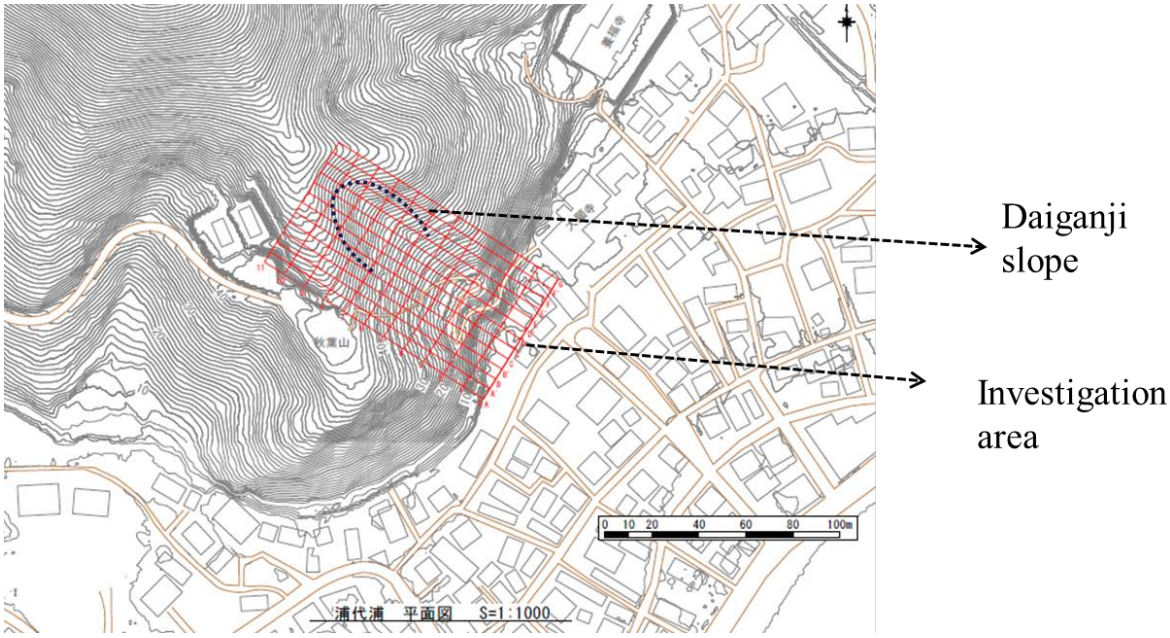

Figure 4.14 The counter map of the slope area

The counter map of the Daiganji slope can be transferred to the raster map easily by the ArcGIS, as Figure 4.15 shows. Because of the slope has been located by the field investigation, after getting the raster map of this area, the raster map of the slope can be obtained by the “mask” function that mentioned before. Then, the 3D model can be visualized and modified in the 3ds Max platform (figure 4.16). Surely, by the data, the model can be recognized by the 3D DDA.

Figure 4.15 Transfer counter map of the Daiganji area to Raster

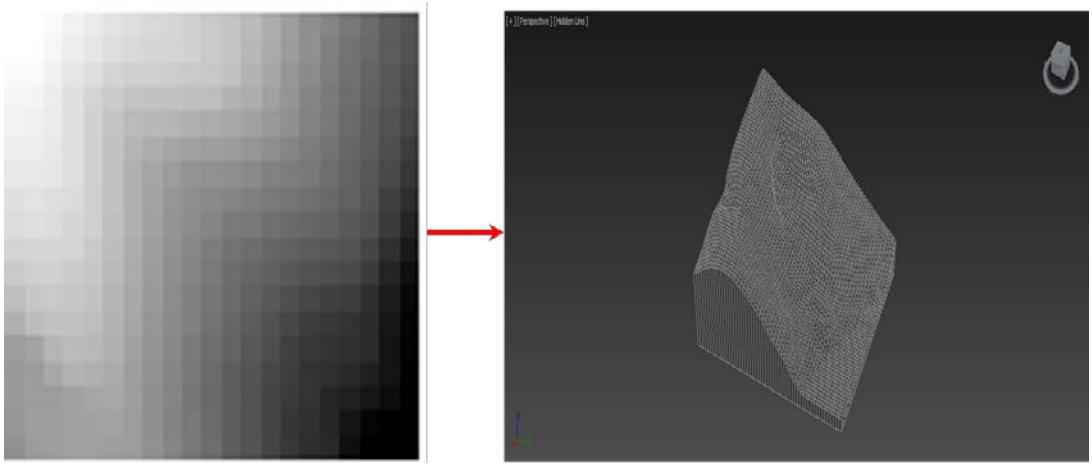

Figure 4.16 Transfer from Raster to 3D model

Because the slope area and the slide surface have been located by the field investigation, the 3D terrain model should be modified. The slide body can be easily constructed by the pre-processor, as illustrated in figure 4.17 (a). It should be cautious that the block number should be proper. If it is too large, the calculation efficiency can be greatly influenced, while if it is two small, it is impossible to make sure the accuracy. In this model the block number is around 70. The slide part and the constructed 3D DDA model can be found in figure 4.17.

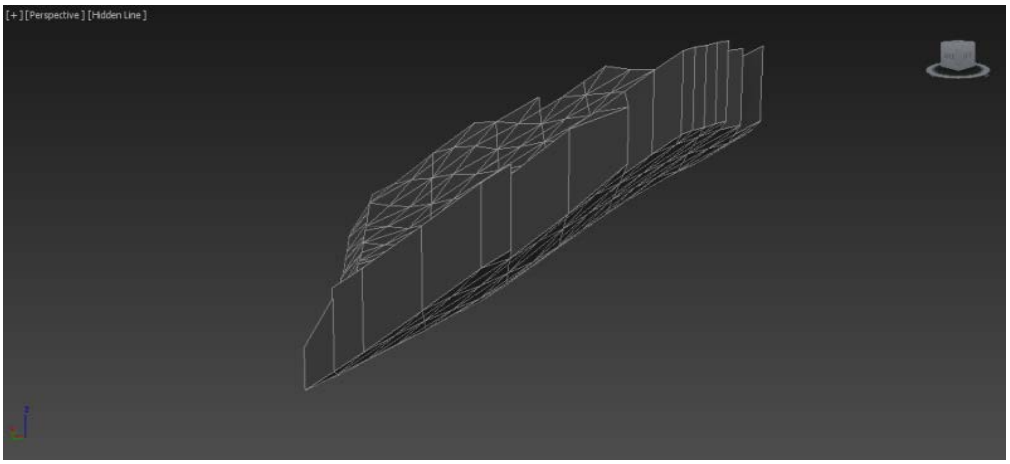

(a)

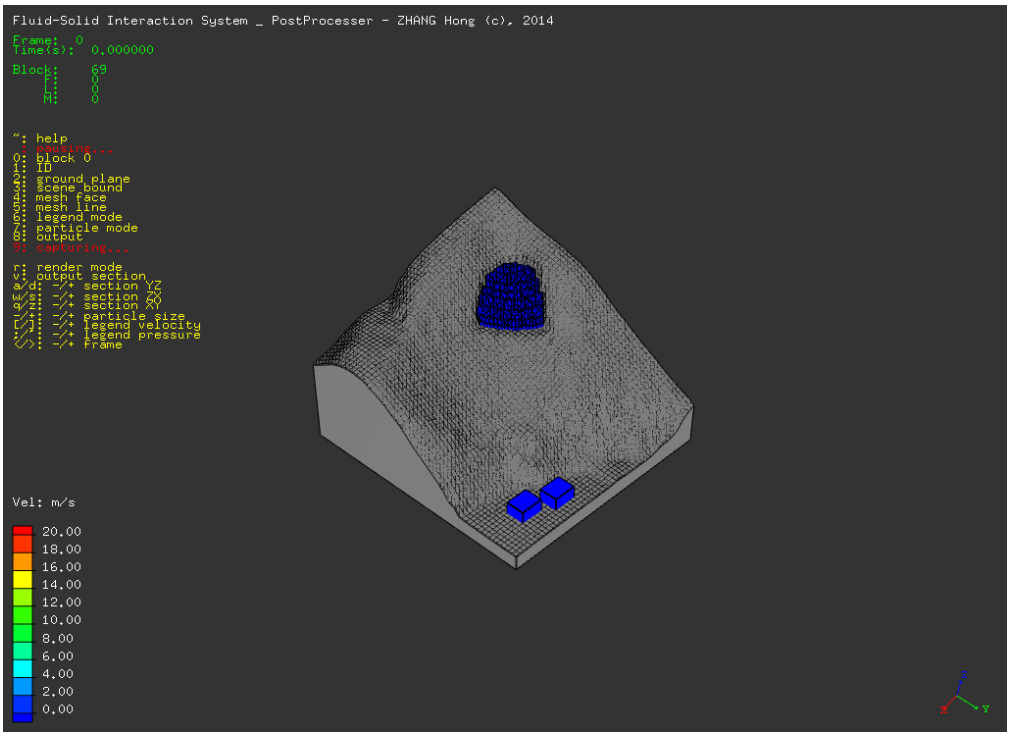

(b)

Figure 4.17 The slide part (a) and the 3D DDA model (b)

4.7 CONCLUSIONS

1) A practical pre-processor has been developed by combing the commonly used commercial software: 3ds Max and ArcGIS. Arbitrary-shaped 3D blocks are made with 3ds Max and complex slope terrain mesh data are obtained from the ArcGIS.

2) A pre-process program is developed to combine the output data from both 3ds Max and ArcGIS and translated them to the 3D DDA model format.

3) The effectivity of the newly developed 3D DDA pre-processor has been verified by building the 3D Daiganji slope model, which makes it possible for applying 3D DDA to practical landslide study.

REFERENCES

Cundall PA and Hart RD. (1992). Numerical modeling of discontinua. Engineering computations, 9(2), 101-113.

Cundall PA and Strack OD. (1979). A discrete numerical model for granular assemblies. Geotechnique, 29(1), 47-65.

Doolin DM and Sitar N. (2004). Time integration in discontinuous deformation analysis. Journal of engineering mechanics, 130(3), 249-258.

Hatzor YH, Arzi AA and Tsesarsky M. (2002). Realistic dynamic analysis of jointed rock slopes using DDA. In Proceedings of the 5th International Conference on

Mikola RG and Sitar N. (2013). Next generation discontinuous rock mass models: 3-D and rock-fluid interaction. Frontiers of Discontinuous Numerical Methods and Practical Simulations in Engineering and Disaster Prevention, 81-90.

Munjiza AA, Knight EE and Rougier E. (2011). Computational mechanics of discontinua. John Wiley and Sons.

Oger G, Doring M, Alessandrini B and Ferrant P. (2006). Two-dimensional SPH

simulations of wedge water entries. Journal of Computational Physics, 213(2), 803-822.

Shi GH. (1988). Discontinuous deformation analysis: a new numerical model for the statics and dynamics of block systems (Doctoral dissertation, University of California, Berkeley).

Shi GH. (2001). Three dimensional discontinuous deformation analysis. In Proceedings of the 4th International Forum on Discontinuous Deformation and the Simulation of Discontinuous Media, Glasgow, UK, 1 (Vol. 21).

Wang Y, Hu MS and Rutqvist J. (2013). Confined-unconfined seepage analysis using Numerical Manifold Method with an energy-work-based model. Frontiers of Discontinuous Numerical Methods and Practical Simulations in Engineering and Disaster Prevention, 349.

Wu JH. (2010). Compatible algorithm for integrations on a block domain of any shape for three-dimensional discontinuous deformation analysis. Computers and Geotechnics, 37(1), 153-163.

Zheng, L., Chen, G., Zhang, Y. and Zhang, H. (2013). Review of rock stability analysis using discontinuous deformation analysis (DDA). Rock Characterisation, Modeling and Engineering Design Methods, Chap. 83, 491-500.

CHAPTER 5

EXTENSION OF ORIGINAL 3D DDA BY ADDING FUNCTION OF SEISMIC LOADING AND ANCHOR REINFORCEMENT

5.1 INTRODUCTION

To evaluate the seismic performance of a slope during seismic loading is of great importance in geotechnical engineering. The existing methods fall into three categories: 1) force-based pseudo-static methods; 2) displacement-based methods; 3) numerical methods;

In the pseudo-static analysis, the earthquake acceleration is treated as a permanent body force acting on the potential landslide mass. Based on the limit-equilibrium analysis, the performance of the slope is evaluated by the factor of safety. When the factor of safety drops below unity, 'failure' is predicted. The earthquake acceleration need to reduce the factor of safety to unity is called the yield acceleration. However, the pseudo-static analysis tells the user nothing about what will occur when the yield acceleration is exceeded (Jibson 1993).Usually, earthquake damage is associated with displacements, and just knowing when the damage happen is not enough. Therefore, earthquake-induced slope failure should be evaluated in terms of permanent displacement.

The displacement-based methods were generally known as the 'Newmark' analysis, which is firstly introduced by Newmark (1965) and by Goodman and Seed (1966). The Newmark analysis is a rigid block sliding on a plane approach. The

permanent displacement of a block can be accumulated by numerically integrating twice the seismic acceleration over time when the acceleration exceeds the yield acceleration of the sliding block. The Newmark's method is a powerful tool to estimate the displacement a mass would experience during ground shaking. However, there are two disadvantages: (1) the analysis is limited to a single and rigid mass, and (2) the failure is restricted to sliding. For rock engineering, the occurrence of discontinuities in rock results in a discrete system. Moreover, the failure models for rock mass during earthquake can be sliding, toppling and slumping. Therefore, using the Nemark's method is too simplified to comprehensively evaluate the seismic performance of landslide during earthquake.

To use the numerical methods is another way to evaluate the seismic performance of slope. The DDA method is a powerful numerical tool that can model the static and dynamic behaviors of discrete blocks. Being different with the Newmark's method, it can analysis a blocky system with discrete blocks, and the failure model of the blocky system can be not only sliding but also toppling and slumping. As summarized by MacLaughlin and Doolin (2006), its availability on dealing with block kinematics has been verified by various examples. For the seismic related problems, this method can be used in the rock-falls (Sasaki et al. 2004) and run-out simulations of landslide (Zhang 2013). However, these studies focus on the two-dimensional scope and verification of the 3D-DDA's availability on the seismic induced block sliding problem is necessary.

Modeling the rock anchor mechanism in rock masses is a difficult work. The 2D DDA has been used to simulate the anchor mechanism by some researches. Yeung (1993) presented the qualitative validation of the mining roof reinforced by rock anchors. Shi (2009) analysed the rock block topping with anchor reinforced. The 2D DDA uses the simplified linear elastic anchor model and shows the reasonable result, which can help us to make basic assessment of the block mass reinforced by anchors. During the simulation, the anchor can be treated as an elastic Newton element, which is a basic simplified model and used in the 2D DDA simulation. Recently, He (2014) proposed a new kind of anchor (He anchor), which serves constant resistance and

large deformation (CRLD). This anchor has been used in engineering and shown excellent performance. However, how to simulate the anchor using 3D-DDA is still a problem.

5.2 THE PROCEDURE OF ADDING SEISMIC LOADING

The equations of motion of the DDA method are derived by the principle of minimization of potential energy, which is similar to the method used in the finite element method. By solving the global equilibrium equations, the displacement unknowns can be get during each simulation step. For a blocky system, the total energy is sourced from the internal and external energy as well as contacts. The Fig.5.1 (a) shows a basic flow chart of the 3D-DDA method, and some parts of the procedure are omitted because it will be out of the range of this paper. The Fig.5.1 (b) illustrates the memberships of the 'assemble of non-contact terms'. When adding the seismic loading to the DDA method, the red terms in the Figure.1 should be modified.

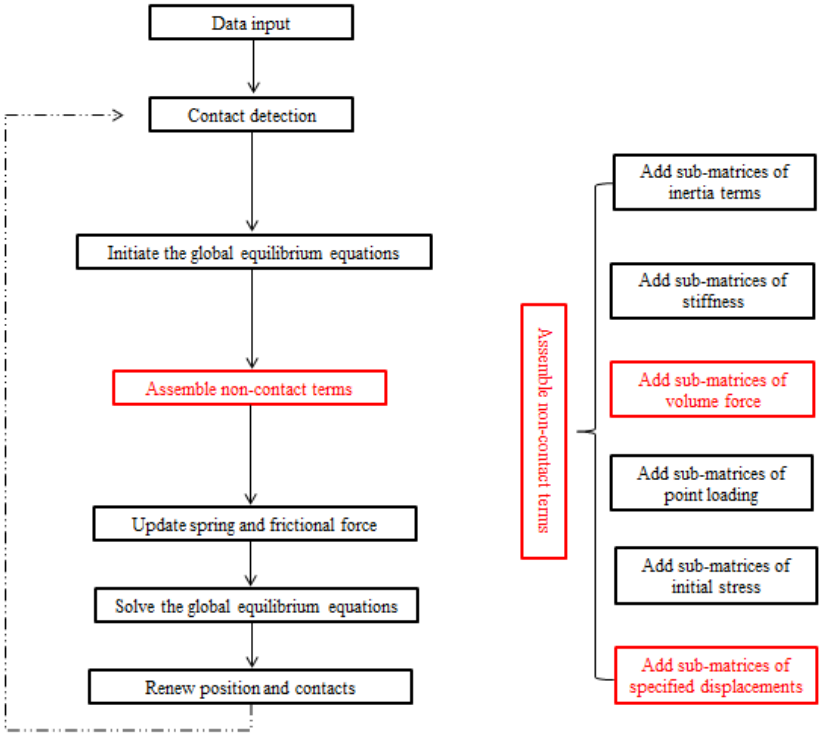

Fig.5.1 (a) The simplified procedure of DDA method; Fig.5.1 (b) The memberships of the 'assemble non-contact terms'.

5.2.1 TIME-DEPENDENT ACCELERATION INPUT METHOD

In the time-dependent acceleration input method, the acceleration is treated as the volume acceleration and works as the volume force on the relevant block. The sub-matrices of volume forces should be added to the 'Assemble non-contact terms'. Assuming that $(f_x,\ f_y, f_z)$ is the volume force caused by the seismic acceleration acting on the entire volume Vi of block i. By minimizing the potential energy of the volume force, the corresponding 12 × 1 sub-matrices is obtained and added to the global force matrices in the global equilibrium equation, as shown below:

$$\left[f_x V_i \quad f_y V_i \quad f_z V_i \quad 0 \quad 0 \quad 0 \quad 0 \quad 0 \quad 0 \quad 0 \quad 0 \quad 0 \right]^T \rightarrow \mathbf{F}_i \tag{5.1}$$

The acceleration can be input into the sliding block or the base block (Fig. 5.2). When the former way is used, the simulation equals to a Newmark's type analysis. Using this way, Hatzor and Feintuch (2001) attempted firstly on validation of the DDA method by simulating the block sliding on an inclined plane with different sinusoidal horizontal accelerations. Tsesarsky et al. (2005) tested the accuracy and validation of DDA method by comparing the simulation results with the analytical solutions and shaking table experiments. Alternatively, the time-dependent acceleration can be applied on the base block not to the sliding block. Sasaki et al. (2004) applied DDA to simulate the seismic behavior of a slope with sliding blocks using this input method. It should be noted that in order to avoid the influence of gravity and the contact force between the base block and the sliding block on the applied acceleration, the base block is assumed to be not submitted to gravity and the density must be significantly large (Zhang, 2013) .Moreover, because of the movement of the base block, there is no need to add constraint points on the base in the DDA simulation.

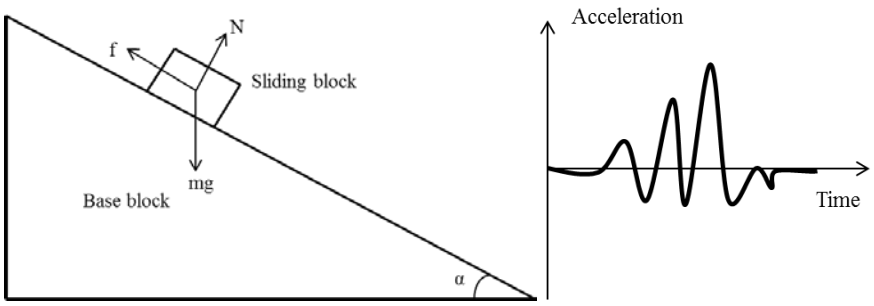

Fig.5.2 The sketch of time-dependent acceleration inputs.

5.2.2 TIME-DEPENDENT DISPLACEMENT INPUT METHOD

The time-dependent displacement can be input into the base block on the prescribed displacement-constraint points (Fig.5.3). During simulation, the displacements of these points are enforced to following the value of time-dependent displacement input. The behavior of the upper sliding block is governed by the gravity force, frictional and contact forces. This input method was used by Nishiyama et al. (2004) on simulation the behavior of a masonry retaining wall in Japan.

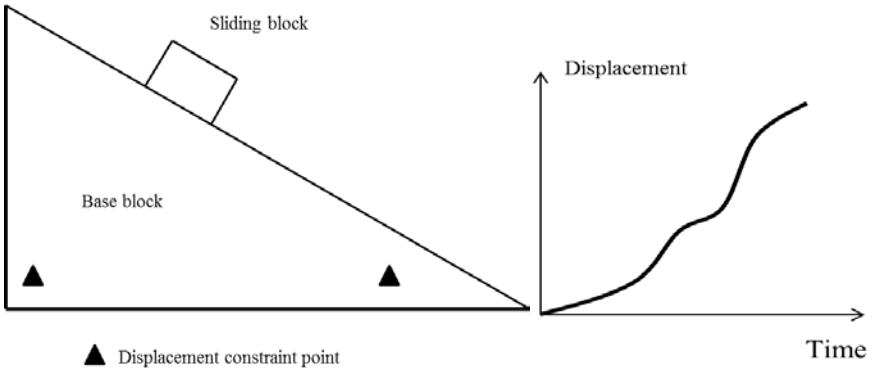

Fig.5.3 The sketch of time-dependent displacement inputs.

Assuming (u,v,w) as the displacement of the prescribed displacement constraint point (x_0,y_0,z_0) in block i, a stiff spring is used to force its virtual displacement to (u,v,w). By minimizing the strain energy of the spring, the corresponding 12 × 12 sub-matrices and 12 × 1 sub-matrices are obtained and added to the global stiffness matrices k_{ii}, and the global force sub-matrices, F_i , in the global equilibrium equation respectively, as shown as below

$$kT_i^T(x_0, y_0, z_0)T_i(x_0, y_0, z_0) \to k_{ii} \tag{5.2}$$

$$kT_i^T(x_0, y_0, z_0)\begin{bmatrix} u \\ v \\ w \end{bmatrix} \to F_i \tag{5.3}$$

Where, k is the stiffness of the spring, and T_i is the displacement function of block i. This method is an indirect method because the input displacements are double integrated from the time-dependent accelerations. Therefore, in theory, this method can get the same result as acceleration input method.

5.2.3 VERIFICATION BY THEORETICAL SOLUTION

The time-dependent acceleration input method is used in the following 3D-DDA simulation. When the sliding system is excited by seismic loading added on the base block (Fig. 1), the velocity and displacement of the base can be calculated by the Newmark's iterative equations. When the sliding block slides, it will be displaced under the seismic loading, the supporting force N, and the friction force f. If the upper block slides downwards relatively to the base, it can be derived that

$$mg\sin\alpha - f = m\left(a_{2x}\cos\alpha - a_{2y}\sin\alpha\right) \tag{5.4}$$

$$N - mg\cos\alpha = m\left(a_{2x}\sin\alpha + a_{2y}\sin\alpha\right) \tag{5.5}$$

where a_{2x} and a_{2y} are the accelerations of the upper block in the x and y direction, respectively. Defining a_{1x} and a_{1y} are the accelerations of the base block in the x and y direction, respectively. The requirement of the upper block of the upper block to slide along the base incline can be represent as

$$-\left(a_{2y} - a_{1y}\right) = \left(a_{2x} - a_{1x}\right)\tan\alpha \tag{5.6}$$

Combined with the sliding friction law $f = N\tan\phi$, the downward acceleration of the upper block in x direction can be deduced as

$$a_{2x}{}^{d} = \frac{(\cos\alpha\tan\phi - \sin\alpha)(g + a_{1x}\tan\alpha + a_{1y})}{(\cos\alpha\tan\phi - \sin\alpha)\tan\alpha - (\sin\alpha\tan\phi + \cos\alpha)} \tag{5.7}$$

where the superscript 'd' indicates the downward movement of the upper block relatively to the base. When the upper block slides upwards relatively to the base, the sliding friction law is $f = -N\tan\phi$. The upward acceleration of the upper block in x direction can be deduced as

$$a_{2x}{}^{u} = \frac{(-\cos\alpha\tan\phi - \sin\alpha)(g + a_{1x}\tan\alpha + a_{1y})}{(-\cos\alpha\tan\phi - \sin\alpha)\tan\alpha - (-\sin\alpha\tan\phi + \cos\alpha)} \tag{5.8}$$

here the superscript 'u' indicates the upward movement of the upper block relatively to the base.

Defining the velocity of the base block and upper block in the x direction as v_{1x} and v_{2x} respectively, the acceleration of the upper block in x direction a_{2x} can be drowned by the following criteria:

$$\begin{array}{lll}
\text{if } v_{2x} = v_{1x} & \text{if } a_{1x} < a_{2x}{}^{d} & a_{2x} = a_{2x}{}^{d} \\
 & \text{if } a_{1x} > a_{2x}{}^{u} & a_{2x} = a_{2x}{}^{u} \\
 & \text{if } a_{2x}{}^{d} \le a_{1x} \le a_{2x}{}^{u} & a_{2x} = a_{1x} \\
\text{if } v_{2x} \neq v_{1x} & \text{if } v_{1x} < v_{2x} & a_{2x} = a_{2x}{}^{d} \\
 & \text{if } v_{1x} > v_{2x} & a_{2x} = a_{2x}{}^{u}
\end{array} \tag{5.9}$$

A similar 3D model (Fig. 5.4) is used by DDA to compare the simulation result with the above theoretical solutions. In Fig. 3, the inclined angle is set to 30 degree

and the friction angle between the two blocks is 15 degree. Only the horizontal acceleration is used for simulation. A harmonic function is added to the base block as the excitation of the system, which is $a_{1x} = 5\sin(2\pi t)$.

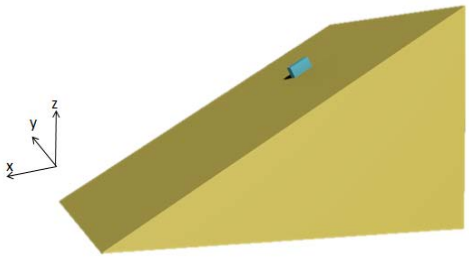

Fig. 5.4 The simulation model

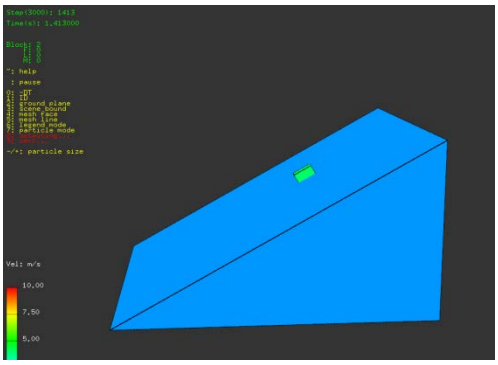

Fig. 5.5 The snapshot of DDA simulation process, simulation time is 1.413s

In Fig. 5.4, the color has no physical meaning and is used to distinguish the sliding block and the base. The Fig. 5.5 shows a snapshot of the simulation process, the color represents the magnitude of the velocity. The simulation period is 2 seconds, with a time step of 0.001s. As the excitation is add on the base block, with a simple harmonic form, the theoretical displacement can be get by twice time integration. The Fig. 5.6 shows the simulated displacement of the base block coincide greatly well with the theoretical solution.

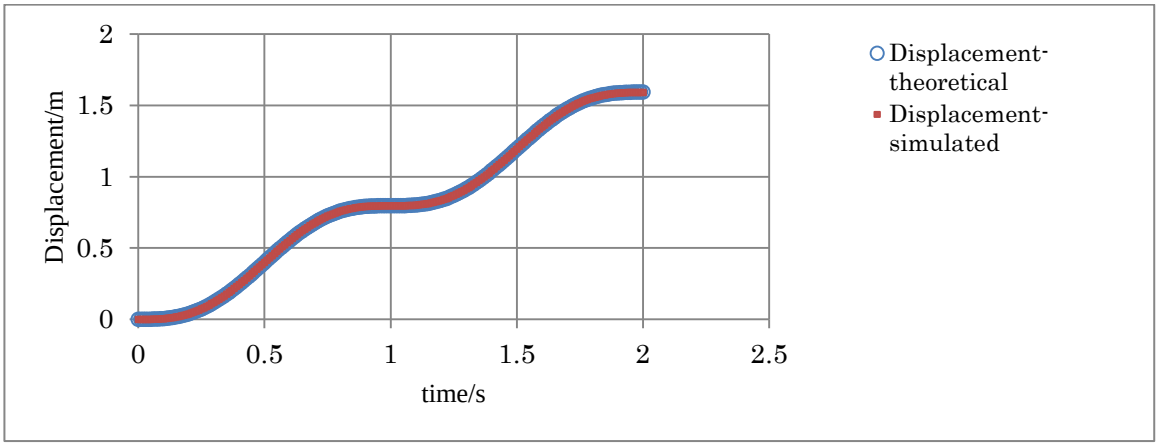

Fig. 5.6 A comparison between the simulated and the theoretical result of base block's horizontal displacement

A compare between the analytical solution and simulation result of the

horizontal displacement of sliding block is shown in Fig. 5.7. It can be seen that the DDA simulated result agrees well with the theoretical solution.

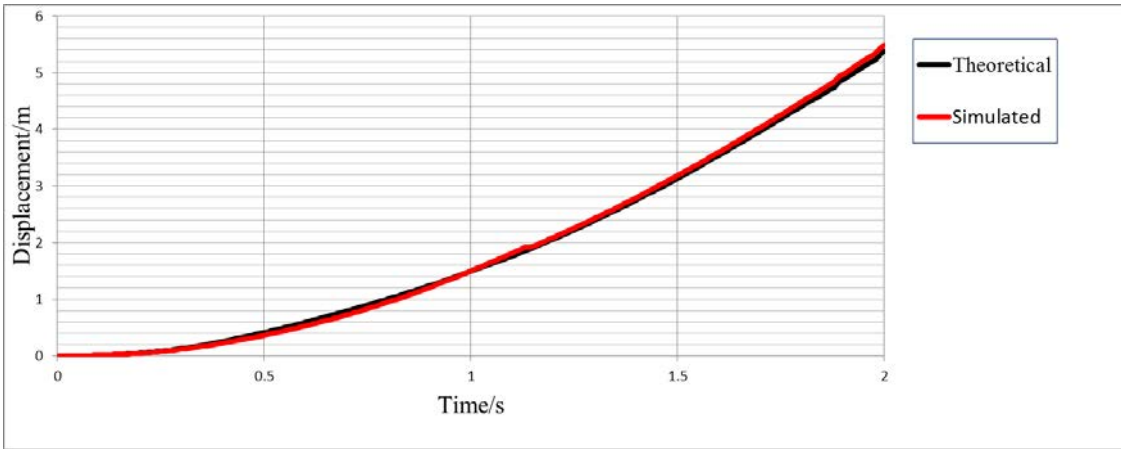

Fig. 5.7 A comparison between the simulated and the theoretical result of sliding block's horizontal displacement.

Although the DDA simulation result agrees well with the theoretical solution, the simulation result can not coincide exactly with the theoretical solution. One reason is the theoretical solution is based on the assumption that both the sliding block and the base are rigid bodies. Another reason is the simulate result somewhat depend on the control parameters it used. One important parameter is the simulation time step. If we take the theoretical solution as the true value, the relative difference between the simulated result and the theoretical solution can be seen as the relative error. When using the different time step, the relative error of the simulated displacement is different. Fig.5.8 shows the relative error when time step is 0.01s and 0.001s respectively. It can be found that when time step is 0.001s, the relative difference is easier to get close to zero than the 0.01s. In order to get a more accurate simulation result, a smaller time step is needed.

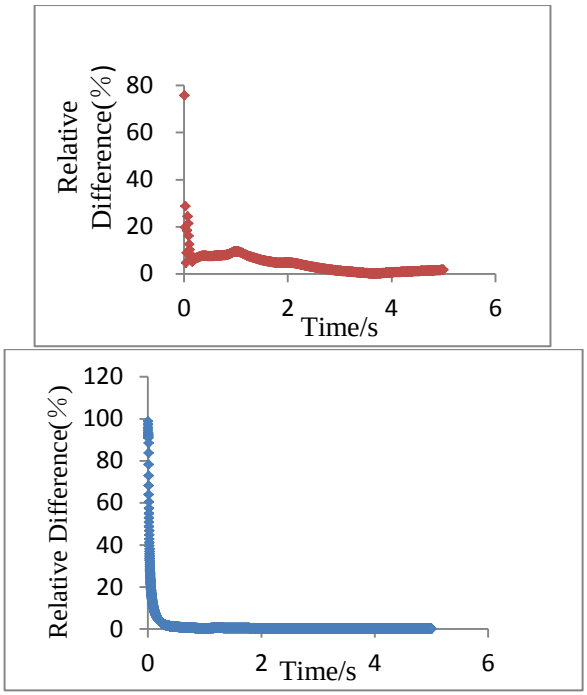

Fig. 5.8 The relative difference of displacement when the simulation time step is 0.01s (top) and 0.001s (bottom).

5.3 ADDING ANCHOR REINFORCEMENT FUNCTION IN DDA

5.3.1 THE ALGORITHM OF ADDING ANCHOR REINFORCEMENT

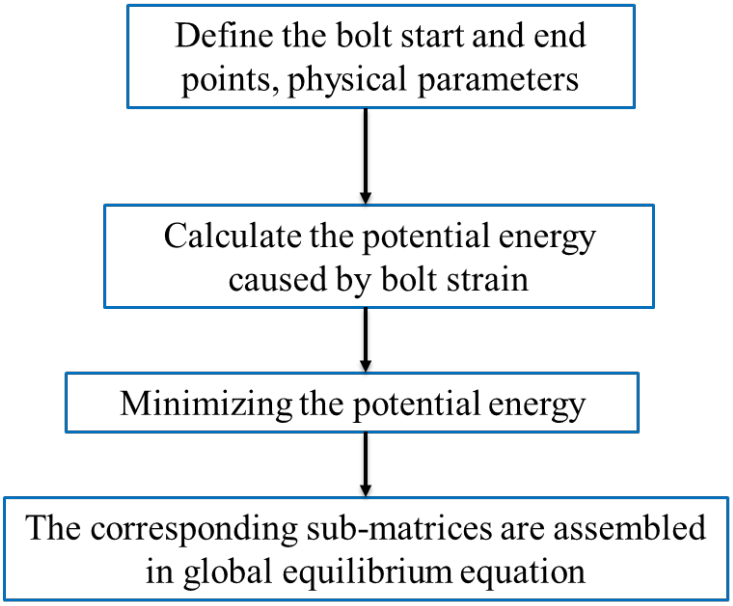

Figure 5.9 The main process of adding anchor function in DDA

Consider a anchor passing through point a $(x_1 \quad y_1 \quad z_1)$ and b $(x_2 \quad y_2 \quad z_2)$ belonging to blocks i and j, separately as shown in Fig.5.10.

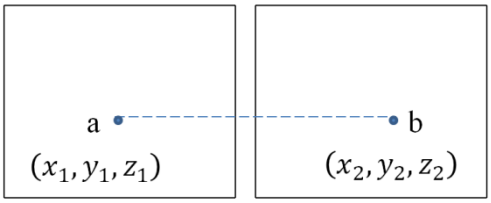

Fig5.10. Geometry of the anchor

The length of the anchor is $l = \sqrt{(x_1 - x_2)^2 + (y_1 - y_2)^2 + (z_1 - z_2)^2}$. Defining the direction cosines of the blot are $l_x = (x_1 - x_2)/L$, $l_y = (y_1 - y_2)/L$ and $l_z = (z_1 - z_2)/L$. If the blocks move, the integral is the blot length dl can be expressed by

$$dl = \left[\left[D_i\right]^T \left[T_i\right]^T \begin{Bmatrix} l_x \\ l_y \\ l_z \end{Bmatrix} - \left[D_j\right]^T \left[T_j\right]^T \begin{Bmatrix} l_x \\ l_y \\ l_z \end{Bmatrix} \right] \tag{5.10}$$

The potential energy can be expressed as

$$\Pi_b = \frac{k}{2l} dl^2 \tag{5.11}$$

Where k represents the elastic stiffness of the anchor.

Minimizing the potential energy by taking the derivatives, the corresponding four sets of 12 × 12 sub-matrices are obtained and added to the global force matrices in the global equilibrium equation, as shown as below

$$\frac{k}{l}\left[E_i\right]\left[E_i\right]^T \rightarrow \left[k_{ii}\right] \tag{5.12}$$

$$\frac{k}{l}\left[E_j\right]\left[E_j\right]^T \rightarrow \left[k_{jj}\right] \tag{5.13}$$

$$-\frac{k}{l}\left[E_i\right]\left[E_j\right]^T \rightarrow \left[k_{ij}\right] \tag{5.14}$$

$$-\frac{k}{l}\left[E_j\right]\left[E_i\right]^T \rightarrow \left[k_{ji}\right] \tag{5.15}$$

In the above four functions the E_i and E_j are expressed by $E_i = \left[T_i\right]^T \left[l_x \;\; l_y \;\; l_z\right]^T$ and $E_j = \left[T_j\right]^T \left[l_x \;\; l_y \;\; l_z\right]^T$ separately. During the simulation the length of anchor is updated after each time step. The limit of the anchor extension length can be set beforehand. Besides the simple elastic model, the elastic-plastic anchor model can also be used.

5.3.2 THE NEW TYPE ANCHOR MECHANISM

As a kind of elastic-plastic model, the constant resistance and large deformation are two main characteristics of the CRLD anchor, of which He anchor (2014) is one typical example. This anchor consists of mass element, spring element, and a stick-slip element. For the spring element, it can be simulated easily. The stick-slip behavior can be seen in Fig. 5.11. The $P_{\max}$ and $P_{\min}$ represents the maximum and minimum resistance force. The constant resistance zone exists between these two

values. The elongation of this kind of anchor can reach 1000mm showing the pattern of large deformation.

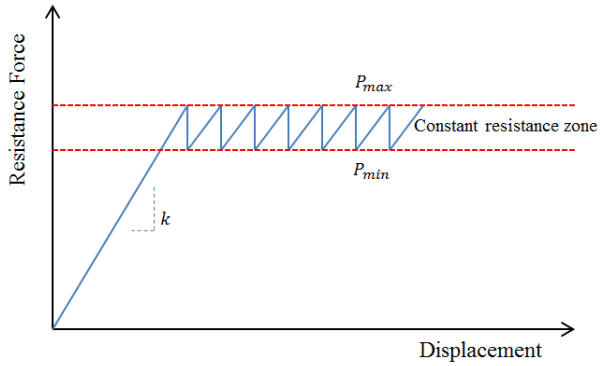

Fig. 5.11 Force- displacement relationship showing the stick-slip behavior, after He (2014).

This paper uses a simplified model, which uses a constant resistance force. The simplified model performs like a elastoplastic model as Fig. 5.12 shows.

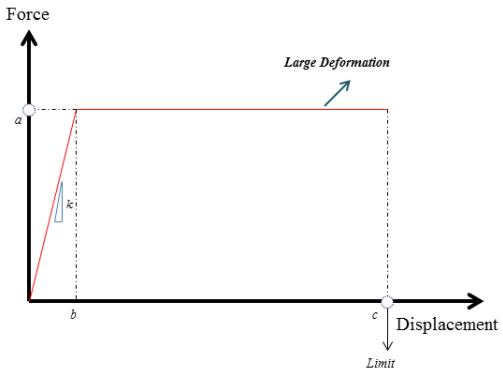

Fig. 5.12 Simplified model of the CRLD anchor

In the Fig. 5.12, the point a represents the constant resistance when the elastic displacement completes, which can be seen as a tension limit. The point b is the maximum elastic displacement, c is a displacement limit, the maximum displacement of the anchor when the anchor lost its efficiency, and k is the elastic stiffness of the anchor.

5.3.3 SIMULATION VERIFICATION

To verify the anchor is very important before using it. A simple but direct simulation model is built containing two blocks. Two blocks are both cubic with side length of 5 meters having a separation distance of 1 meter. The red block is fixed by eight fixed points at corners. The blue one owns the gravity force of 2500kN, with density of 2000 kg/m3. A anchor is added shown as write dash line, which is located at the center of each block with a length of 6 meters as Figure 5.13 shows.

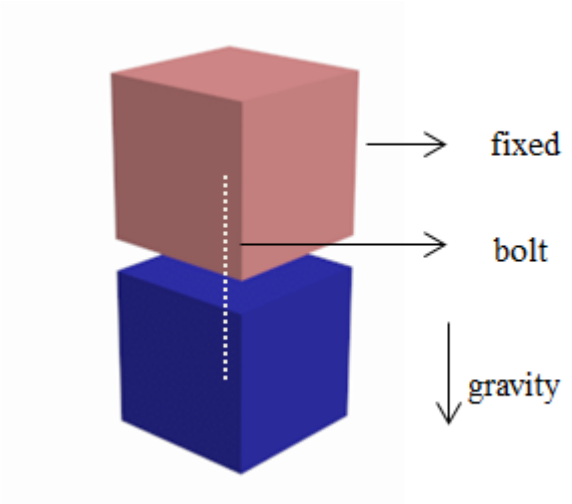

Fig. 5.13 The example with two blocks

Firstly, the simplified anchor model is completed by testifying the coincidence between the pre-set model type and the simulated result. The pre-set parameters for the He anchor model are constant resistance, anchor stiffness and displacement limit, which are 2000kN, 100Mpa and 1.5m. Using the dynamic mode, the simulated result of the relationship between the anchor displacement and anchor force can be seen from Fig. 5.14. We can see that the anchor mechanism behaves a well consistency with the pre-set model.

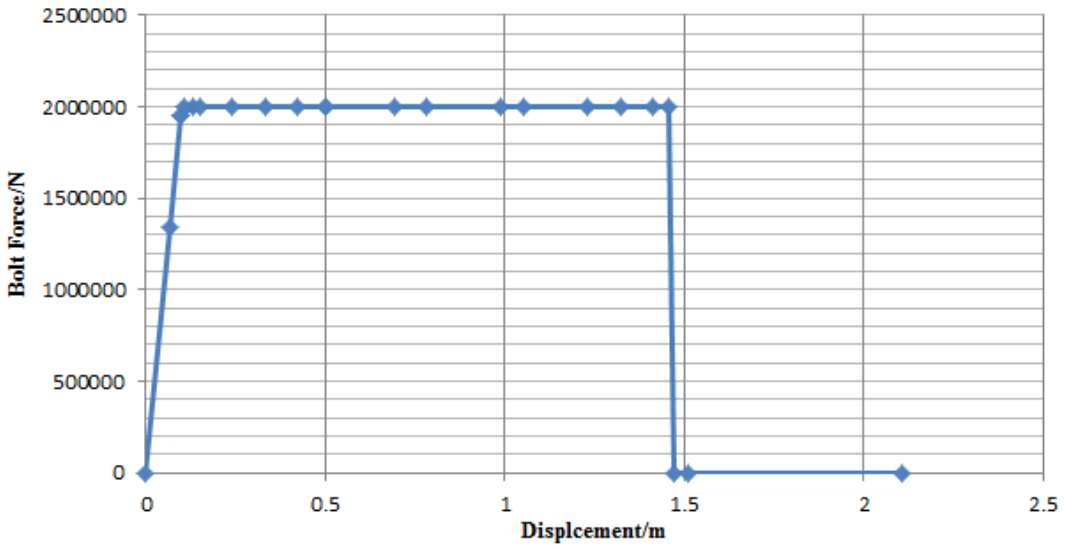

Fig. 5.14 The relationship between anchor displacement and anchor force

In the above example, the below anchor will finally drop because the gravity force 2500kN is larger than the constant resistance 2000kN. If the value of anchor's constant resistance is increased to be equal or larger than the gravity force, the under block will finally stop. Fig. 5.15 shows two kind of situation when the simulation time is one second, the left one with a constant resistance of 2200kN and right one of 2800kN.

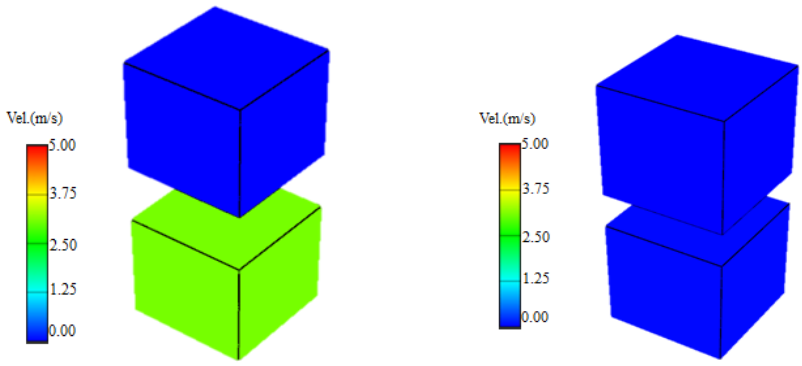

Fig. 5.15 Compare the block state of different constant resistant force, left one 2200kN and right one 2800kN; Simulation time is one second.

A simplified slope model is built, as Fig. 5.16 shows. There are total 347 blocks

in the simulation. The dip angle of foliation plane is 60°. A horizontal anchor is set inside the slope shown as a green line. Some parameters of the 3D DDA simulation are listed as Table 5.1.

Table5.1. Mechanical properties and computational parameters

Parameters	Value
Density ρ (kg/m3)	2,000
Young's modulus E (GPa)	5
Poisson's ratio υ	0.2
Gravitational acceleration (m/s2)	9.8
Friction angle (°)	10
Penalty spring stiffness k (kN/m)	5.0 × 1010
Time step (s)	10-3

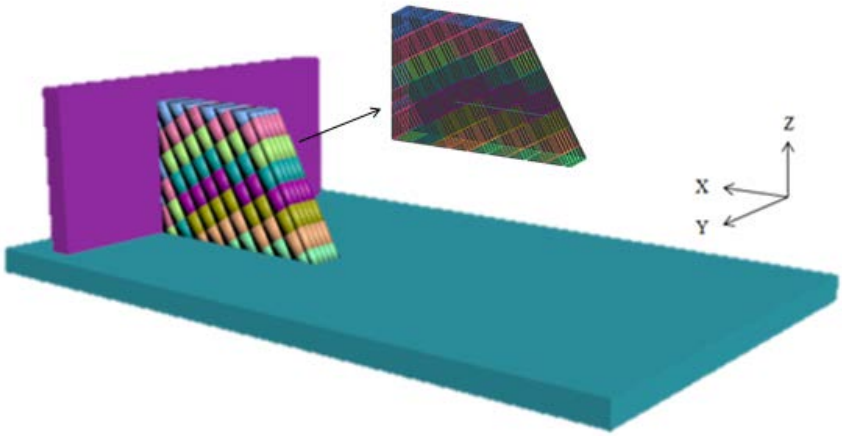

Fig. 5.16 Geometry of the simulation model

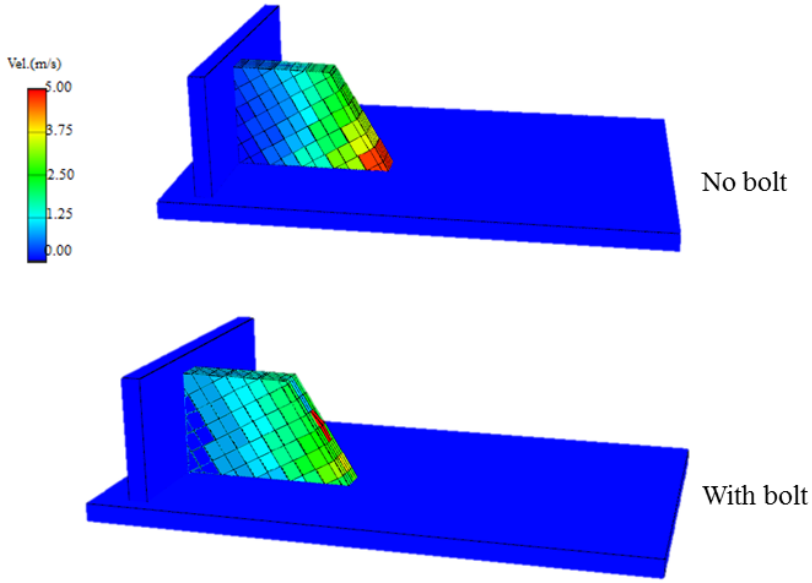

Fig. 5.17 The simulation of the anchor effect; simulation time is 1s

Computation of three dimensional DDA uses 10000 time steps, 0.001 second per step. The dynamic ratio is 1.00. It means the next time step inherent all of the velocity from the previous time step. The slope will failure as the friction angle 10

degree is much smaller than the dip angle of the plane. The final failure situation needs a rather long time, and the simulation result just shows the state of the beginning of the failure happens. As shown in Fig. 5.17, the anchor has an evident influence on the deformation of the slope. The two blocks locating above the reinforced block are extruded, which does not happen when blot is not added. The anchor has influence on the block at the toe area resulting in a different velocity pattern compared with no anchor example.

5.4 CONCLUSIONS

The existing 3D DDA method can be extended by adding the function of seismic loading and the anchor reinforcement. These two extensions are necessary and meaningful as the seismic loading is one of the major factors that can induce the landslide and the anchor reinforcement is a common and useful technique for the reinforcement of the slide-prone slides.

For the adding of seismic loading function, there are two major adding methods, adding the displacement wave or the acceleration wave, the chosen of which depends on the data available. Then, the verification has been made to demonstrate that not only the base block, on which the seismic loading is applied, but also the relevant slide block can perform accurately when compared with the theoretical solution. Moreover, the time steps affect the simulation accuracy when the seismic loading is applied. In theory, the smaller the time step is the more accurate the simulation result can be got if the efficiency is not considered.

For adding the function of anchor reinforcement in the 3D DDA program, the sub-matrices sourcing from the anchor's strain energy can be implied into the 3D DDA program, and the anchor's mechanism can be simulated accurately. Moreover, not only the common anchor function but also the new type of blot can be simulated by the 3D DDA method.

REFERENCES

Hatzor Y H, Feintuch A. 2001. The validity of dynamic block displacement

prediction using DDA. International Journal of Rock Mechanics and Mining Sciences, 38(4): 599-606.

J. Liu, X. Kong, & G. Lin. (2004). Formulation of the three-dimensional discontinuous deformation analysis method. Acta Mech Sinica, 20 (3), 270–282.

Jibson R W. 1993. Predicting earthquake-induced landslide displacements using Newmark's sliding block analysis. Transportation Research Record, 9-9.

M. He, Weili Gong etal. (2014). Development of a novel energy-absorbing bolt with extraordinarily large elongation and constant resistance. International Journal of Rock Mechanics & Mining Sciences, 67, 29–42.

MacLaughlin M M, Doolin D M. 2006. Review of validation of the discontinuous deformation analysis (DDA) method. International Journal for Numerical and Analytical Methods in Geomechanics, 30(4), 271-305.

Nishiyama S, Ohnishi Y, Yanagawa T, et al. 2004. Study on stability of retaining wall of masonry type by using discontinuous deformation analysis. Proceedings of the ISRM International Symposium 3rd ARMS, 1221-6.

N.M. Newmark. 1965 Effects of earthquake on dams embankments. Geotechnique, 15, 139-160.

R.E. Goodman, H.B. Seed. 1966. Earthquake induced displacements in sands and embankments. J Soil Mech Foundation Div ASCE, 92, 125-146.

Shi G. & Goodman R. E. (1989). Generalization of two- dimensional discontinuous deformation analysis for forward modelling. International Journal for Numerical and Analytical Methods in Geomechanics. 13, 359-380.

Shi GH. (2001). Three dimensional discontinuous deformation analysis. In Rock Mechanics in the National Interest, Proceedings of the 38th U.S. Rock Mechanics Symposium, Elsworth D, Tinucci JP, Heasley KA (Eds). American Rock Mechanics Association, Balkema: Rotterdam, Washington DC, 1421–1428.

Shi, G. H. (2009). Applications of discontinuous deformation analysis (DDA) to rock engineering. Computational Mechanics (pp. 136-147). Springer Berlin Heidelberg.

Shi G, Goodman R E. 1984. Discontinuous deformation analysis[R]. Lawrence Berkeley Lab., CA (USA).

Shi GH. 1988. Discontinuous deformation analysis: a new numerical model for the statics and dynamics of block systems. Doctoral dissertation, University of California, Berkeley.

Sasaki T, Hagiwara I, Sasaki K, Yoshinaka R, Ohnishi Y, Nishiyama S. 2004. Earthquake response analysis of rock-fallmodels by discontinuous deformation analysis. In Proceedings of the ISRM International Symposium 3rd ARMS, 1267–1272.

Tsesarsky M, Hatzor Y H, Sitar N. 2005. Dynamic displacement of a block on an inclined plane: analytical, experimental and DDA results. Rock Mechanics and Rock Engineering, 38(2): 153-167.

Yeung, M. R. (1993, December). Analysis of a mine roof using the DDA method. International journal of rock mechanics and mining sciences & geomechanics abstracts, 30 (7), 1411-1417, Pergamon.

Zhang Y, Chen G, Zheng L, et al. 2013. Effects of near-fault seismic loadings on run-out of large-scale landslide: a case study. Engineering Geology, 166, 216-236.

CHAPTER 6

VERIFICATIONS AND APPLICATIONS

6.1 INTRODUCTION

The Daiganji slope located at the coastal area of Oita prefecture, as Figure 6.1 shows.

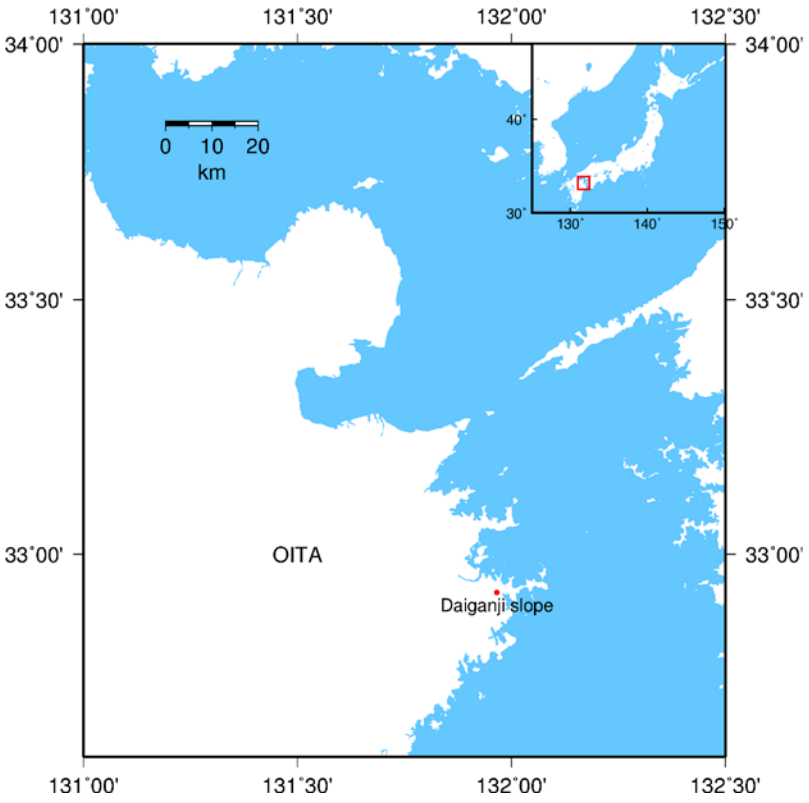

Fig. 6.1 The location of the Daiganji slope

A field investigation of this slope has been made and found that this slope has just located upward the tsunami excavation road and the houses (Figure 6.2)

Fig. 6.2 The houses and tsunami excavation road downward the Daiganji slope

Once the tsunami happens, the Daiganji slope may failure under the earthquake, which may lead to the damage of not only the houses but also the excavation road. When the excavation road is destroyed by the earthquake, the threat of earthquake induced tsunami will be enlarged, and the catastrophe may happen. In history, the big earthquake and tsunami has happened, as we can found from the monument shown in Figure 6.3. Therefore, it is of practical meaning to make a research about this slope.

table

Fig. 6.3 The monuments of the historical big earthquake and tsunami

The field investigation and laboratory tests have been made on this slope to prepare for the deep research. The investigation net can be found in the Figure 6.4 and the blue points represent the sites that the simple penetration tests are performed (Figure 6.5). According to simple penetration tests, the depth of the upper slide-prone parts can be determined. This depth is very useful for the estimation of sliding surface for the 2D and 3D analysis.

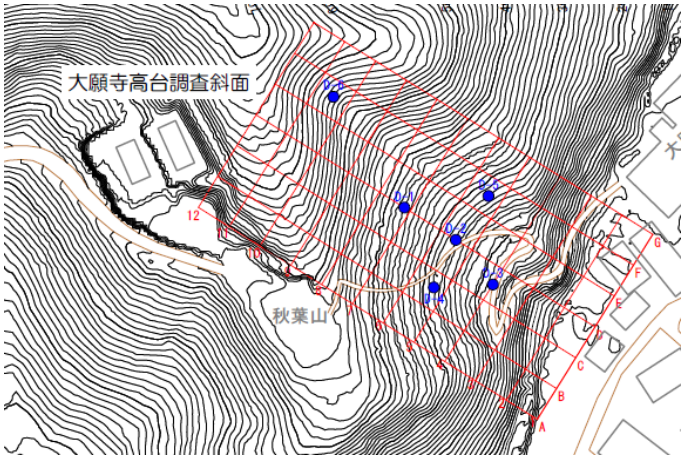

Fig. 6.4 The investigation area and the sites of simple penetration test

Fig. 6.5 The operation of simple penetration test

According to the simple penetration test (SPT), the Nd value can be got, which is the impact number for the penetration depth of 10 cm. This Nd number can be used to estimate the slide-prone depth under rain or earthquake condition (Figure6.6). The estimated sliding depth can be found in Figure 6.7. It should be mentioned that the colors used in these two figures are kept in consistence.

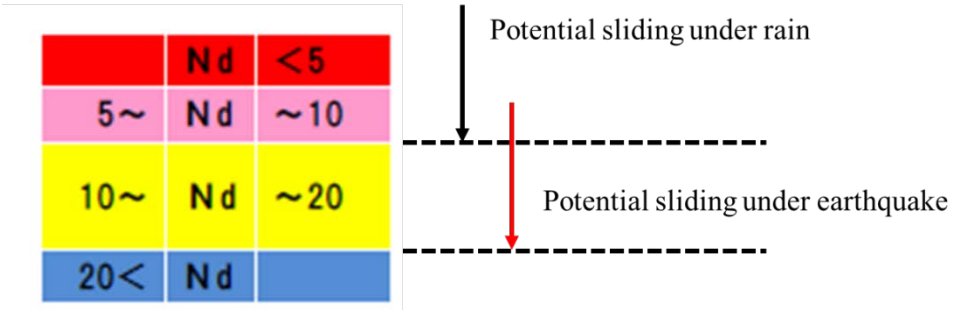

Fig. 6.6 The estimation of sliding depth based on Nd

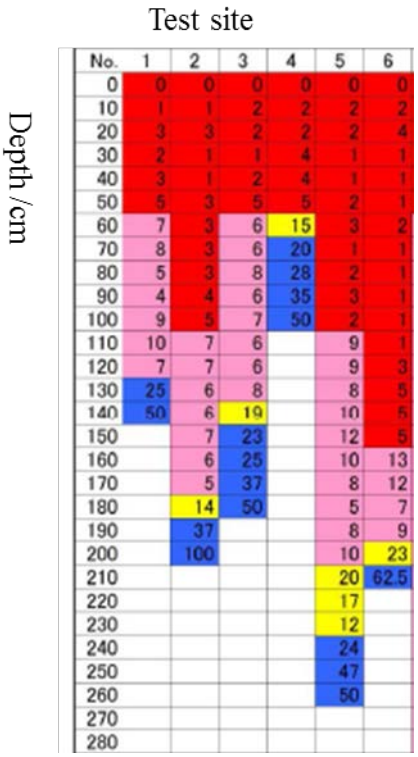

Fig. 6.6 The estimated slide depth for different test sites based on Fig. 6.5

According to the laboratory test, the physical parameters such as the density, the frictional angle and the cohesion strength can be obtained (Figure 6.7). The soil distribution of all sections in Figure 6.4 can be obtained, for instance the profile of section E can be found in Figure 6.8.

浦代浦(大願寺)地区

土層名	Nd分布	地盤定数		
		湿潤重量 γt (kN/m3)	内部摩擦角 φ (度)	粘着力 c (kN/m2)
表土・崩積土	0 ＜ Nd ≦ 5	16	30	5
崩積土	5 ＜ Nd ≦ 10	16	30	5
風化土 [強風化岩]	0 ＜ Nd ≦ 10	18	35	10
風化岩	10 ＜ Nd ≦ 20	21	40	10
弱風化岩	20 ＜ Nd	23	40	1000

Fig. 6.7 The physical parameters obtained from laboratory tests

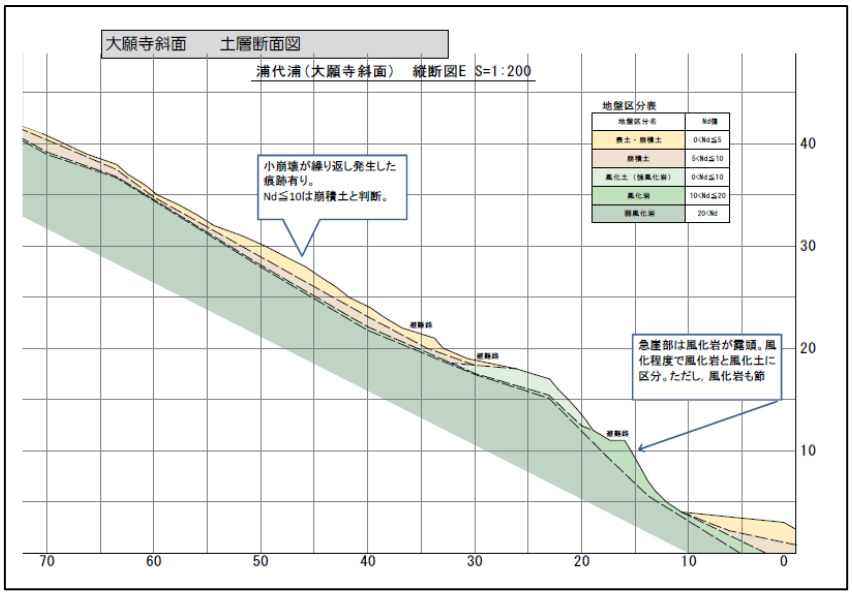

Fig. 6.8 The profile of the Section E according to the Nd value

Moreover, the GIS data has been prepared. Therefore, according to the introduction above, the condition for the deep research of the Daiganji slope is enough, and which will be performed in the following section parts.

6.2 THE STABILITY ANALYSIS WITHOUT SEISMIC LOADING

Firstly, the 2D DDA analysis is performed. For the section E (Figure 6.9), which can be considered as the symmetry section of the slope, the 2D DDA mode is constructed (Figure 6.10). There are totally 24o blocks are used for the simulation. The physical and simulation parameters that are used is listed in Table 6.1.

Table 6.1 The physical and simulation parameters for the 2D DDA simulation

Parameters	Value
Density ρ (kg/m^3)	2000
Young's modulus E (GPa)	5

Poisson's ratio υ	0.3
Cohesion (KPa)	5
Frictional angle(°)	30
Penalty spring stiffness (GPa)	10
Step allowed displacement ratio	0.001
Time step (second)	0.001

The shear strength reduction method that mentioned in 3.2.2 will be used to determine the factor of safety.

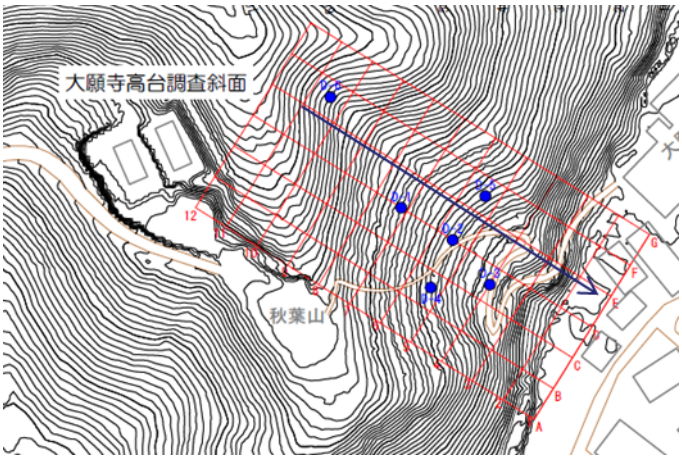

Fig. 6.9 The location of the section E

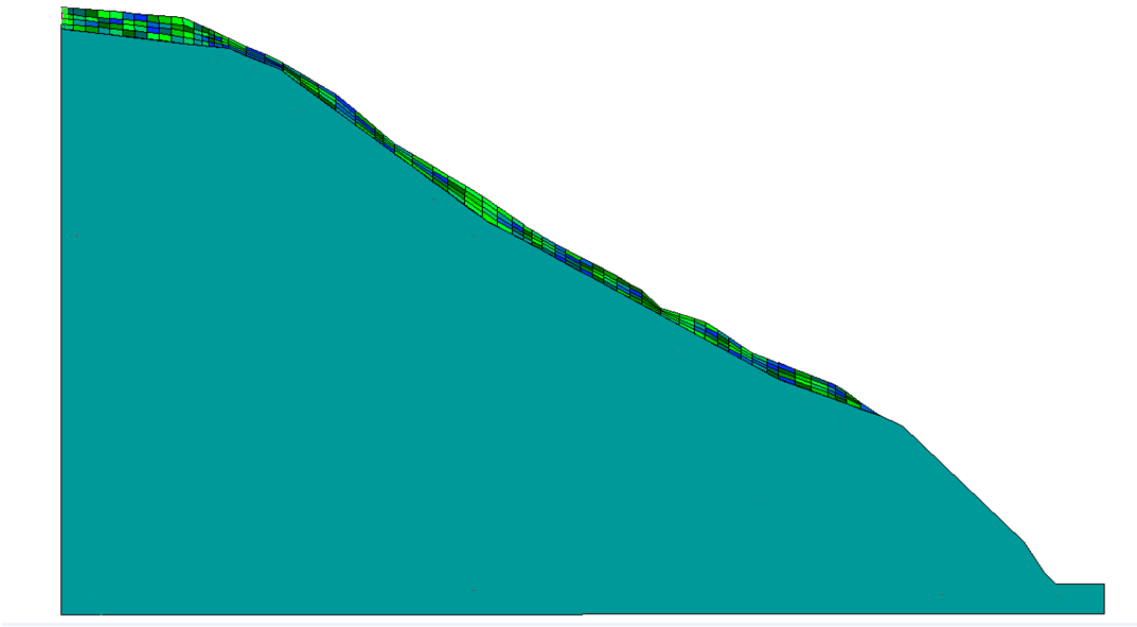

Fig. 6.10 The 2D DDA model for the section E

The toe block is set as the monitored point. The change of horizontal displacement with the shear reduction factor (SRF) when the simulation time is five seconds can be found in Figure 6.11. It is obvious that when the SRF is bigger than 1.31, the horizontal displacement will increase seriously, so this limit SRF is considered as the factor of safety.

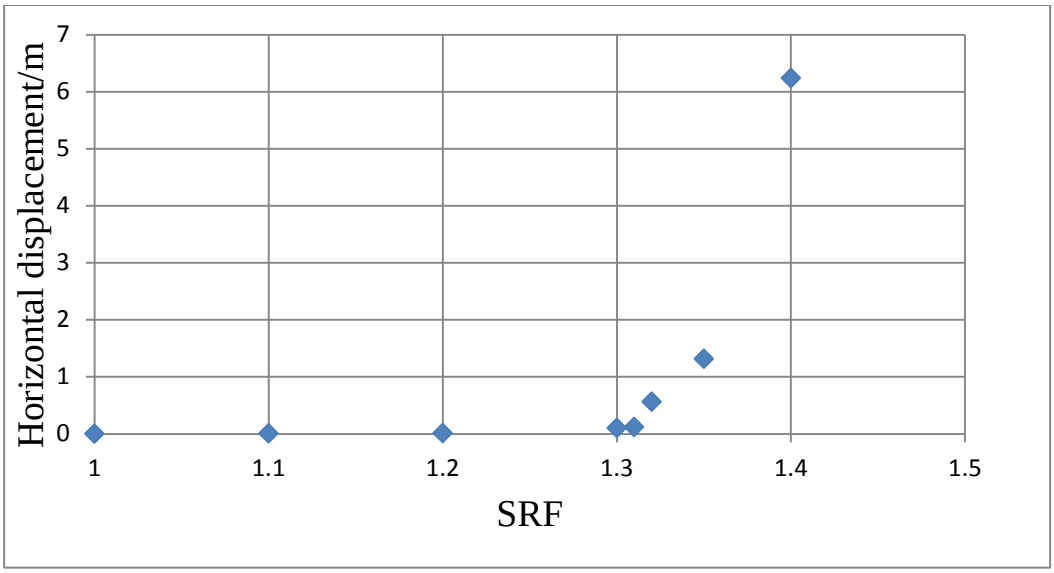

Figure 6.11 The change of SRF with the toe block's horizontal displacement

when the simulation time is five seconds

Another way to evaluate the factor of safety is the traditional limit equilibrium method. In this method, the potential circular sliding surfaces will be searched until the minimum factor of safety is achieved. The result of the equilibrium method can be found in Figure 6.12, in which factor of safety is 1.43.

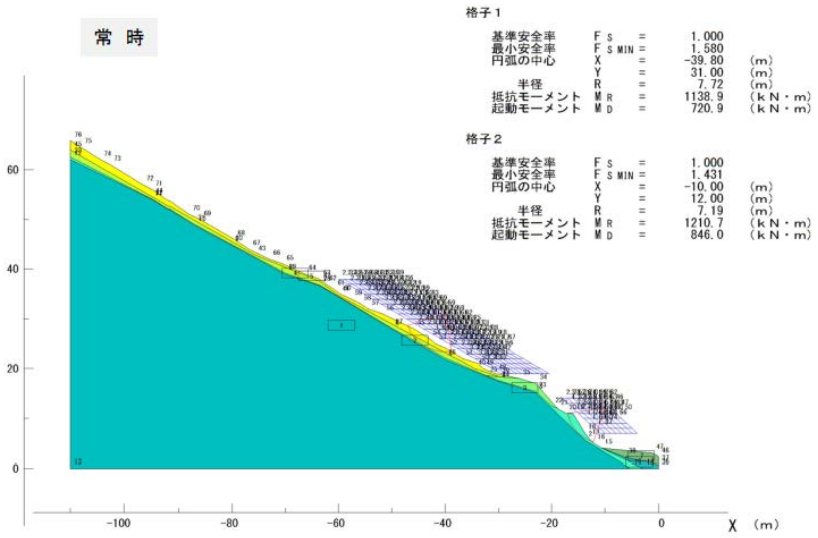

Figure 6.12 The factor of safety from the limit equilibrium method

The 3D DDA model was created for the 3D analysis of stability of the Daiganji slope, as shown in Figure 6.13. There are totally 67 blocks for the slide body.

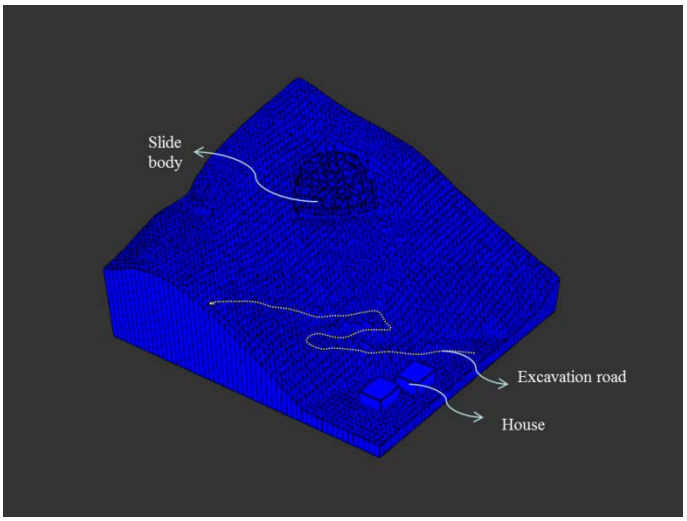

Figure 6.13 The 3D DDA model for the stability analysis

Similar to the 2D DDA analysis, the simulation uses the strength reduction method. The physical and simulation parameters for the 3D DDA simulation are listed as Table 6.2.

Table 6.2 The physical and simulation parameters for the 3D DDA simulation

Parameters	Value
Density ρ (kg/m^3)	2000
Young's modulus E (GPa)	5
Poisson's ratio υ	0.3
Cohesion (KPa)	5
Frictional angle(°)	30
Penalty spring stiffness (GPa)	5
Step allowed displacement ratio	0.01
Time step (second)	0.0001

Table 6.2 The physical and simulation parameters for the 3D DDA simulation

The monitored block is block 57, which is locating at the toe of the slope (Figure 6.14). When the strength reduction performs each time, the displacement of the monitored block will be recorded at a certain simulation time.

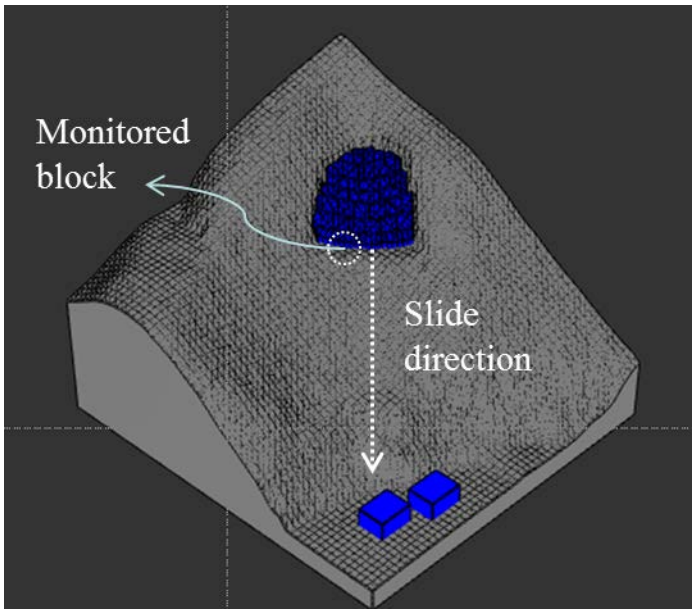

Figure 6.14 the monitored block for the 3D DDA simulation

The Figure 6.15 shows the horizontal displacement along the slide direction various when the SRF changes, using the monitored time of two seconds. It can be found that the limit of SRF, also the factor of safety (FOS) is around 1.7. The Table 3 summarized the result of three methods when calculating the FOS without considering the seismic loading. It can be seen from table 6.3 that: 1) the FOS got from the 3D DDA is almost 25% bigger than the result from the 2D analysis; 2) the FOS from the 2D methods, the DDA or limit equilibrium is nearly the same with the DDA's is slightly higher than the limit equilibrium.

Method	3D DDA	Limit equilibrium method	2D DDA method
FOS	1.70	1.43	1.31

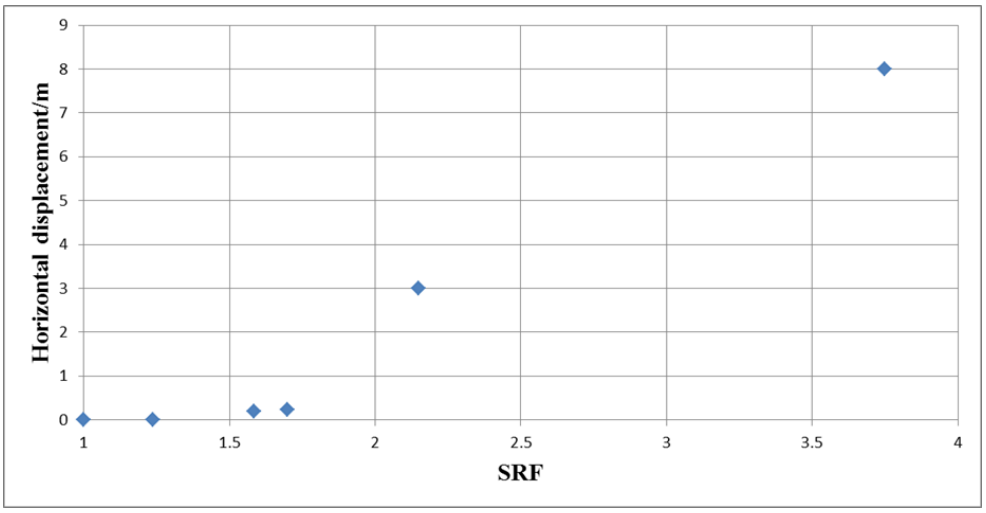

Figure 6.15 the horizontal displacement of the monitored block when the SRF changes (time=2seconds)

6.3 THE STABILITY ANALYSIS WITHOUT SEISMIC LOADING

In this section, the analysis of the Daiganji slope under the seismic load by the 3D DDA method will be performed. Before doing the seismic analysis, it is necessary to make sure that the seismic loading is accurately reflected especially when it is applied to the huge 3D terrain. Therefore, preliminarily, the relevant verification is executed. Then the focus is on two objects: 1) the failure under seismic loading; 2) the influence of seismic loading on the stability.

6.3.1 THE VERIFICATION OF APPLIED SEISMIC LOADING

The applied seismic loading is on the base 3D terrain (Figure 6.15). This is more proper than other seismic applied methods. If the seismic loading is considered on the sliding parts no matter the real seismic loading or the weight related factor as that in the quasi-static method, they all deviates the real situation. For the real earthquake, the seismic shake directly happened on the ground, and the performance of the sliding parts is just the indirect result.

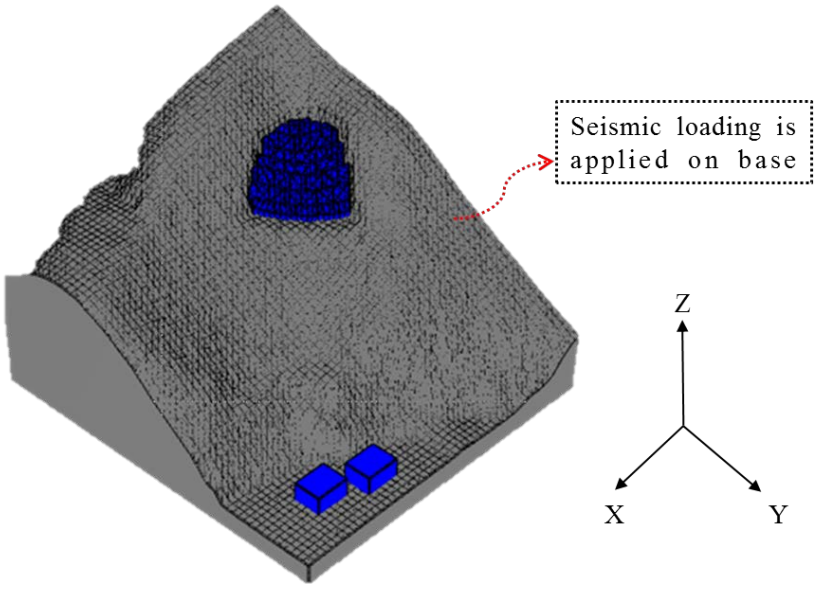

Figure 6.15 the seismic loading on the base for the 3D DDA model

In this section, no vertical seismic loading is considered. The applied seismic loading a_{xy} is almost on the same as the slide direction (Figure 6.16). The components a_x and a_y are applied on the x and y direction separately.

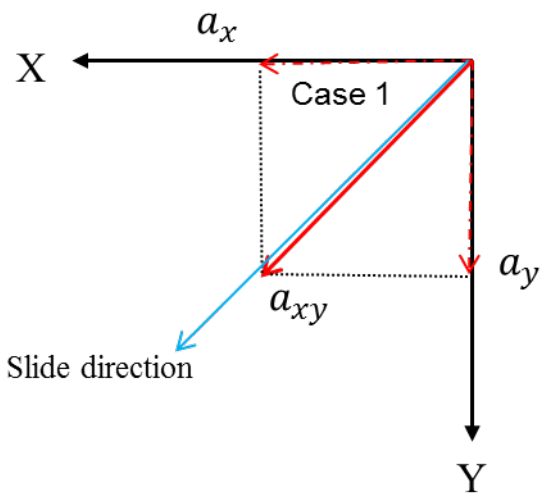

Figure 6.16 The illustration of the direction of seismic loading

These two components are necessary because of the data structure in the 3D DDA makes only the seismic on three directions, x, y, and z, can be read directly. In this section, the $a_x = a_y$= 15sin (8πt), which will lead the $a_{xy} = 21.21\sin(8\pi t)$, shown as Figure6.16. It is clearly that the peak acceleration of the applied sine-shape acceleration wave is 21.21m/s^2, and the period is 0.25s.

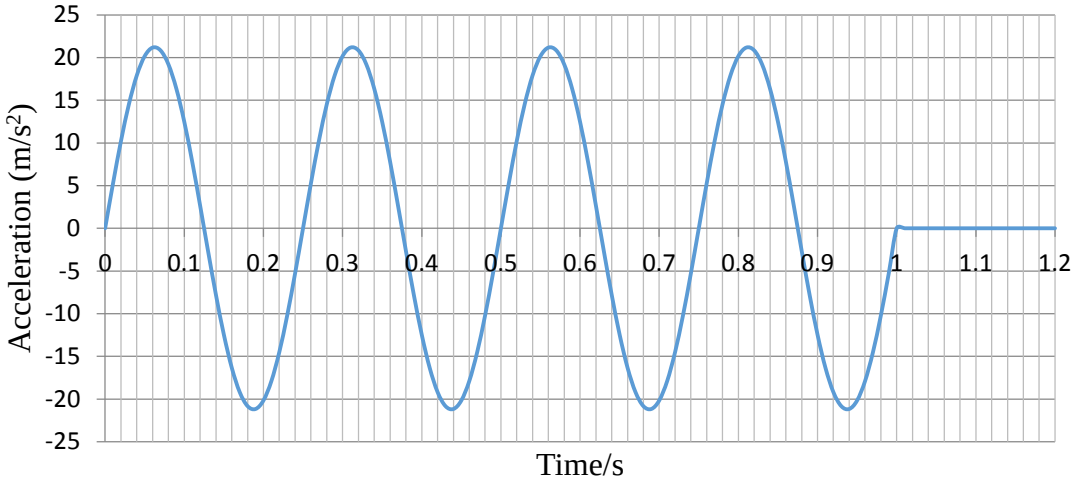

Figure 6.17 The applied acceleration pattern

If the initial velocity and displacement is set to be zero, that is $v_{ini} = 0$ and

$d_{ini} = 0$. The relevant velocity and displacement can be calculated by once and twice time integration individually. The calculated velocity and displacement are $v_{xy} = 21.21(1 - \cos(8\pi t))/8\pi$, and $d_{xy} = \left(-\frac{21.21\sin(8\pi t)}{64\pi^2}\right) + \frac{21.21t}{8\pi}$ shown as Figure 6.18(a), (b).

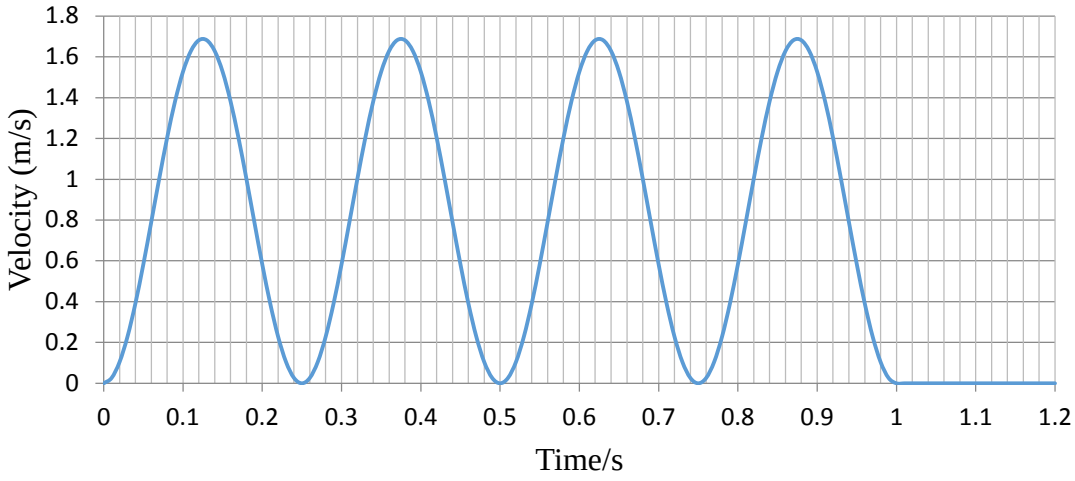

(a) The calculated velocity pattern, v_{xy}

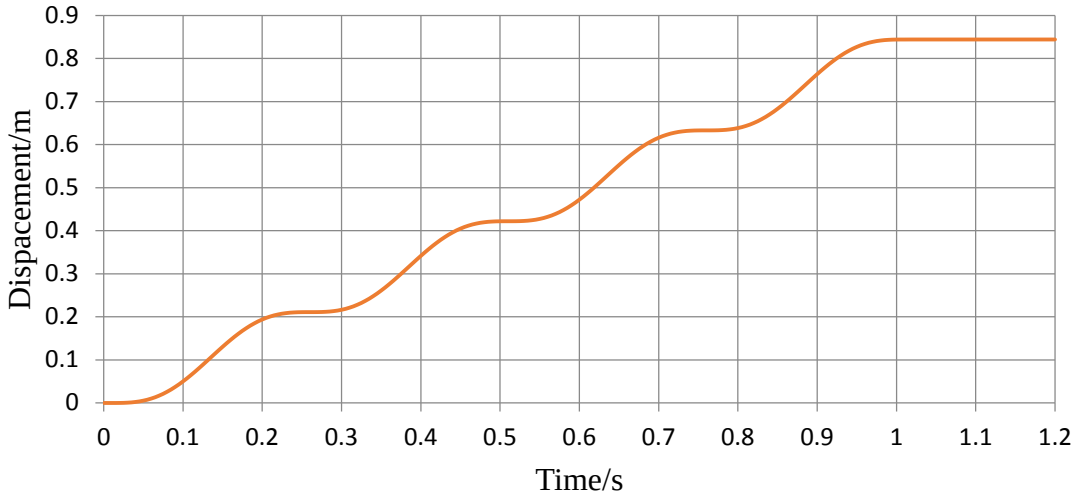

(b) The calculated displacement pattern, d_{xy}

Figure 6.18 The calculated velocity and displacement pattern, v_{xy} and d_{xy}

Then the acceleration will be applied on the base terrain of the 3D Daiganji model. There are important points that are needed to be illustrated: 1) using the difference method to resolve the inconsistent between the input accelerated data's time interval and the 3D DDA's time interval. The normally input time interval of acceleration wave is 0.01s. However, for the 3D DDA simulation, the time interval for calculation is almost ten or thousand times smaller than this value so, the difference method is used to make 3D DDA get the more accurate result; 2) the set of velocity to be zero when the seismic loading is finished loading. In the example of this section, it is not obvious because of the full for period of sine-shaped acceleration makes the velocity to be zero at the end. However, if the real earthquake acceleration wave is input, there is normally a residual velocity at the end of seismic loading during the simulation, for the real situation, there will be no velocity left after the earthquake. So, it is necessary and of practical meaning. As just an example to show the dynamic movement of the 3D terrain, two snapshots during the simulation are given in Figure 19 (a) and (b).

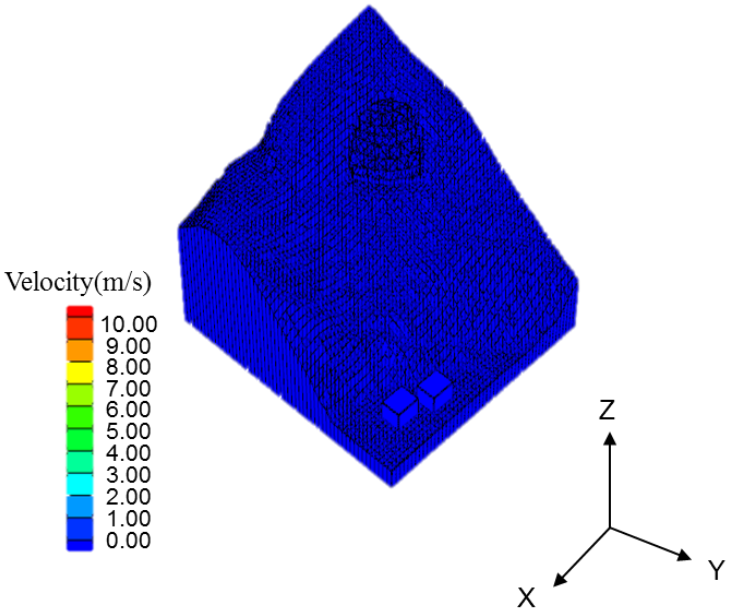

(a)

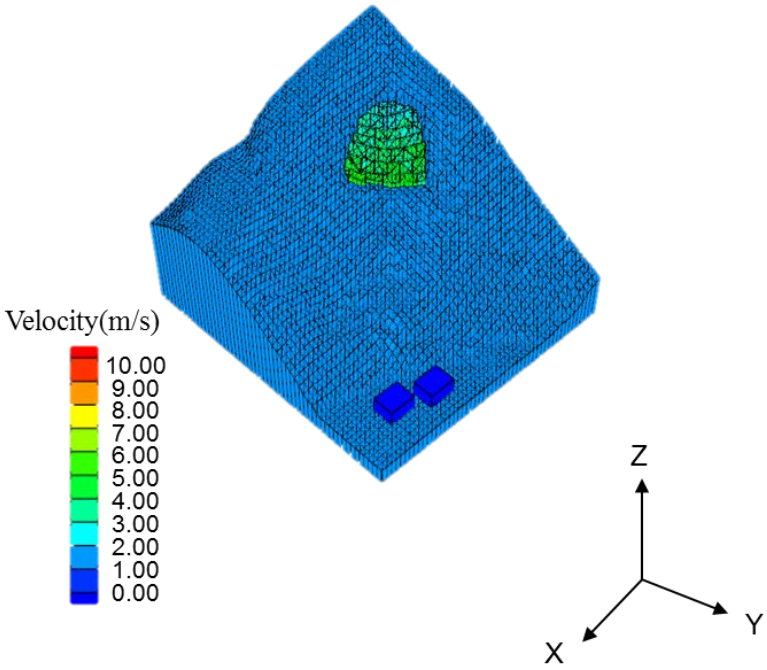

(b)

Figure 6.19 The snapshots to show the movements of the 3D terrain. (a) time=0.25s, (b)time=0.9s.

The comparison between the simulated velocity and the above mentioned calculated theoretical solution is shown on Figure 6.20. It can be found that this is a great consistent between the velocity result of 3D DDA and the theory.

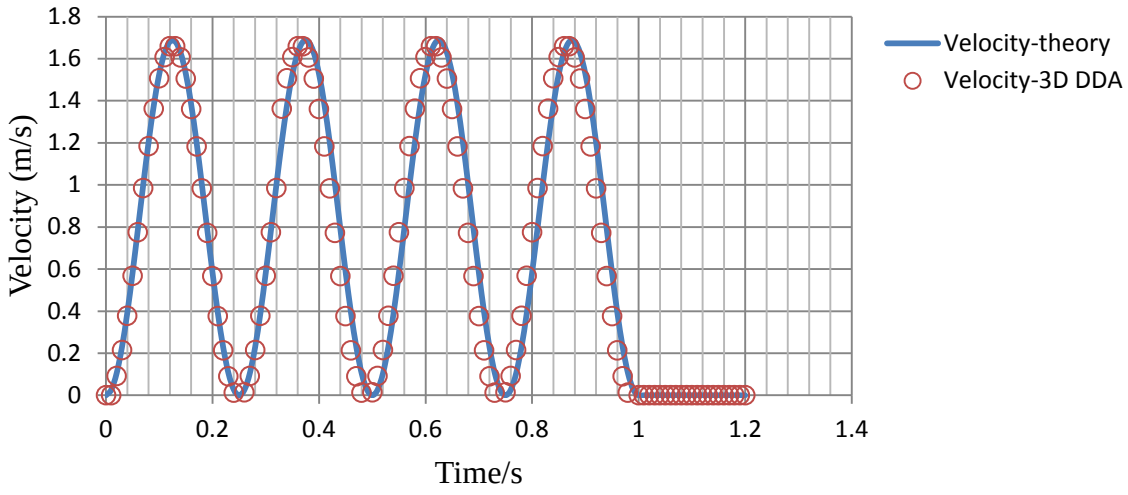

Figure 6.20 Comparisons between the 3D DDA and the theoretical solution on velocity

The comparison on the displacement between the 3D DDA and the theoretical solution can be found on Figure 6.21. The very consistency can be discovered. Although there is a difference about 2cm between them, compared with the whole displacement around 80cm, this very small error is acceptable.

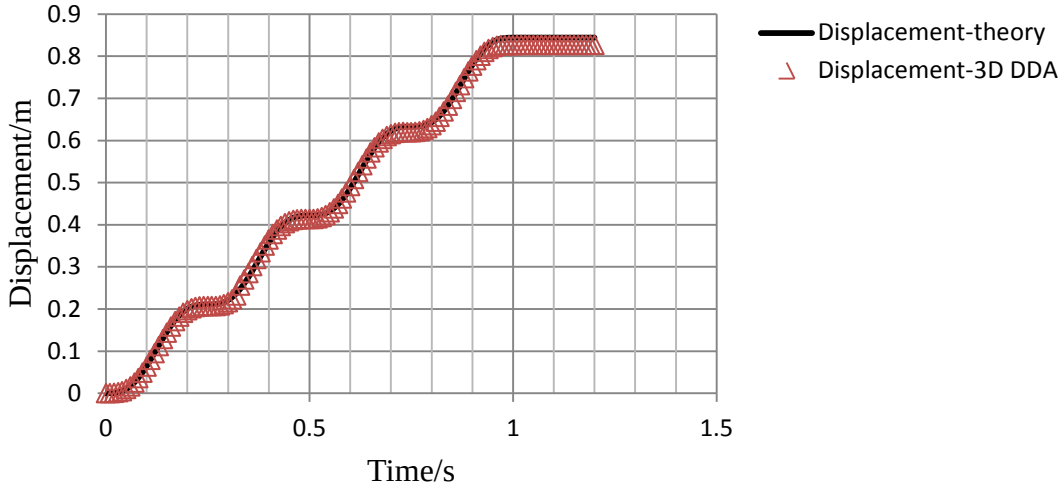

Figure 6.21 Comparisons between the 3D DDA and the theoretical solution on displacement

Therefore, it can be conclude that when the 3D terrain is used, the 3D DDA can reflect the seismic loading accurately according to the close comparison between the 3D DDA simulation result and the theoretical solution. This step makes sure the accuracy of the subsequent research.

6.3.2 THE FAILURE UNDER SEISMIC LOADING

The seismic loading $a_{xy} = 21.21\sin(8\pi t)$ is applied on the Daiganji slope, and the physical and simulation parameters have been illustrated before. Under this seismic loading, the slope tends to be failure. The failure process is shown in Figure 6.21.

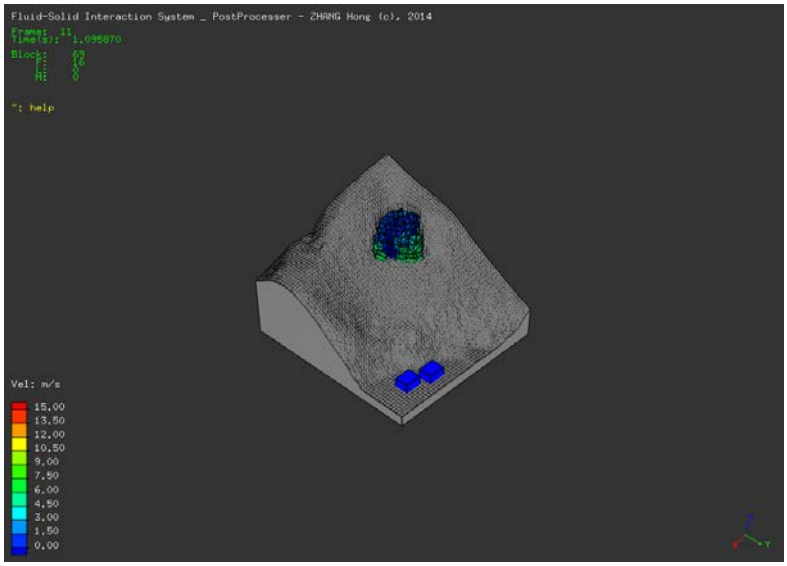

(a) t=1s

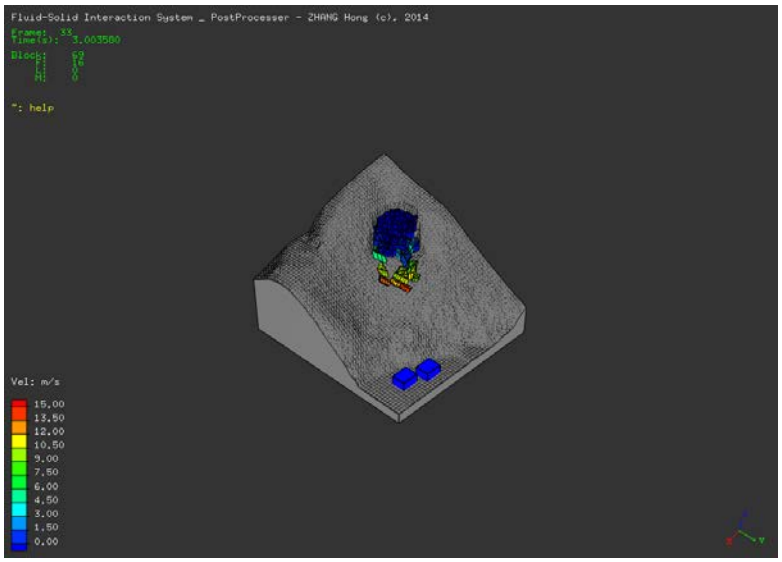

(b) t=3s

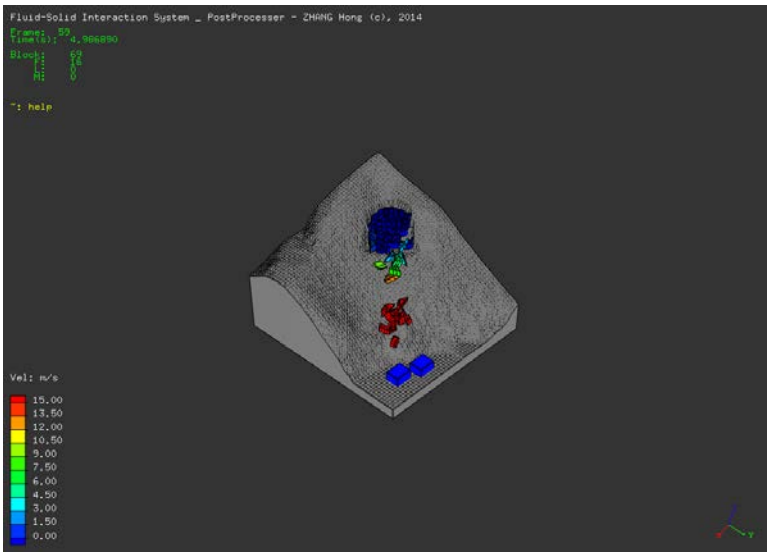

(c) t=5s

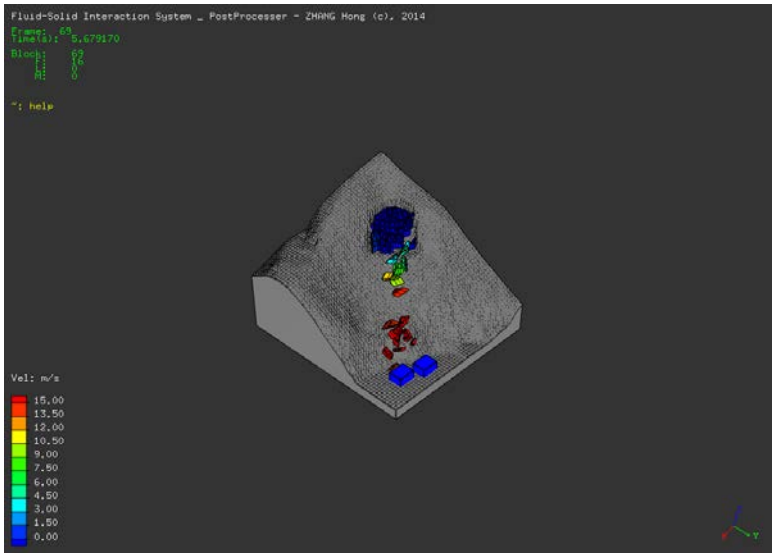

(d) t= 5.68s

Figure 6.22 the failure process under the seismic loading

The color in the Figure 6.22 represents the velocity. It can be seen clearly under this certain seismic loading, the Daiganji slope failures resulting the positon of the excavation road has been influenced which may cause its damage, meanwhile, the houses located downward the slope have been impacted by the failure sliding parts. The detail information of the monitored block's velocity is illustrated by Figure 6.23

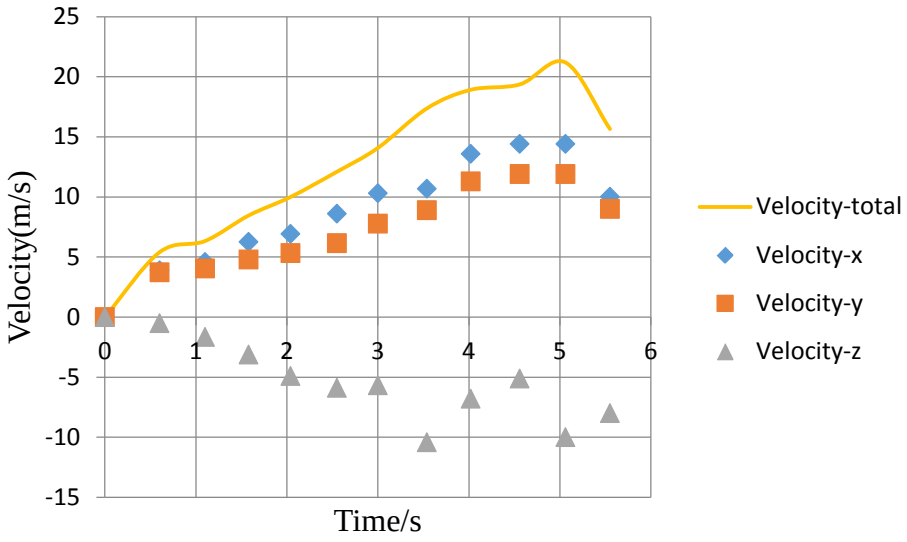

Figure 6.23 the velocity pattern of the monitored block

In the Figure 6.23, the velocity-x, y, z represents the velocity components on the three directions individually. The total velocity is resulted by $v = \sqrt[2]{v_x^2 + v_y^2 + v_z^2}$. The Figure 6.23 shows the following information: 1) the maximum of the total velocity is more than 20 m/s^2, which is very dangerous for both the people and houses;2) a clear decrease of the velocity happens around 5.2s, resulting from the impact on the house downward located; 3)during the whole process, the velocity on the x and y direction is different, which illustrate the development of the lateral movement because the sliding direction is almost on the symmetry of x and y direction.

In order to know exactly how much the factor of safety (FOS) is, the shear strength reduction method is used. As the Daiganji slope is unstable before the reduction, the strength reduction factor (SRF) will be below the unit one until a stable state can be found. The monitored block is just the same as that in stability analysis. Differently, in this section, the whole displacement d is used, $d = \sqrt[2]{d_x^2 + d_y^2 + d_z^2}$, in which the three components are its displacement on the three direction separately.

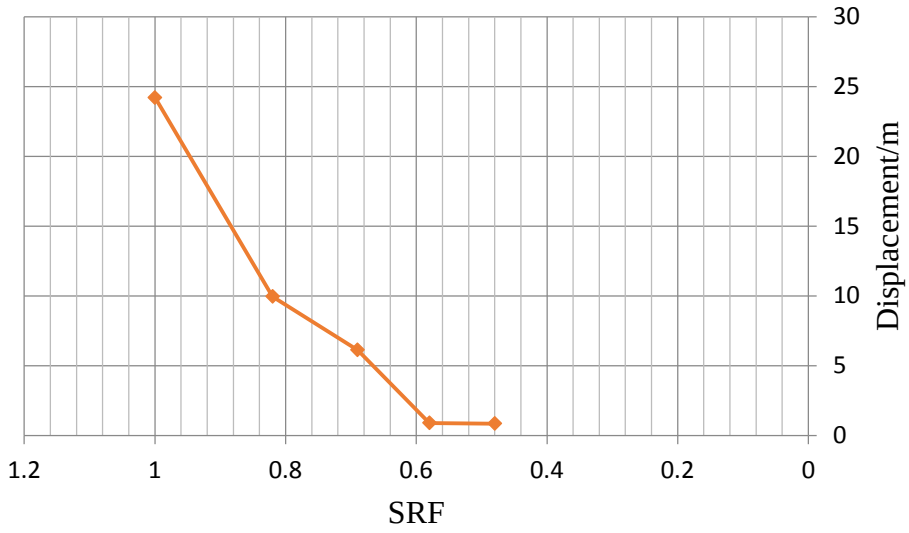

Figure 6.24 The change of SRF with displacement when simulation time is 3s

A strong drop of displacement can be found when the SRF value drops. This means with the increase of the shear strength, the slope will be more stable just as the Figure 6.24 shows. An obvious inflection point can be found when the SRF is 0.58 this point is considered as the value of FOS under this certain seismic loading.

6.3.3 The Influence of Seismic Directivity on The Stability

"Although the presence of site response directivity is not frequently reported in literature, this does not mean that it is uncommon in hillslope areas" (Vincenzo Del Gaudio, 2011). The scheme of the applied directional seismic loading is illustrated in Figure 6.25. There are three pints need to be illustrated:1) the case one is just that in section 6.3.2; 2) for case 3, because the nearly perpendicular on the sliding direction, the seismic loading doesn't make any efforts on the FOS; 3) all the magnitude of the applied directional seismic loadings is kept in consistent.

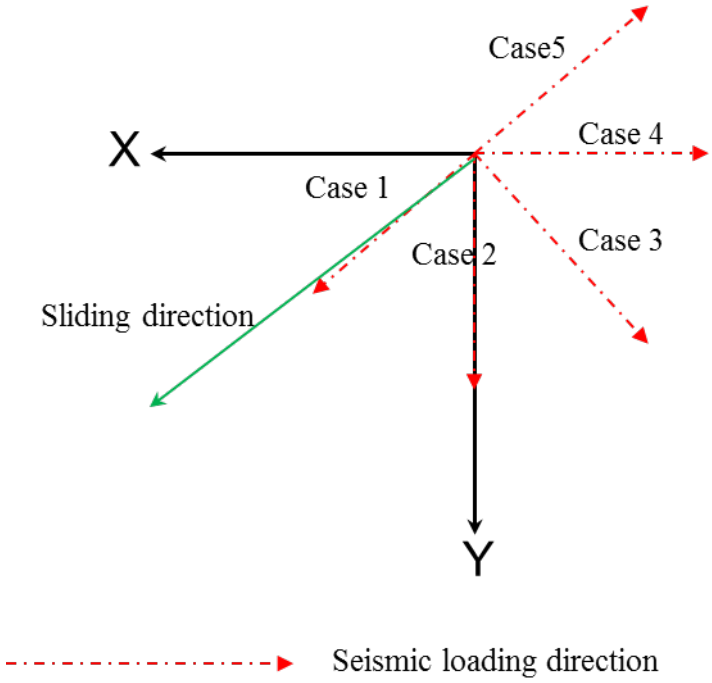

Figure 6.25 The direction of applied seismic loading

Because case 1 has been performed during the section 6.3.2 and case 3 got the very nearly the same result as without seismic loading, only the results of case2, case 4 and case 5 are shown in Figure 6.26 (a), (b) and (c).Jut like before mentioned. The displacement is related the monitored block and the SRF represents the strength reduction factor.

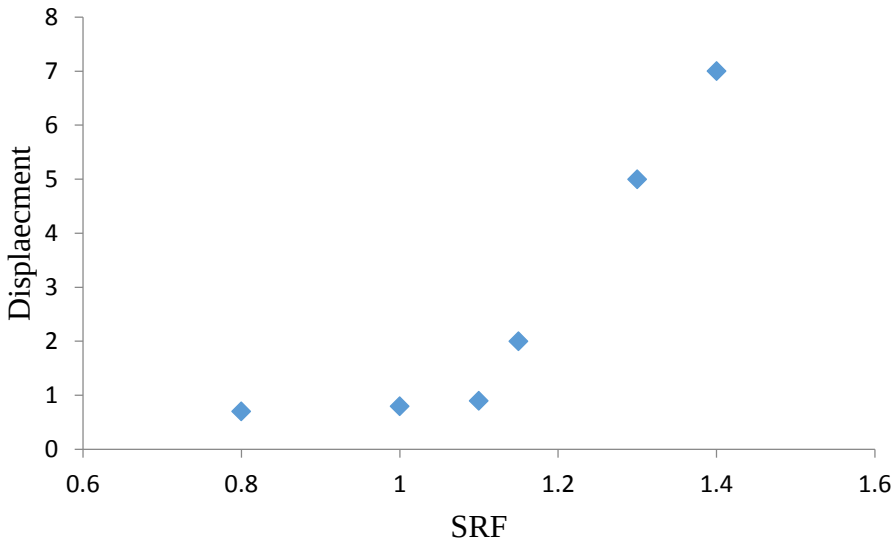

(a) Case 2

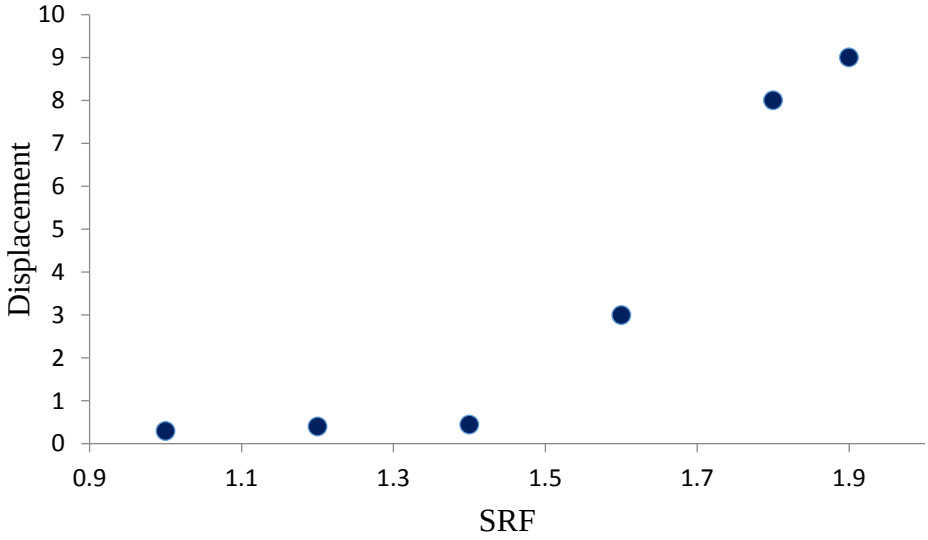

(b) Case 4

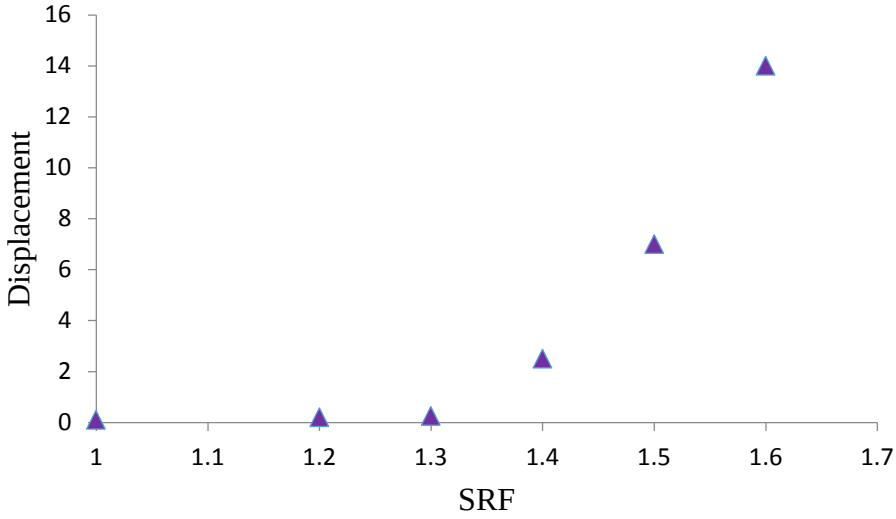

(c) Case 5

Figure 6.26 The change of SRF with the monitored block's displacement for Case 2, 4 and 5.

If we take the SRF at the inflection point as the FOS, then the factor of safety for Case 2, Case 4 and Case 5 are 1.1, 1.4 and 1.3 seperately.

Then, the factor of safety for these 5 cases mentioned in Fig. 6.24 can be listed together as Fig. 6.27 shows.

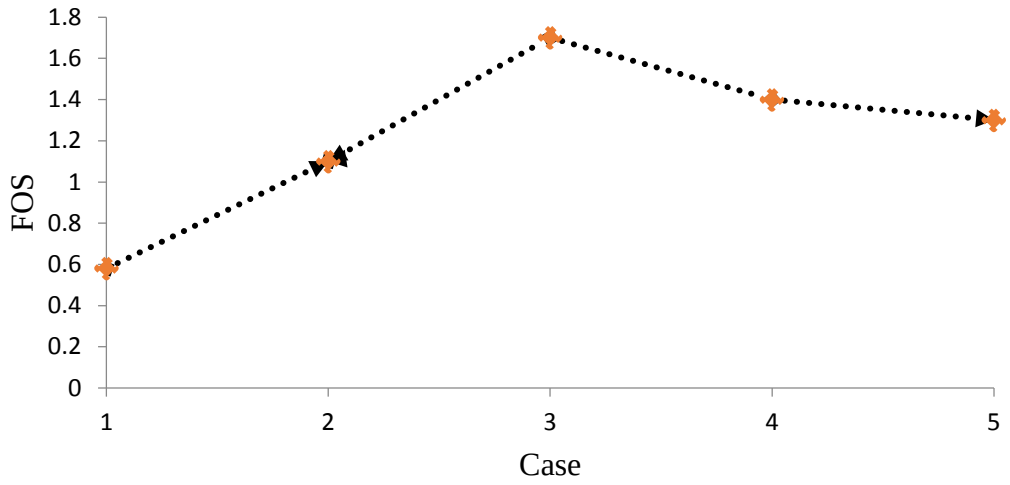

Figure 6.27 The FOS for different seismic loading cases

It can be found that the direction of seismic loading has a huge influence on the slope's factor of safety. Same conclusions can be drawn as: 1) the most dangerous state for the direction of seismic loading is when it is the same as the slide direction (Case1); 2) the most stable case is when the applied seismic loading perpendicular to the slope's sliding direction (Case3); 3) when the direction of seismic loading is opposite to slope's slide direction (Case5), it will cause of a certain small reduction of the factor of safety.

6.4 THE EFFECT OF ANCHOR REINFORCEMENT

The anchor reinforcement is a normal way that is used in the slope prevention. In order to test the function of anchor reinforcement under the earthquake, five anchors are arranged (Figure 6.28).

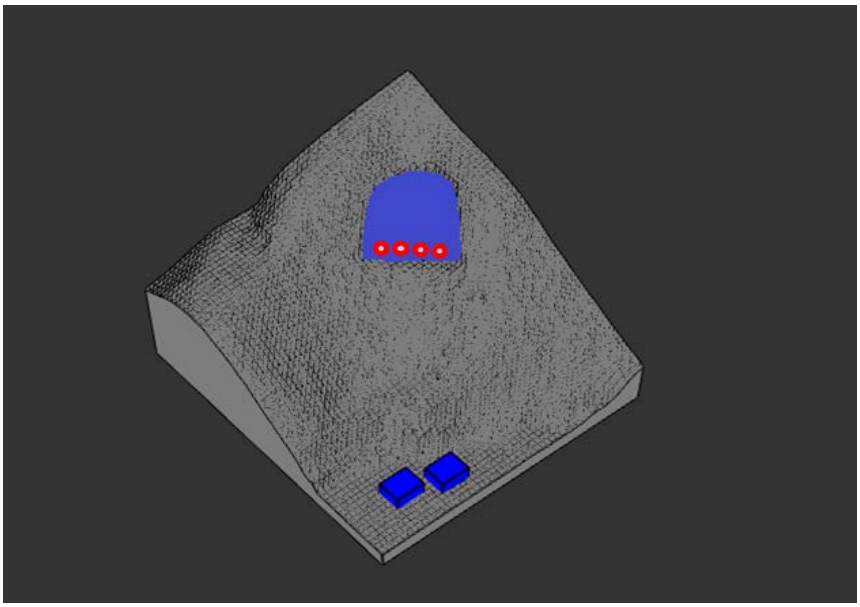

(a)

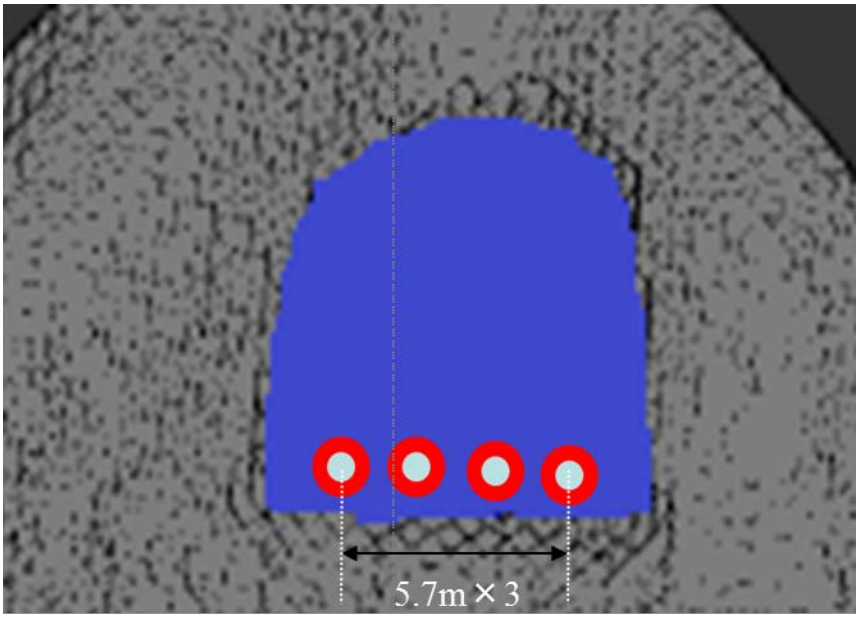

(b)

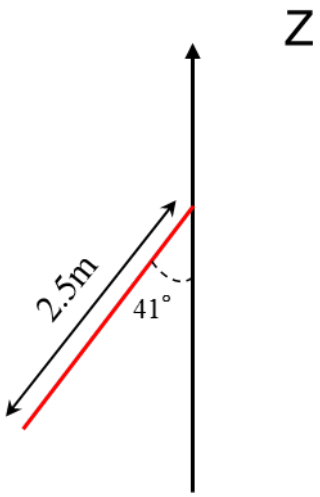

(c)

Figure 6.28 The arrangement of the anchors, (a) the whole view of the anchors, (b) the overlook and the anchor interval, (c) the anchor length and space angle.

During the earthquake, there are four anchors are arranged with a horizontal interval of 5.7m each by each. The seismic loading is just as case 1 shows. The four anchors are of the same physical parameters with the stiffness of 100 MPa (the 50 MPa has been tried), resistance force 10 KN, and limit strain 30%.

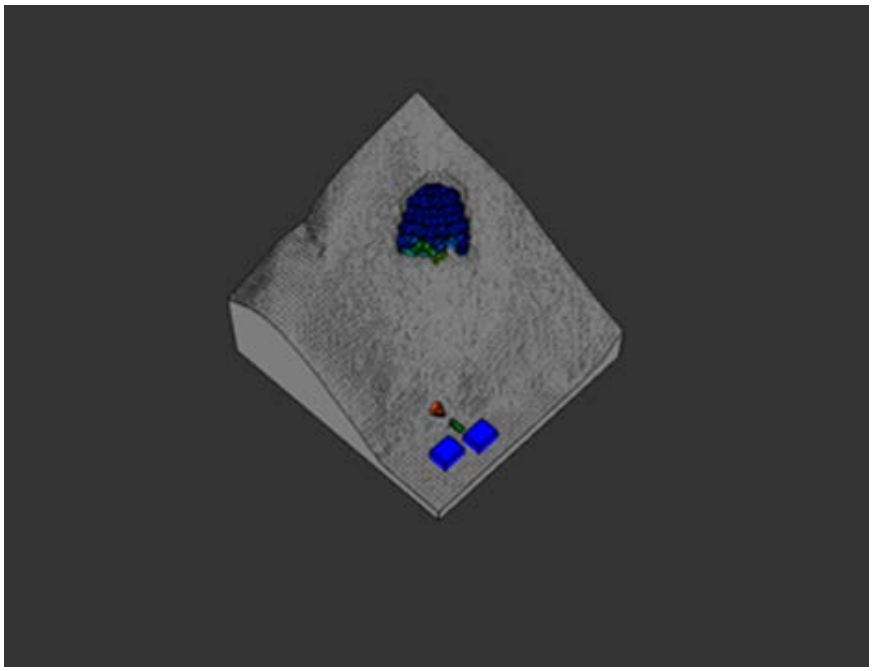

(a) Anchor with stiffness 50 MPa, simulation time around 7s

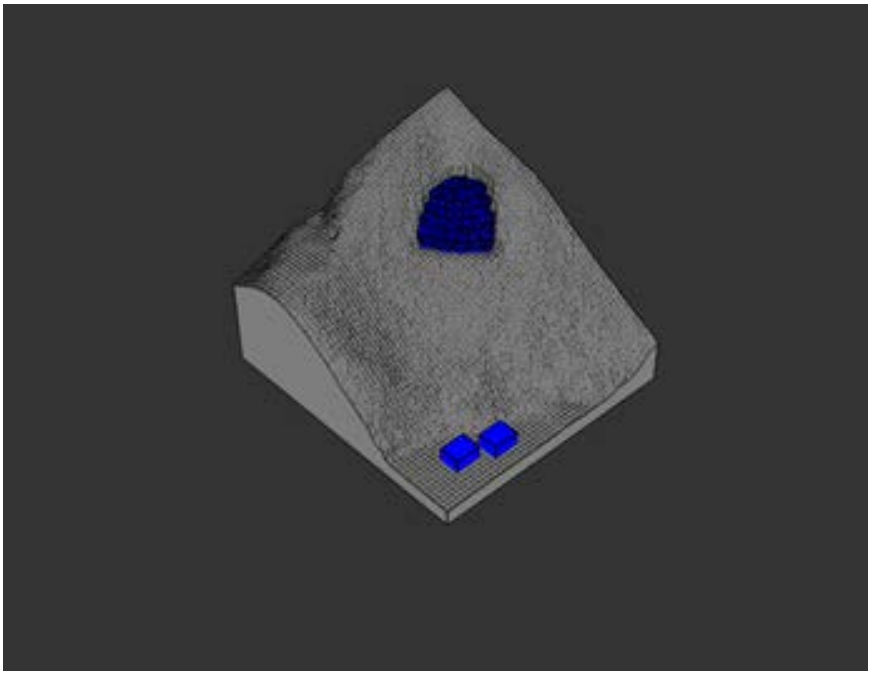

(b) Anchor with stiffness 100 MPa, simulation time around 7s

Figure 6.29 (a) Anchors with stiffness 50 MPa, simulation time around 7s; (b) Anchors with stiffness 100MPa, simulation time around 7s.

It can be found from that with the increase of the anchor's stiffness from 50MPa to 100 MPa, the slope is tender to be stable. When the stiffness of 50MPa is used, the Daiganji slope failures under the seismic loading, While if the stiffness is 100MPa, the slope is stable under seismic loading after a long period of simulation time. The effect of the anchor reinforcement can also be found by the increase of factor of safety as figure 6.30 illustrated. When the anchor stiffness is 0, it means no anchor reinforcement is arranged. If can be found that, when the anchor stiffness is increased from 50MPa to 100MPa, an obvious increase of factor of safety (FOS) happens, which illustrates that the anchor really works and if the parameters of the anchor are suitable the effect of landslide reinforcement under the seismic loading is obvious

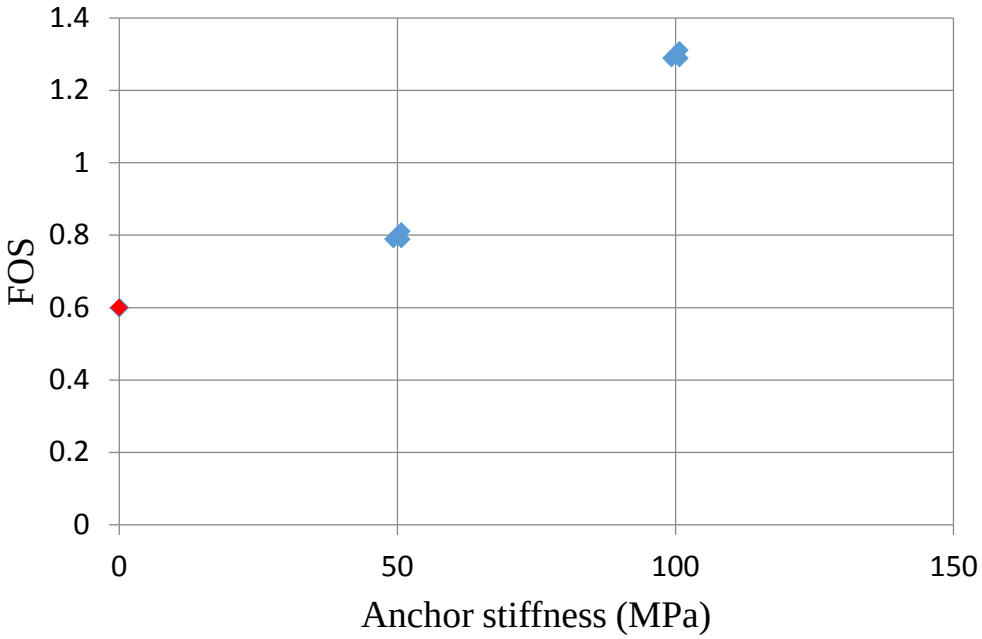

Figure 6.30 The relationship between the anchor stiffness and the FOS

6.5 CONCLUSIONS

(1) In the stability analysis without seismic loading, a great different between the 2D and 3D DDA can be found. For the 3D DDA, it is around 1.7, which is bigger than the 2D, 1.31

(2) When the certain seismic loading is applied on the direction of sliding direction, a great drop of FOS may happen, from 1.7 to 0.58.

(3) The directivity of seismic loading has a huge influence on the stability. The most dangerous case is when its direction is the same as the slope sliding direction.

(4) The effect of anchor reinforcement is obvious. During the most dangerous seismic case, the arranged anchors can improve the FOS from 0.6 to 1.3.

REFERENCES

Ke TC. (1993). Simulated test of two-dimensional heterogeneous and discontinuous rock mass using Discontinuous Deformation Analysis, PhD thesis, Department of

Civil Engineering, University of California, Berkeley.

Lin CT, Amadei B, Jung J and Dwyer J. (1996, October). Extensions of discontinuous deformation analysis for jointed rock masses. In International journal of rock mechanics and mining sciences and geomechanics abstracts (Vol. 33, No. 7, pp. 671-694). Pergamon.

Popov EP. (1996). Mechanics of materials. 2nd ed. New York: Prentice-Hall; 1996.

Wyllie, DC and Mah C. (2004). Rock slope engineering. CRC Press.

CHAPTER 7

CONCLUSIONS

7.1 SUMMARIES AND RESULTS

(1) A close comparison between the 2D and 3D DDA has been performed to reveal the limitation of the 2D analysis and the necessity of 3D DDA. Their advantages and disadvantages are illustrated based on slope stability analysis and run-out simulation. The limitations of 2D analysis is obvious, without considering the lateral effect, the factor of safety is often underestimated and lateral spread movement cannot be estimated in run-out analysis. On the other hand, the lateral friction and the lateral spread movement can be considered in 3D DDA analysis, the factor of safety can be estimated and the reasonable run-out can be simulated more accurately. Some meaningful conclusions have been drawn: 1) The factor of safety is different from section to section. The 2D analysis underestimates the factor of safety around 20% as the lateral friction cannot be considered, and the relative error may increase when the strength parameters increases. 2) When the run-out analysis is compared it can be concluded that run-out distance of the 2D DDA analysis is greatly different from the 3D DDA solution, and the run-out distance is different from section to section. Moreover, the lateral spread can be considered in the 3D DDA method, a lateral spread of 30 meters can be found, which is of practical meaning for the disaster mitigation.3) The FOS from the 3D DDA is in good agreement with the theoretical solution. Therefore, it is more meaningful and accurate to use the 3D analysis than the 2D.

(2) A practical pre-processor to easily construct a complex 3D slope model for the 3D DDA program has been developed. There are two major barriers for constructing a real and complex 3D slope model for 3D DDA: (1) how to generate the blocks; (2) how to consider the 3D slope terrain. The developed pre-processor solves these two problems by taking the advantage of the commonly used commercial software: 3ds Max and ArcGIS. Arbitrary-shaped 3D bocks are made with 3ds Max and complex slope terrain mesh data are obtained from the ArcGIS. A pre-process program is developed to combine the output data from both 3ds Max and ArcGIS and translate them to the 3D DDA model format. The example of building the Daiganji slope has shown that the 3D DDA slope model can be easily and effectively made for any real slope with complex terrain by using the newly developed 3D DDA pre-processor, which makes it possible for applying 3D DDA to practical landslide study.

(3) The existing 3D DDA program has been extended by adding the function of seismic loading and the function of anchor reinforcement. The stability analysis and run-out estimation of a potential earthquake induced landslide need the function of dealing with seismic loading in a 3D DDA program. The added seismic loading function can use either displacement wave or acceleration wave, which depends on the data available. In addition, when a slope is judged unstable under a potential earthquake, the slope should be reinforced in general. Rock anchor reinforcement is one of typical preventive methods. Thus, it is necessary to evaluate the preventive effect and provide the useful information for optimum design of the size and number of rock anchors. By adding these two functions, the new 3D DDA program makes it possible to assess the hazard of earthquake induced landslides for securing the safety of tsunami evacuation sites and access roads.

(4) The application of the new 3D DDA program on practical hazard assessment of earthquake induced landslides for securing the safety of tsunami evacuation sites and access roads in the coastal area of Oita prefecture has been performed. The Daiganji slope is taken as an example. An access road to a tsunami evacuation site and several houses are located at the slope downward. At first, the slope stability is

analyzed by using both 2D and 3D DDA. The results are compared with those from the commonly used limit equilibrium method. The adaptability of DDA and the difference between 2D and 3D analysis are shown. Secondly, the factor of safety is analyzed by using earthquake loading. And the influence of seismic directivity on the slope stability is analyzed. The landslide run-out is estimated by using the new 3D DDA program under the condition of the earthquake. It is shown that the access road and some houses are threatened by the potential landslide. Finally, the stability analysis of an anchor reinforced slope is performed to evaluate the preventive effect. It has been shown that the new 3D DDA is very useful and powerful enough for hazard assessment of earthquake induced landslides.

7.2 RECOMMENDATION AND FUTURE STUDIES

1) For the original 3D DDA program, the contact detection and contact mechanism theory is not mature, especially when the concave blocks are taken into consideration. It is necessary to put efforts on this issue.

2) It is necessary to introduce the viscous boundary into the 3D DDA, which is necessary when simulation the press wave propagation. Although some efforts have been made on the 2D DDA, it is still a blank for the 3D DDA.

3) The fluid flow should be considered in the 3D DDA. For the fractured rocks, the fluid flow has a significant influence on the solid deformation. However, up to now, the relevant research by the 3D DDA is just in the very beginning.

4) It needs a deep research on the joint's constitutive model in the 3D DDA. In the current 3D DDA program, the Mohr-Coulomb is used to simulate the mechanism of the rock joint. How to simulate the residual strength of the rock joint and how to consider the strength reduction under cyclic loading are two issues need to be solved.

5) To improve the computation efficiency of the 3D DDA. Besides of the contact detection, the other aspect that greatly influences the computation efficiency is the 3D DDA's program organization, which is not designed for the parallel

computation. It is believed that if the 3D DDA program can be re-organized and edited to be the parallel edition, with the help of the GPU (Graphic Processing Unit), the computation efficiency of the 3D DDA should be greatly improved.

6) Deep research on the coupling the 3D DDA with the FEM. By coupling these two programs, not only the block's large deformation can be considered but also its inner stress and deformation can be obtained. Although some efforts have been made on this, this research is just on the preliminary level and should be continued.

7) More practical applications should be performed such as the 3D slope，rock-fall, underground cave and etc.. Because the powerful pre-processor has been developed, it is necessary and meaningful to make more practical applications.